AD-A269 037

MENTATION PAGE

Form Approved
OMB No. 0704-0188

REPORT DATE	3. REPORT TYPE AND DATES COVERED
	Final Report 1 May 91 - 29 Feb 92

4. TITLE AND SUBTITLE

Optical Millimeter-wave interactions: measurements, generation, transmission and control

5. FUNDING NUMBERS

AFOSR-91-0209

6. AUTHOR(S)

Dr Robert T Wangemann

7. PERFORMING ORGANIZATION NAME(S) AND ADDRESS(ES)

IEEE/LEOS
445 Hoes Lane
P. O. Box 1331
Piscataway NJ 08855-1331

AFOSR-TR-

8. PERFORMING ORGANIZATION REPORT NUMBER

93 0662

9. SPONSORING/MONITORING AGENCY NAME(S) AND ADDRESS(ES)

AFOSR/NE
110 Duncan Avenue Suite B115
Bolling AFB DC 20332-0001

10. SPONSORING/MONITORING AGENCY REPORT NUMBER

2301/A1

11. SUPPLEMENTARY NOTES

12a. DISTRIBUTION/AVAILABILITY STATEMENT

UNLIMITED

DISTRIBUTION STATEMENT A
Approved for public release;
Distribution Unlimited

12b. DISTRIBUTION CODE

13. ABSTRACT *(Maximum 200 words)*

TOPICAL MEETING WAS HELD

93-20503
174pp

14. SUBJECT TERMS			15. NUMBER OF PAGES
			16. PRICE CODE
17. SECURITY CLASSIFICATION OF REPORT	18. SECURITY CLASSIFICATION OF THIS PAGE	19. SECURITY CLASSIFICATION OF ABSTRACT	20. LIMITATION OF ABSTRACT

SUMMER TOPICAL MEETINGS

LEOS 1991
Summer Topical Meetings

on

Spaceborne Photonics: Aerospace Applications of Lasers and Electro-Optics

July 22-24

Sponsored by the IEEE Lasers and Electro-Optics Society and in cooperation with the IEEE Aerospace and Electronic System Society and the Optical Society of America

and

Optical Millimeter-Wave Interactions: Measurements, Generation, Transmission and Control

July 24-26

Sponsored by the IEEE Lasers and Electro-Optics Society and in cooperation with the IEEE Microwave Theory and Techniques Society and the Optical Society of America

Sheraton, Newport Beach
Newport Beach, California

IEEE

IEEE LASERS AND ELECTRO-OPTICS SOCIETY LEOS

Spaceborne Photonics: Aerospace Applications of Lasers and Electro-Optics

July 22-24, 1991

Sheraton Newport Beach
Newport Beach, California

Support provided by:
NASA Langley Research Center
Defense Advanced Research Project Agency

IEEE# 91TH0345-9

Library of Congress #: 90-85245

The papers in this book comprise the digest of the meeting mentioned on the cover and title page. They reflect the authors' opinions and are published as presented and without change, in the interest of timely dissemination. Their inclusion in this publication does not necessarily constitute endorsement by the editors, the Institute of Electrical and Electronics Engineers, Inc.

IEEE#: 91TH0345-9
Library of Congress #: 90-85245
ISBN: 0-87942-618-7 Softbound
0-87942-619-5 Microfiche

F O R E W O R D

Welcome to the first summer topical meeting on Spaceborne Photonics! With a total of 46 scheduled papers, it will provide an up-to-date review of the use of lasers and electro-optics for future space missions and advanced aeronautics applications. Special emphasis will be placed on the uniqueness and significant mission-enhancing features provided by photonics technologies, and comparisions will be made, where possible, with alternative approaches.

The comprehensive program starts with a Plenary Session consisting of four speakers who will each give a unique perspective on the use of photonics for aerospace applications. The conference will continue with technical sessions in the following areas: Flight Applications; Nonintrusive Measurement for Aeronautics; Automation, Robotics, and Humans in Space; Optical Communications & Storage, Lasers and Lidar Systems; and Remote Detection and Identification. Each session will be introduced by at least one prominent Invited Speaker followed by a series of state-of-the-art contributed papers.

Spaceborne Photonics will also include a Panel Discussion involving high-level executives, program managers, and scientists. They will present their ideas on current and future aerospace applications of photonics technologies and systems, then participate in a question-and-answer session with the attendees. The Panel Session will be folllowed by the Conference Reception which will allow time for more informal discussions.

E.D. Hinkley
TRW Space and Technology Group

Frank Allario
NASA Langley Research Center

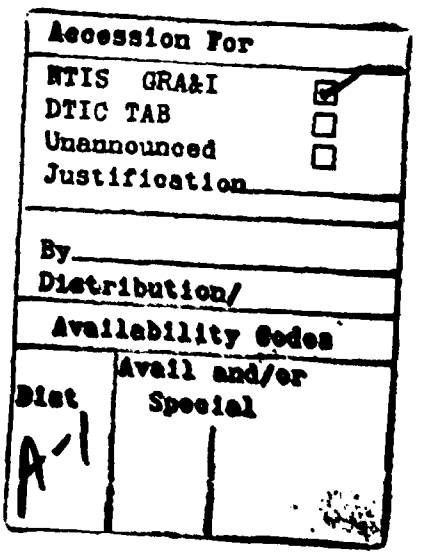

TECHNICAL COMMITTEE

General Co-Chairmen

E. David Hinkley
TRW Space & Technology Group

Frank Allario
NASA Langley Research Center

Program Committee

John Bowers
University of California, Santa Barbara
Robert Byer
Stanford University
Ramon dePaula
NASA Headquarters
Mario Dagenais
University of Maryland
Thomas Giallorenzi
Naval Research Laboratory
Brian Hendrickson
Rome Lab
Alan Johnston
Jet Propulsion Laboratory
Louis G. Kelly, Jr.
Litton Data Systems
Louis S. Lome
Strategic Defense Initiative Office
Richard Miles
Princeton University
Stewart Ocheltree
NASA Langley Research Center
Robert Rice
McDonnell-Douglas
Chandra Roychoudhuri
United Technologies Optical Systems
S.C. Wang
Lockheed Research Laboratory
Andrew Yang
DARPA

TABLE OF CONTENTS

MONDAY, JULY 22, 1991

PLENARY SESSION

MA: FLIGHT APPLICATIONS

MB: NON-INTRUSIVE MEASUREMENTS FOR AERONAUTICS

TUESDAY, JULY 23, 1991

TuA: AUTOMATION, ROBOTICS, & HUMANS IN SPACE

TuB: OPTICAL COMMUNICATION

TuC: SENSING FOR GLOBAL CHANGE

TuD: OPTICAL COMPUTING AND STORAGE

TABLE OF CONTENTS

WEDNESDAY, JULY 24, 1991

Monday

July 22, 1991

P1

Photonics: Past, Present, and Future

S. R. Forrest
National Center for Integrated Photonic Technology
University of Southern California
Los Angeles, CA 90089-0241

Abstract

We will review advances in materials, devices and systems now at the forefront of photonic research. Emphasis will be placed on discussing the state-of-the-art in optoelectronic integrated circuits (OEICs) and photonic integrated circuits (PICs), and their future use in numerous applications.

P2 Photonics for Future NASA Missions

RAMON P. De PAULA
NASA HEADQUARTERS
WASHINGTON DC, 20546
(202) 453-2742

Photonics is a relatively new and still rapidly developing discipline that can change the means of implementing future NASA missions and should receive strong support from future mission planners.

The goal of the photonics program is to support future NASA missions by developing hybrid photonic / electronic devices and systems in the areas of sensing, communications, computation and control that will have an order of magnitude improvement in performance relative to existing technology. These systems will be of particular significance in meeting the requirements of Earth-Observing Platforms, Astrophysics Missions, and Mars and Lunar exploration missions.

Photonics will enable or enhance operations such as: hazard avoidance for autonomous Mars and Lunar landers, autonomous rendezvous and docking, advanced vision for robotic systems, very high data rate transmissions, multi-spectral infrared imaging, high-speed processors, fault-tolerant networks, continuous health monitoring of space structures (smart skins), and special purpose processing, including data systems, image processing, mission operations, and advanced remote sensing instruments operating at unprecedented wavelengths.

Table 1 shows a summary of future mission requirements, performance goals and identifies the future photonic system that can meet the requirements. Additionally, state-of-the-art capabilities are identified. In order to meet these requirements we must establish an R&D program in the following areas: (1) photonic materials, components and devices, including optoelectronic integrated circuits (OEIC's), special purpose lasers, a spacial light modulator, and optical amplifiers; (2) optical processing and advanced optical pattern recognition; (3) networking for tight coupling of large distributed data systems such as those necessary for lunar or Mars bases; (4) In situ sensors for structure monitoring.

The key payoffs of photonics is that it will provide spacecraft systems with very high reliability, less power consumption, size, and weight with an order of magnitude improvement in performance. For example, high data throuput in the order of 10^4 to 10^5 MIPS at a power consumption of 10^3 MIPS/Watt will be possible. Increased high rate networks system capacity with power consumption of 1 W/node and decreased error rates. New laser wavelengths will provide unique capabilities in atmospheric sensing not available today.

TABLE 1. MISSION REQUIREMENTS AND PERFORMANCE GOALS FOR PHOTONIC SYSTEMS

TOP LEVEL MISSION REQUIREMENTS	TECHNOLOGY PERFORMANCE GOALS	PRESENT STATE-OF-THE-ART PERFORMANCE	FUTURE PHOTONIC SYSTEM
Hazard detection during autonomous landing	• Real-time detection of >0.5m objects, >15° slopes • Input power <50W	• Digital algorithm • Scanning laser rangefinder • Capability does not exist now	• Compact photonic pre-processor • Optical neural processor, off-loads lander general purpose digital computer
Order of magnitude improvement in data system capability for handling science data, images, and mission operations	• Networking to support multi-gigabit data streams • Terabyte storage • Real-time manipulation of HDTV images	• Ethernet, few Mbit, or FDDI, 100 Mbit • Magnetic tape or optical CD storage	• Fiber networking for 3-10 Gbit/sec data rate; 1μsec latency • Optical volume memory for mass storage
Multi-spectral imager for visible and IR wavelengths	• Simple, small, agile, staring mode multi-spectral imager • 200 pixels • 70 wavelengths	• Filter wheel camera or complex instrument, for example HIRIS or AVIRIS	• Acousto Optic Tunable Filter instrument • Separate electronically tunable instruments for the visible and the IR wavelengths ranges
Sub-millimeter wave receiver	• 3THz devices working at 10 times the quantum limit	• Semiconductor or superconductor devices for 500 – 1 THz	• Non-linear optical elements to up-shift or mix sub-millimeter images to detectable optical frequencies
Superlattice detectors for far-IR, sub-millimeter waves	• λ's up to 20μm IR • ≥65K working temperature • Submillimeter mixer array	• Not available	• New devices would simplify existing instruments
Metrology sensor for inter-spacecraft positioning	• Scannable beam • 10^{-7} metrology	• Surveying type instruments (accurate, but slow)	• Phase-locked semiconductor laser system for rapid, scannable measurements
Scene correlation for landmark guidance	• 30 images/sec • 300-1000 pixel image format • 30 W total power	• Digital algorithm on video data • 8x8 pixel search • 256x256 final correlation	• Stand-alone optical processor for real-time correlation; off-loads general-purpose computer
Specialized laser sensors	• Tunable, high-power laser at accurately predetermined λ's	• Not available	• New laser would enable compact spectral sensor for atmospheric composition
100 Gbit/sec cross-correlator	• ≤10W optical preprocessor	• Digital on-line special purpose chips	• Optical in-stream filter to perform special processing functions
Microwave antenna arrays	• Micro-second beam scanning capability	• Arrays are built up from discrete components • Very costly	• Array integrated into composite skin structures • Feed and control by optical fibers and optoelectronic chips
Health monitoring of space structures	• Continuous monitoring of temperature, strain and vibration	• Laboratory demonstration	• In situ fiber optic sensor network imbedded in composite skin structures

P3

Photonics: A View from an Astronaut

Ellen Ochoa

NASA Johnson Space Center
Astronaut Office
Houston, TX 77058

Summary

Photonics technology is attractive for space-based applications because of the need for high speed processors with low weight and power requirements. This talk concentrates on the optical information processing aspect of photonics, because that is the area I performed research in before being selected for the astronaut program in 1990. Several examples are presented of how optical information processing can contribute to manned space flight objectives, either by assisting in tasks that are time-consuming, repetitive, or dangerous, or by accomplishing tasks that may be too difficult for humans, especially after long spaceflights.

These examples are based on the use of an optical processor which usually takes the form of a correlator. The correlator consists of a coherent light source, a set of Fourier transform lenses to transform spatial information into spectral information, input and filter plane spatial light modulators, and a detector. The spatial light modulators are programmable so the input and/or filters can be rapidly changed to accomplish the desired task, generally a recognition problem. Other types of transform and matrix operations are also possible. The optical processor should be thought of as one component of a heterogeneous computing system that will have the capability to make decisions based on the results of the optical processors and provide feedback to it.

One very important use of photonics is in vision processing section by a robotic servicer, perhaps used for building and maintaining structures in space. The Space Station is going to require many hours of EVA (extravehicular activity or "space walks") to build. Over its proposed lifetime of 30 years, it will need to be maintained, inspected and repaired. The same is true for structures to be used in a lunar base or a Mars outpost. While astronauts are more than happy to volunteer for space walks, there are considerations that limit the amount of time that can be spent in EVA, and the amount of work that can be done in a given time.

One problem is the physical difficulty of working in a space suit. The suits are many layers thick to protect against the space environment, and certain motions are difficult to achieve. Even the simple motions may become tiresome after a few hours, and EVA is particularly hard on the forearms and hands. The gloves are thick compared to fingers, and require constant tension to keep them in the proper configuration while working. Astronauts are currently not scheduled to do space walks two days in a row to allow time for their muscles to recover. The physical exertion coupled with the need to be restrained at all times mean that tasks are completed slower in suits than they would be in a shirt-sleeve environment.

The use of crew time is another consideration. EVAs currently require the full-time attention of three crew members - two EVA astronauts and an astronaut inside the shuttle monitoring their actions. There is also time allotted to don and doff the suits, and to complete a pre-breathe protocol that protects astronauts from the bends. For routine maintenance tasks, a robotic servicer that only required the attention of one monitoring astronaut would free up crew time to pursue scientific and engineering experiments.

Another concern is the overall safety of the crew. EVAs are currently scheduled so that astronauts receive no more radiation that they would if they remained in the orbiter. It may not be possible to always schedule them so advantageously, and medical standards call for limiting the amount of radiation that each person receives. Another safety measure is to send out EVA astronauts in pairs and to keep both of them in sight from inside the orbiter. This rule limits the types of activities that can be done on the shuttle (for example, tiles on the underside of the shuttle cannot be repaired) and will have a similar impact on building the station.

There is also a small chance that a space suit will malfunction or be penetrated by a micrometeoroid. While astronauts, and the space program in general, are willing to accept that risk to accomplish the country's space goals, it makes sense to consider robotic devices for routine inspection and maintenance tasks. The astronauts can then use their EVA time to perform more difficult procedures.

On a space station or planetary outpost, there will be a variety of housekeeping tasks inside the station that will be repetitive and costly of crew time. On the shuttle today, the crew needs to change out lithium hydroxide canisters twice a day for the effective removal of CO_2 from the air. While a different system will probably be used in the station, it is an example of a task that could be done robotically. The station or outpost will also need to be wiped down periodically, a task that no astronaut will mind handing over to a robotic system. The more intelligent vision processing capability that a robotic servicer has, the less crew time will be required to monitor these housekeeping tasks, resulting in more science accomplished.

Although the previous examples involve images, similar optical systems can be used as matrix processors for other types of data. One application is the real-time spectral analysis of rocket plumes. This analysis would provide information on the quality of combustion, and the optical system is even envisioned as part of a feedback system that provides for an optimal combustion throughout the launch. Another example is the processing of data on spacecraft health. There are currently over 2000 sensors on the orbiter. Most of the data cannot be processed onboard and are downlinked to Mission Control. With the Space Station, the amount of data will go up by at least an order of magnitude. Even on the ground, it will be difficult to process the data in a timely manner. It would be very helpful to have the capability to do some processing in space for health trend analysis and as a backup to the ground in case of loss of communications.

Finally, there are cases where an intelligent robotic vision system will be necessary to successfully complete a mission. NASA is currently planning robotic missions to Mars as precursors to manned missions. One of the most challenging tasks is to land safely in a predetermined, geographically interesting area. The vision system will be required to provide navigation information as well as to perform hazard avoidance in the final seconds of landing. It is possible that such a system may even be used for a manned mission, since there is concern that humans may have difficulty performing such a complex task after months of space travel.

Given these scenarios, there are many areas of photonics that need to be developed further in order for the technology to be sufficiently mature when needed. These areas include fast programmable I/O devices with low power and weight, new filters to deal with three-dimensional objects and provide noise immunity, hazard avoidance techniques, and efficient interfaces between optical and electronic systems. Several NASA field centers including Ames Research Center, Johnson Space Center and the Jet Propulsion Laboratory are currently working on these issues, though the funding levels limit the effort. Perhaps through collaborative efforts with industry, the technology will be advanced to the point of flight tests within a few years - and we will have an opportunity to test the technology in the space environment.

P4 Aeronautics Applications of Photonics

R. Miles, *Princeton University, Princeton, NJ*

New optical instrumentation has the capability of nonintrusive, multicomponent point and field measurements in unseeded air flows. Approaches include molecular light scattering, fluorescence, and molecular tagging. These devices are currently being implemented in ground test facilities and are under development for flight applications.

MA.1 Fiber-Optics Technology for Aircraft Applications

N. Albion, L. Figueroa, C.S. Hong, D. Gangsaas,
Q. Mendoza, J. Polky and C. Porter

Boeing Defense & Space Group
PO Box 3999, M/S 7J-05
Seattle, WA 98124-2499
(206) 865-3135

Over the last several years, it has become widely recognized that electromagnetic interference (EMI), electromagnetic pulse (EMP), high intensity radio frequency (HIRF), and new threats such as directed-energy weapons can jeopardize the flight safety of vehicles with Fy-By-Wire (FBW) systems, unless adequate shielding precautions are taken. In addition, the long-term trend is for the aerospace community to increasingly use composite materials in airframes, thus eliminating the shielding inherent to the metal skins used in the past. Lastly, with the increasing use of computers and digital transmission, the electrical power and data distribution channels must be heavily shielded. This leads to weight and maintenance penalties. Preliminary estimates by a variety of sources indicate a weight penalty (compared to FBL) of approximately 250 to 500 pounds for transport aircraft having a FBW fight control system. In addition, the assurance of maintaining the integrity of the shielding may become a problem. The penalties are sensitive to the assumed level of threat. Thus, there are strong technical and economic incentives to develop FBL systems for both military and commercial transports.

The presentation reviews the various fiber-optic technologies which are required to implement FBL systems.(1) The future is also explored to see where fiber optics technology might be implemented in areas other than flight control, such as data communications. Technologies which will be discussed include: fiber-optic position sensors, sensor interfaces, sensor multiplexing, fiber-optic transmitters/receivers, semiconductor opto-electronic devices, electronic packaging and opotical interconnections. With the increasing need for higher information bandwidth, fiber optics appears to be positioned for future significant growth and for providing new system architectures with reduced complexity.

Lastly, we will discuss some of the major problems and limitations that need to be overcome for implementing the technology.

(1) L. Figueroa, C.S. Hong, R. Huggins, G. Miller, A. Popoff, C. Porter, D. K. Smith, and B. Van Deventer, "*Fiber-Optics for Military Aircraft Flight Systems*, " IEEE LCS, V.2, P. 52 (1991)

MA.2 Photonic-Based Smart Structures and Engine Control Systems for Aerospace Applications

F. J. Leonberger, J. R. Dunphy and W. L. Glomb
United Technologies Research Center
East Hartford, CT 06108

In the past few years, there has been increasing interest in fiber optic systems for aircraft and space applications. In particular, fiber optics opens new possibilities for diagnostics and controls compatible with new aerospace designs and materials. This presentation will focus on the use of embedded fiber sensors to monitor and control smart composite materials and the use of fiber sensors and optical interconnects for aircraft engine control. Special attention will be given to two types sensors, fiber Bragg grating (FBG) sensors and position sensors (PS), and their system implementations.

A FBG sensor is a narrow-band reflector (30GHz) formed in the core of a single mode fiber.[1,2] When subject to temperature or strain, a variation in the wavelength of reflection will be obtained. These gratings are typically 1 cm long and are formed transverse to the fiber using a noninvasive technique. Gratings have been formed in a large variety of fibers over the .5 to 1.6 micron range and are permanent and robust. An attractive feature of FBGs is that they are an absolute, rather than a relative sensor since the measurand is a wavelength shift.

Arrays of gratings can be formed in a single fiber to form a quasi-distributed sensor. They lend themselves to a variety of multiplexing arrangements including time and wavelength division. The distributed sensors permit ease of multiplexing since multiple sensors can be read from a single input/output port. Examples of demonstrated applications include polymer cure monitoring, static and dynamic strain measurements, structural diagnostics and active damping systems.[3]

For use in a wavelength-division-multiplexing mode, a tunable diode laser source would be highly desirable. By forming an external cavity laser in which the cavity mirrors are the back facet of the laser and a grating in the pigtail, a narrow-line source tunable over 2nm has been demonstrated.[4] Extension to 10nm seems feasible. The tuning is accomplished by piezeoelectrically straining the grating.

Optical fibers and other photonic devices are also under active development for aircraft engine control.[5] Such a "fly-by-light" control system can be built around a central electronic computer that contains electro-optic interface circuits for fiber optic sensors. One attractive architecture[6] contains common, multiplex interfaces to seven sensor groups: (1) self luminous sensors; (2) high temperatures; (3) low temperatures; (4) speeds and flows; (5) vibration; (6) pressures; and (7) mechanical positions. Nine distinct fiber optic sensor types could provide these sensing

functions: (1) CW intensity modulators; (2) TDM digital optic codeplates; (3) TDM analog self-referenced sensors; (4) WDM digital optic code plates; (5) WDM analog self-referenced intensity modulators; (6) analog optical spectral shifters; (7) self-luminous bodies; (8) coherent optical interferometers; and (9) remote electrical sensors. The purpose of this design is to reduce the size and weight attributed to inputs and outputs by multiplexing arrays of functionally similar sensors on a single pair of optical fibers through common electro-optical interfaces. These circuits feature passive optical multiplex of groups of sensors through a common electro-optic interface. Each interface is standardized to multiplex a set number of measurements of a given parameter through a single circuit card in a modular mechanical design.

The most numerous type of sensor on an aircraft engine is a position transducer. At this time the most promising types of fiber optic position sensors are the time domain multiplex (TDM), wavelength domain multiplex (WDM) and coherent frequency modulated carrier wave (FMCW) types.[7]

For photonic systems to be implemented on aircraft and other aerospace vehicles by the turn of the century, accelerated development of components is required to meet the size and environmental requirements for the electro-optic architecture in aircraft control systems. In the area of optical sources, development should address increased optical power for all applications, broader spectra for WDM systems, and lasers for operation at 125 C. Maximum utilization of hybrid optoelectronic packaging and monolithic integrated electronic circuit arrays will be required to produce electro-optic interfaces that fit within the confines of the control enclosure. These components will be in the form of multi-application, general purpose pigtailed functional modules to ease electrical and mechanical design. The performance of optical components (e.g. optical power levels, spectral properties, noise levels, optical loss, and failure rates) must be maintained over the environment. In particular, the performance models used for electro-optic architectures require that over the lifetime (typically on the order of 10,000 hours) and the environment a variety of special conditions must be maintained. Optical source power, spectra, receiver noise and link loss must not drift by more than 3dB, 50nm, 1dB and 3dB respectively. Finally, the failure rate of an interface circuit must be less than 4×10^{-6}/hour.

1. G. Meltz, W. W. Morey and W. H. Glenn, Opt. Lett. 14, 823 (1989).
2. W. W. Morey, G. Meltz and W. H. Glenn, Proc SPIE 1169, 98 (1989).
3. J. R. Dunphy, G. Meltz, F. P. Lamm and W. W. Morey, DoD Fiber Optics Conference '90, p. 410.
4. W. W. Morey, G. Meltz and C. M. Ferrar, Tech. Digest LEOS 1990 Top. Mtg. on New Semiconductor Laser Devices and Applications, p. 16.
5. F. J. Leonberger, W. L. Glomb and J. R. Dunphy, Tech. Digest of OFC '90, p.48.
6. W. L. Glomb, NASA CR 159468 (NTIS).
7. W. L. Glomb, Proc SPIE 1367, 162 (1990).

MA.3

Optically Powered Sensor Technology for Avionics and Flight Control Systems

Paul E. Bjork
Honeywell Inc. Systems & Research Center
MN65-2600
3660 Technology Drive
Minneapolis, Minnesota 55418

Abstract

Future aerospace missions require sensors which are both lightweight and immune to EMI. Honeywell's optically powered sensor approach combines the light weight and EMI immunity inherent in optical fiber data links together with the robustness of existing electrical transducers.

A typical sensor system is composed of an aircraft interface board, an optically powered sensor, and an optical fiber data link. A semiconductor laser diode on the aircraft interface board transmits optical power to the sensor over the optical fiber. At the sensor, a GaAs photodiode is used to collect the optical power. A proprietary dc-dc converter transforms this to well regulated electrical power. A ratiometric synchronous demodulator and an analog to digital converter converts signals from a micropower electrical transducer into binary words. These words are then transmitted back to the aircraft interface board for flight control or system status indication.

Two complete engine throttle lever angle sensors including aircraft interface boards are being delivered for flight tests on NASA's ATOPS aircraft. Temperature stability of less than 0.5% full scale readout error is shown in figure one. We are currently testing temperature, linear position and proximity switches. Operation from -65° to +125°C has been demonstrated.

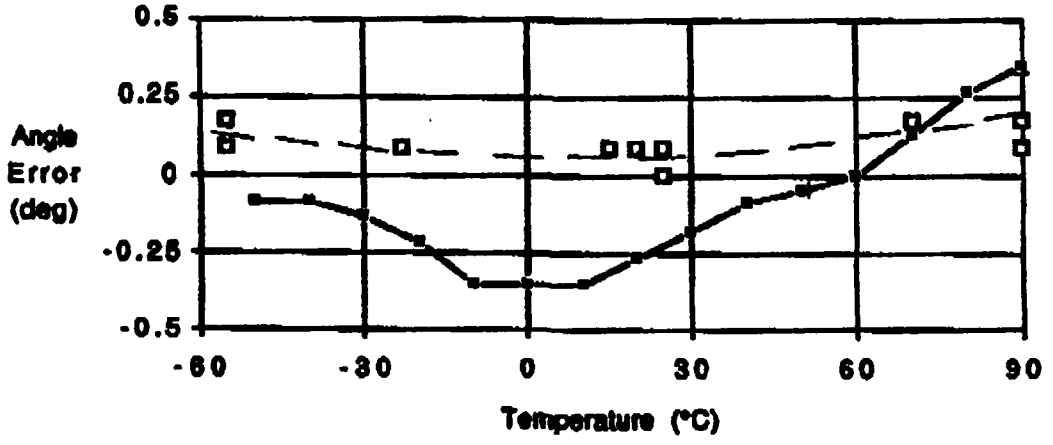

Figure 1: Temperature stability for throttle lever angle sensor (solid line) and aircraft interface board (dashed line)

MA.4 NDE Fiber Optic Experiment in Space

Robert S. Rogowski and Bobby G. Batten
Nondestructive Evaluation Science
NASA Langley Research Center
Hampton, VA 23663-5225

Background

The development of fiber optic sensors for measurement of many chemical and physical properties has provided the opportunity for instrumenting aircraft and spacecraft with lightweight, unobtrusive sensing elements which are immune to electromagnetic interference. The nondestructive evaluation (NDE) of critical parts can now be a continuous process with sensors monitoring the health of a structure in a manner analogous to a nervous system in living organisms. This enabling technology has prompted the description of a new class of materials and structures, "Smart Structures with Nerves of Glass".[1]

Health monitoring of structures in space poses a unique challenge to the NDE community. Space platforms are designed for long duration deployment in a hostile environment. Structural integrity becomes critical when astronauts occupy a space platform as in the present space station concept and when large investments have been made in systems required to perform reliably over long time periods. Continuous health monitoring by remote sensors and robotic test modules will likely be necessary.

Fiber optic sensors for smart structure applications have been developed at the Langley Research Center NDE laboratory and at the Fiber and Electro-Optics Research Center (FEORC)/Virginia Tech with the support of a NASA grant. Several methods are available for strain and vibration measurement with embedded or attached optical fibers. For space deployment these sensors would have to be attached to the structure and survive the environment for many years. A flight experiment will provide valuable information for the retrofitting of a space platform with an optical fiber sensor .

Fiber optic sensors have the potential for continuous monitoring of critical elements of space platforms and spacecraft to insure proper functioning and to detect environmentally induced damage which may compromise safety and performance. If the initial phases of space station are to be instrumented for this purpose, methods of attaching the fibers to the structural elements must be developed. The bond between the optical fiber and the structure

must assure proper transfer of stresses to the fiber and withstand the harsh environment in low earth orbit. The most effective way to test the concept of instrumenting space structures with fiber optic sensors is to subject the sensors and associated electronics to the rigors of a space launch and subsequent exposure to the space environment. Although many environmental effects can be simulated on earth it is diffucult to simulate the synergistic effect of all the environmental factors on an insrument's performance. Therefore the ultimate test for space implementation of a device is a space experiment.

Space Experiment

The space experiment proposed would involve instrumenting an existing platform with optical fibers for sensing dynamic strain. A planned experimental platform is the LITE shuttle experiment. This platform has a reinforcing strut structure to provide stability to the instrument table. One purpose of the initial flight test is to evaluate the structure - hence the struts are instrumented with strain gauges, accelerometers and temperature sensors. We propose to instrument one or two struts with fiber optic sensors and compare our data with the other sensors already manifested. It may be possible to replace one of the aluminum struts with an instrumented composite strut to gain valuable additional data on new materials likely to be used in space. This is an excellent opportunity for testing fiber optic sensors in space without the expense of an independent space flight.

The systems proposed for this experiment are an optical phase locked loop(OPLL) which integrates strain along a sensing fiber and a Fabret - Perot etalon which provides point strain data.[2,3]

References

1. R. M. Measures, "Smart Structures With Nerves of Glass", Prog. Aerospace Sci., vol. 26, pp289-351, (1989).

2. R. S. Rogowski, J. S. Heyman, M. S. Holben, Jr., C. Egalon, D. W. Dehart, T. Doederlein and J. Koury, "Fiber Optic Strain Measurements in Filament Wound Graphite-Epoxy Tubes Containing Embedded Fibers", Fiber Optic Smart Structures and Skins, E. Udd, ed., vol. 986, pp. 194 -199, Proceedings of SPIE - The International Society for Optical Engineering, Boston, 1988.

3. K. A. Murphy, C. E. Koob, A. J. Plante, S. E. Desu and R. O. Claus, "High Temperature Sensing Applications of Silica and Sapphire Fibers" Fiber Optic Smart Structures and Skins III, E. Udd and R. O. Claus, eds., vol. 1370, pp. 169 - 178, Proceedings of SPIE - The International Society for Optical Engineering, San Jose. 1990.

MB.1 Flight Assessment of Optical Air Data Measurement Concepts

by
Rodney K. Bogue
NASA Ames-Dryden Flight Research Facility
Edwards, California

At the NASA Dryden Flight Research Facility, a flight demonstration project is underway and a second project to evaluate optical air data measurement concepts in flight is in the planning stages. The demonstration project to assess the state of the technology in optical air data measurements was initiated by NASA at the request of DARPA. NASA is conducting and managing the flight demonstration project, serving as the technical agent for DARPA, and evaluating the performance of the test systems. The rapid progress in photonics technology has provided new options and enabled new concepts for air data measurement. NASA-Dryden is planning for a flight test-bed facility to provide a realistic environment for evaluating measurement concepts.

The flight demonstration project was initiated in September 1989 and is scheduled to be completed in about two years. A Time-of-Flight (TOF) optical airspeed measurement technique is currently in the flight test phase on a high performance NASA aircraft. The DARPA goals of this flight project are to investigate the state of this technology for applications in high speed agile aircraft and to assess the capability and maturity of this technology for use as a primary aircraft air data system. In addition to the DARPA goals, the NASA goals for the project are to assess the technology for applications to flight research and to a broad class of military and civilian aircraft.

Vector airspeed (the motion of the vehicle with respect to the local air mass) and local air pressure and temperature combine to form the complete air data measurement set. Reference free stream air data is very important in flight research. The correlation of wind tunnel and flight test results relies on free stream air data for comparison. For most commercial and military aircraft, air data is used for gain scheduling in flight control systems. Because of the important role that air data plays both in flight research and in operational control of aircraft systems, much effort is expended to obtain accurate and repeatable air data for these purposes.

The desired air data conditions are those which exist in the unperturbed flow field in the vicinity of the aircraft in flight.

Conventional methods of air data measurement rely exclusively upon measurements obtained from pressure orifices or temperature probes on the surface of an air data measurement boom or on the aircraft surface itself. Because the aircraft disturbs the surrounding air, a local flow field is created in the vicinity of the vehicle. Ideally, all air data measurements reflect the "free stream" conditions outside the local flow field of the aircraft. With conventional techniques, this is approximately achieved by using an air data boom which extends as far as is practical ahead of the aircraft to avoid the local flow field effects. Optical air data measurement techniques show promise of being able to acquire information much further away from the aircraft than is possible with the air data boom (and thereby reduce the local flow field effects). At the same time, optical techniques acquire the air data information without disturbing the conditions being measured (a goal of all measurements). Unlike conventional methods, optical techniques require little or no calibration, little maintenance, and are expected to be very reliable.

The operation of most optical airspeed measurement systems relies on the availability of naturally suspended atmospheric particulate material. This material must be of an appropriate size and be present in sufficient quantity to reflect a laser signal to a detector. A Time-of-Flight (TOF) optical airspeed measurement technique is currently in the flight test phase at Dryden. This concept measures the transit time of individual suspended particles between two projected laser beams to derive the airspeed. Another airspeed measurement concept, called Laser Doppler Velocimetery (LDV), is less mature, but also offers an attractive set of characteristics well matched to the flight air data measurement requirement. The LDV concept detects the frequency shift (Doppler frequency) between a transmitted laser beam and the reflected signal from a collection of suspended particles at a focused measurement point. At this time, there are no LDV systems available which can be accommodated in the high performance NASA aircraft. These concepts have the potential for accurately measuring the three dimensional airspeed vector. Neither of these above concepts address the measurements of static pressure or ambient temperature which are also required to obtain a complete air data measurement set. Several optical concepts have been proposed to acquire these additional measurements and there is a high level of interest in developing and flight testing these concepts in addition to the airspeed measurement.

NASA-Dryden is in the early stages of planning for a flight test-bed facility to provide a realistic environment for evaluating both of the optical airspeed concepts (TOF) and (LDV) as well as competing embodiments of each concept. The atmospheric particulate environment, and system variables such as: radiated wavelength, radiated power, continuous or pulsed operation, and detector concept and sensitivity, are important design factors. The test-bed aircraft would be instrumented to acquire accurate baseline air data information as well as atmospheric particulate information and would provide a hospitable test environment for assessment of absolute and comparative performance of air data measurement concepts and systems at the "breadboard" stage of maturity. Accurate air pressure and temperature measurements would be provided for baseline comparisons of performance of optical measurement concepts for these parameters. This test-bed aircraft would be operated by NASA on a cooperative basis with the prototype developer with NASA providing baseline air data and particulate characterization as well as analysis assistance for each system tested. NASA would protect proprietary issues and would provide strict isolation for data from competing systems.

The oral paper will address the air data measurement problem, the significance of the air data information, several air data measurement concepts, and preliminary details of the NASA program.

MB.2 Nonintrusive Diagnostics at NASA Langley

Richard R. Antcliff and Jeffrey R. Balla
Nonintrusive Diagnostics Branch
NASA Langley Research Center
Hampton Va 23665

NASA Langley is currently involved in fundamental research in many areas of laser based nonintrusive diagnostics. These areas include coherent Raman techniques such as coherent anti-Stokes Raman spectroscopy (CARS) and Raman Doppler Velocimetry (RDV). Also work involving planer techniques is being utilized such as Rayleigh scattering and Laser Induced Fluorescence (LIF). The field of velocity measurements from seeded particles also constitutes a major research area. These techniques include laser Doppler velocimetry (LDV), Particle Imaging velocimetry (PIV) and Doppler global velocimetry (DGV). In addition, several less complex techniques based on absorption measurements are being investigated. This paper will describe some examples of the scope of this research and present the most recent research results.

Although many of these techniques are "well developed" the application of these techniques to actual facilities has been very limited. The thrust of our effort at Langley has been twofold, first to investigate new techniques for possible wind tunnel application; and second, to develop prototype systems to be used to acquire data in harsh wind tunnel environments.

The CARS technique has been under investigation at Langley for several years. It has been applied to a series of combustion systems of increased complexity. Most recently it has obtained measurements inside a supersonic combustion ramjet nozzle. These studies have shown the robustness of this complex laser system under very harsh conditions. In previous studies this system was applied to obtain simultaneously temperature and the densities of two major species.

The RDV technique produces simultaneous measurements of temperature, pressure and velocity. This technique has been applied to a large scale wind tunnel to obtain freestream values of these variables. Unique engineering considerations were required to allow the generation and collection systems to be on the same side of the tun-

nel. This system is currently being upgraded to decrease the measurement volume and the system noise.

Rayleigh measurements have been made with both Nd:YAG and Excimer lasers. Initial measurements in a Mach 6 environment have discovered previously unknown levels of molecular clustering. This clustering is a major noise source for Rayleigh measurements and is also of concern to the aerodynamicists. We have been able to quantify this clustering problem to understand the measurement limits. Excimer based Rayleigh measurements have been obtained in supersonic mixing and combustion experiments. As these data are analyzed, new information and relationships are being discovered.

Fundamental studies have been performed to understand the spectroscopy of oxygen LIF. These studies hold the potential of unlocking a new diagnostic technique for this important species in combustion chemistry. LIF studies of the hydroxyl radical have also been applied to fundamental combustion systems. Currently, this system is being applied to obtain measurements from a supersonic combustor.

LDV measurements have been developed for wind tunnel application in a large number of facilities at Langley. We continue to make breakthroughs in the areas of signal processing, optical access, seeding and ease of use. Although a mature technology, each individual application poses new obstacles and challenges.

PIV is a relatively new technique which has recently been applied to a Langley wind tunnel. This technique allows the acquisition of two dimensional fields of velocity data. The technique involves double exposing the detector to track individual particles as they traverse the flow system. We have spent considerable time improving data interrogation techniques and algorithms to improve the precision and accuracy of the technique. Several additional real world test are planned for this novel technique.

DGV has been developed jointly with the Northrup Corporation. This technique allows a three-dimensional field to be probed and relies on a molecular filter to detect the Doppler shift of an aggregate of the particles. A prototype of this system has already been successfully demonstrated in a Langley wind tunnel. A program is currently underway to apply this technique to an aircraft in flight.

MB.3

Technology, Design and Flight Tests of an Optical Air Data Velocity Sensor

Dr. Anthony E. Smart
TITAN SPECTRON Division
3535 Hyland Avenue, Suite 102
Costa Mesa, California 92626-1439

Brief Abstract

An optical air data velocity sensor system implementing sheet-pair transit-time technology with band-gap engineered devices was successfully demonstrated on F-16 and F-104 aircraft. Details of packaging, signal retrieval, performance and future potential are discussed.

Contents Summary

We describe the technology, implementation and performance of the sheet-pair transit-time optical velocity sensor implemented as part of an optical air data system. This sensor was designed, built to flight worthy standards and test flown on an F-16 in 1990 and on an F-104 in 1991 over envelopes exceeding 80,000 feet and Mach 2. Although pneumatic sensors use simple technology, they have become mechanically complicated and difficult to calibrate. Compared with conventional probes the optical sensor system offers the potential advantages of improved accuracy, latency, calibration, dynamic range of speed and attitude, robustness, and possibly life, cost, and range of application, without modification of the vehicle skin contour. Optically derived vehicle speed and attitude can extend the safe envelope of intrinsically unstable vehicles which rely on computer synthesis of several inputs including air data to make them flyable.

Of the two possible technologies, transit-time and Doppler homodyne laser velocimetry, each of which offers potential advantages, only the former has so far been demonstrated over the range discussed here. Originally identified major risks included doubt about the sufficiency of particles in the atmosphere, retention of geometrical calibration, the possible need for aerodynamic compensations, and the usual opto-avionic system concerns of size, weight, power demand and, of course, cost. These risks are now quantified well enough to confirm viability of the technology. Sufficient particles have been found everywhere the system has so far been flown.

Such a system is made possible by recent developments that include the availability of miniaturized band-gap engineered components such as GaAlAs diode lasers and avalanche photodetectors with outstanding performance, the establishment of a suitable optical geometry and the creation of non-linear signal discrimination and retrieval algorithms. The pattern of light-sheets is projected into a test volume four feet from the vehicle from six 1W laser diodes at a wavelength of 810 nm. The lasers are thermally wavelength stabilized using inferred true junction temperature. The laser drivers are a new design which is small, simple and of high efficiency. We outline opto-mechanical design techniques to meet three needs; laser and receiver lenses with adequate performance, a receiver optical system capable of separating the six channels while maximizing system étendue, and the achievement of sufficient rigidity for calibration retention.

Advantages of newly available avalanche photodiodes include a quantum efficiency of 85%, a gain of 50 A/W and an NEP of 10^{-14} W/$\sqrt{Hz}$ for a 1 mm diameter active area. Adaptive bias and temperature control circuits were developed to exploit these qualities while preserving dynamic range. Non-linear signal discrimination techniques and algorithms realized the 0.1% velocity accuracy required from individual particle measurements - up to 0.01% over 40ms integration times - to be achieved at update rates of the order of tens per second.

Data from installations looking upward and to starboard in the radome of the F-16 and downward from the belly of the F-104 are presented to demonstrate features of the system and to show comparisons with the pneumatic data for various flights and atmospheres. Flight conditions include altitudes from ground to 80,000 feet, speeds from take-off to Mach 2, and the extreme maneuvers of which each vehicle was capable. Weather conditions varied from extremely clear to cloud and heavy rain, and included a brush fire. Background light conditions, which can affect sensor performance, included darkness, clouds, snow, sea and earth illuminated by sunlight and the solar image itself.

Measurements corresponding well with existing pneumatic aircraft systems were obtained under almost all conditions and a brief review of these is presented with comparative data plots. Software enhancements during the winter of 1990 made possible improved data from the more recent F-104 flights.

System design was established by computer modeling of aspects of the physics, phenomenology and implementation geometry. The importance of such modeling for software and hardware design optimization is exemplified and quantitative elements of the final design listed. We show the dependance of accuracy on the two critical parameters, ability to find a particle in the presence of background light and noise, and timing error with which its position in the sheet pattern may be identified. Against low altitude blue sky the system yields 0.1% velocity accuracy from a single 0.4 μm radius dust particle, which typically gives rise to signals of 100 detected photons.

Analysis of flight data anomalies initially gave insight into phenomena intrinsic to the behavior of the sensor but are now beginning to yield atmospheric information which may be of more general interest. Brief mention is made of problems and solutions in general opto-avionic implementations. Special concerns were thermal management, power supplies, vehicle interfacing and data handling and reporting. System hardware and software architecture was chosen to permit independent module development and testing.

Conclusions are drawn to show that the technology is viable and attractive for many high performance atmospheric vehicles. Other properties of the data can indicate atmospheric aerosol properties. Empirical data so far show that aerodynamic compensations, once thought necessary because the probe volume is only a few feet from the vehicle, are smaller than the disparity between pneumatic and optical probes if the site is well chosen. Indeed, what disparity there is may give insight into the comparison between vehicle measurements and computational fluid dynamic predictions at the distance of the probe volume from the vehicle.

Acknowledgement

The author wishes to thank Spectron for its ongoing support and the many people, who contributed significantly to the successful outcome of this work, with particular acknowledgement to J. B. Abbiss, W. A. Girard, M. D. Henigman, P. D. Kenefick, R. E. Olsen and R. J. Rickey.

MB.4 Proof-of-Concept Test of the Doppler Global Velocimeter

by

James F. Meyers, Joseph W. Lee
NASA - Langley Research Center
Mail Stop 235A
Hampton, Virginia 23665

and

Angelo A. Cavone
Vigyan, Inc.
30 Research Drive
Hampton, Virginia 23665

A new nonintrusive flow velocity measurement technique, Doppler global velocimetry, is being developed for wind tunnel and flight applications. The Doppler global velocimeter, DGV, directly measures the Doppler shift in scattered light from particles passing through a laser light sheet. The edge of an absorption line in Iodine vapor provides a linear relation between optical frequency and optical transmission through the vapor. The optical frequency of an Argon ion laser can be tuned to the mid-point on the downward slope of the absorption line by adjusting the tilt of the intercavity etalon. Thus the intensity of scattered light collected by a video camera viewing the light sheet through an Iodine cell will have a dependency on velocity. This dependency is isolated by using a second camera to view the same scene without a cell to provide a reference image. Normalizing the signal image by the reference removes effects of particle number density, particle size, nonuniformities in the light sheet intensity and in the collecting optics from the collected light intensity.

A proof-of-concept test of a prototype DGV was conducted in the Basic Aerodynamics Research Tunnel. The vortical flow field above a 75 degree delta wing was chosen for this test. At low angles of attack, the flow is highly structured with two opposing leading edge vortices. The laser and the optical system were mounted on the traversing mechanism normally used to move a fringe-type laser velocimeter. The light sheet was placed at the 70 percent chord location and adjusted to be normal to the surface of the delta. The collecting optical system was placed in forward scatter, 53 degrees from the propagation direction of the light sheet in the horizontal plane. This configuration measures the velocity component rotated 26.5 degrees from the free stream direction in the horizontal plane. A view of the system is shown in figure 1. The illuminated vortical flow is shown in figure 2 as viewed from the collecting optical system. Images of the vortical flow for an angle of attack of 20.5 degrees are shown in figure 3. The normalized image clearly shows the expected flow structure. Greater detail is provided by scanning through the center of the vortices where an increase in velocity (a decrease in amplitude) of the normalized image near the core region corresponds with the streamwise flow measurements using a fringe-type laser velocimeter.

This work indicates that the Doppler global velocimeter has the potential to be a valuable addition to fluid mechanic investigations. Continued development will investigate the

addition of components, error analysis, and an assessment of measurement accuracy by comparing results with other techniques.

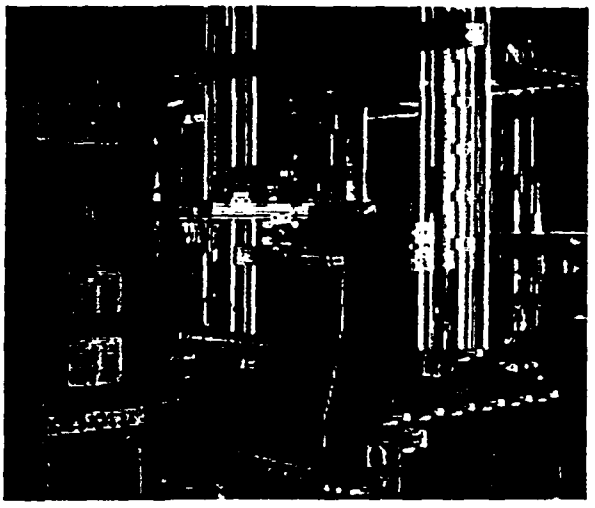

Figure 1.- The Doppler global velocimeter installed in the Basic Aerodynamic Research Tunnel.

Figure 2.- View of the vortex flow field above a 75 degree delta wing.

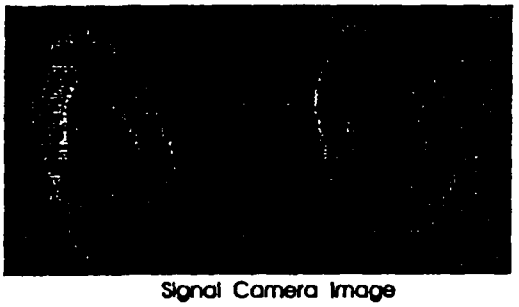

Signal Camera Image

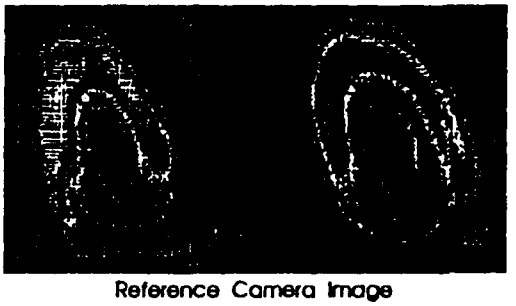

Reference Camera Image

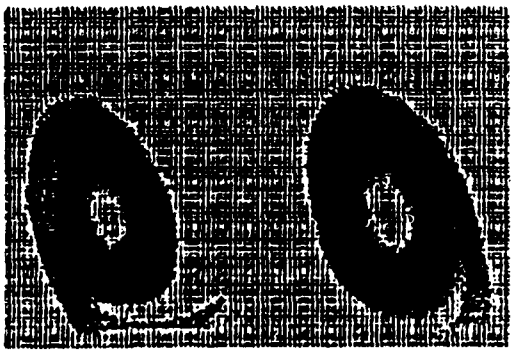

Normalized Image: Color Contours of Velocity

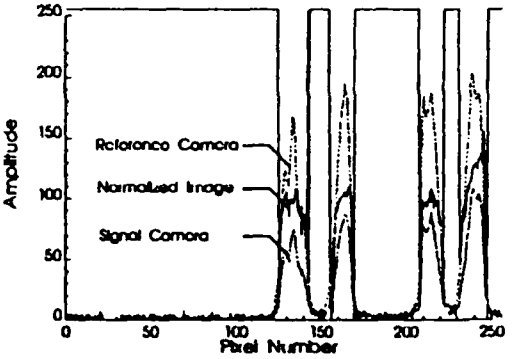

Image Amplitudes
Scan through center of vortices

Figure 3.- DGV images of the vortical flow field above a 75 degree delta wing.

MB.5 An Optical Ultraviolet Sensor for Remote Measurement of Atmospheric Pressure and Temperature

Dr. John B. Abbiss
TITAN SPECTRON Division,
3535 Hyland Avenue, Suite 102
Costa Mesa, California 92626-1439

Brief Abstract

A remote optical atmospheric pressure and temperature sensor based on Rayleigh scattering and oxygen fluorescence and using an ultraviolet light source was constructed and test-flown on an F-16. The results obtained are presented and their significance analyzed.

Contents Summary

Current sensors for aircraft pressure altitude and ambient temperature measurements (e.g., static pitot tubes, pressure transducers and thermocouples) are intrusive and yield pressure and temperature data which require correction factors and wind tunnel calibrations. These problems could be alleviated by means of optical sensors, whose development, however, presents great challenges. The sensor must satisfy stringent flight hardware requirements, which include compact size, low power, robust design and the ability to withstand high vibrational levels, high g's and extreme stresses. Optical sensors must use the molecules in the atmosphere or naturally-occurring aerosols as the source of the data. In addition, the probe volume should be some distance from the aircraft to ensure that the data are unperturbed by its presence.

Developments of optically-based flight instruments to provide data for flight control systems have focused largely on the measurement of aircraft velocity; little has been done on determining the air density and ambient temperature. However, various spectroscopic techniques have been proposed to determine the temperature and species concentrations (and hence the pressure, through the equation of state) in compressible flows both in the laboratory and in wind tunnels. Among these techniques, laser induced fluorescence and Rayleigh scattering have received more attention because of their relatively higher signal levels and lesser complexity. Almost all of these methods require sophisticated lasers, detection systems and data reduction software. In the present approach, which does not require a laser, we measure the temperature and concentration of oxygen molecules using relatively wide-band excitation and detection. At the ultraviolet wavelengths used, oxygen absorption is dominated by the Schumann-Runge system of transitions. The method is suitable for air-borne applications since the sensor can be made compact and does not need the high power levels and the auxiliary equipment typically required for a laser based system. Radiation from a high-pressure xenon lamp is projected into the probe volume and the light scattered from this region collected by two separate detector channels. The first channel receives Rayleigh-scattered light over the excitation wavelength band. This signal is linearly proportional to the number density of air molecules. The second channel monitors the fluorescence from oxygen molecules, which depends upon both temperature and number density of oxygen molecules. Since the oxygen mole fraction in air is invariant with altitude, the Rayleigh and fluorescence channels yield two measurements which are related to atmospheric temperature and number density.

The flight hardware consists of a transmitter, a receiver operating in backscatter, and data acquisition and processing electronics. The system measures 300 × 250 × 350 mm, weighs 35 kg and consumes 150 watts. It was mounted for flight test in the radome of an F-16 fighter aircraft, the transmitted light being directed to port at an elevation of approximately 60°.

The transmitter includes an EG&G model FX193 xenon flash lamp as a source of radiation, three dichroic mirrors which restrict the lamp spectral output approximately to the 185-200 nm range, and a focussing lens. The lamp was operated in flight with an electrical input to the discharge of 1 J per pulse. The receiver system includes separate Rayleigh, fluorescence and lamp monitor channels. The detectors are EMR photo-multiplier tubes equipped with rubidium telluride cathodes having a solar-blind response. The Rayleigh channel uses filters to limit the detection bandwidth to the 185-200 nm range. The fluorescence channel detects radiation in the wavelength band 220 nm to 280 nm approximately. The monitor channel permits measurement of pulse-to-pulse variations in the lamp output. The radiation from the probe volume is collected by a 50 mm diameter lens. The data acquisition and processing system includes gated integrators and 12-bit digitizers. The system acquired data from each of the three channels at 50 Hz. The focal plane of the transmission lens was about 2 meters distant from the airplane. The probe volume was formed by the intersection of the slightly expanding beam and the field of view of the receiving lens and extended from about 0.5 m beyond the aircraft. The probe volume cross-section at two meters was about 100 mm high and 280 mm wide.

The flight hardware optical configuration formed the basis for a numerical simulation of the absorption, scattering and detection processes. With the aid of this model, the numbers of collected photons in both the Rayleigh and fluorescence channels were calculated as a function of temperature and pressure. The results could be used to calibrate the system, and to analyze and predict its performance in flight. The numerical model showed that the fluorescence and Rayleigh signals are, in combination, uniquely related to the atmospheric pressure and temperature. Clearly, a one-to-one relationship between pressure and temperature pairs and the corresponding fluorescence and Rayleigh signals is essential if the flight instrument is to provide unambiguous data.

The pressure and temperature sensor system was mounted in the nose of an F-16 aircraft. The sensor performance was evaluated during flight tests under a wide range of ambient conditions, including altitudes up to 50,000 feet. Results from the flight tests are presented and discussed. Although a faulty monitor channel prevented compensation of the Rayleigh and fluorescence signals for flash-to-flash fluctuations in the transmitted light, which obscure fine detail, the data trends are as predicted, and useful conclusions on system performance can be drawn. Contamination of the Rayleigh signal by scattering from airborne particles, for which corrective schemes are being investigated, is considered. Fluorescence from such particles, on the other hand, does not appear to have been significant.

Acknowledgement

Key roles in the design, analysis and implementation of the instrument described here were played by Drs Medhat Azzazy, Bryan J Brames and Julie Tan at Spectron, and by Dr Robert W. McCullough of TecKnowLogica, Inc, Princeton Junction, New Jersey. Sincere thanks are due to Dr Anthony Smart for many helpful contributions during the program and to Mr Peter Kenefick and members of the engineering staff at Spectron for their devoted efforts at a time of severe pressure.

MB.6 Measurements of Temperature and Density in Hypersonic Flows

Robert L. McKenzie and Douglas G. Fletcher
NASA Ames Research Center, Moffett Field, CA 94035

A renewed emphasis on aerodynamic testing in hypersonic airflows has been introduced by the modern trends in aircraft development toward hypersonic cruise aircraft, single-stage-to-orbit vehicles and aero-maneuverable spacecraft. In support of these advanced designs, new measurement capabilities are required in hypersonic ground facilities for numerical code validation and turbulence modeling and in flight for flight control and design calibration. An important aspect of these new capabilities is the need for nonintrusive methods to determine fluid dynamic parameters such as temperature, density, velocity, and their fluctuations in the flow field away from aerodynamic surfaces.

The use of ultraviolet laser-induced fluorescence (LIF) of O_2 appears be a particularly viable means of obtaining such measurements at the gasdynamic conditions of hypersonic wind tunnels[1,2]. Such conditions are typified by those in the NASA Ames 3.5-foot wind tunnel where, at a free-stream Mach number of 10, temperatures can be as low as 50 K and densities as low as 0.01 amagat. To adequately resolve the turbulent fluctuations in the flow, measurements are desired with uncertainties of 1%, a temporal resolution determined by the duration of a single laser pulse, and a spatial resolution of 1 mm.

This presentation describes an experimental evaluation of the O_2 LIF technique in combination with Raman scattering from the same laser beam, specifically for obtaining point measurements of temperature, density, and their fluctuations owing to turbulence at the very low temperatures and densities encountered in hypersonic wind tunnel flows. The anticipated performance of the technique in the NASA-Ames 3.5-foot hypersonic wind tunnel and preparations for its demonstration there will also be described.

In general, temperature and density measurements based on O_2 LIF rely on the use of a pulsed ArF laser operating at 193 nm to selectively excite ro-vibronic transitions in the Schumann-Runge ($B^3\Sigma_u^- \leftarrow X^3\Sigma_g^-$) band of O_2. If the spectral bandwidth of the laser is narrow, individual rotational transitions which originate from the ground vibrational state may be selectively excited. The resulting fluorescence energy is then proportional to the population density of the initial state which, in turn, is sensitive to both the gas temperature and density. This approach is particularly attractive for measurements at room temperature and below where only the rotational state populations vary significantly with temperature. A notable feature of O_2 fluorescence from the Schumann-Runge band is that all of the important excited vibronic states are strongly predissociated, making the fluorescence lifetime extremely short. Thus, the troublesome temperature- and density-dependent effects of collisional quenching are negligible.

Because the population of an individual state is also proportional to the gas density, the measurement of temperature using a single laser frequency requires an independent measurement of density. Once density and temperature are both known, the pressure may also be determined using the equation of

state for a gas in thermochemical equilibrium. If all measurements are made simultaneously, their temporal correlations are also known. This latter information will provide new insights into the physics of the highly compressible turbulence in hypersonic flows.

In the approach taken here, the density measurement is made using Raman scattering from the same beam that excites the fluorescence. Raman scattering is linearly dependent on density and can be made insensitive to temperature by integrating the scattering from the entire rotational Q-branch associated with transitions from the ground vibrational states of O_2 and N_2. Similar measurements can also be made with Rayleigh scattering, which has a cross section that is typically 1000 times greater than Raman scattering, but competitive scattering by particles and condensates in the flow or by walls and windows are often troublesome in wind tunnel environments. In any case, the Raman cross section for oxygen is exceptionally high, owing to the ultraviolet wavelength and to an enhancement by the near-resonance of 193 nm radiation with the absorbing transition in oxygen used for LIF. Consequently, the Raman process can provide the required sensitivity for measuring density even at the lowest densities considered here.

The O_2 LIF/Raman technique has now been developed to a stage where it can be applied in a large scale, hypersonic wind tunnel. The present development includes a validated spectral model which incorporates all of the physical phenomena believed to be significant in the LIF process except the effects of multi-photon processes. Predictions of the excitation spectra, the dependence of the fluorescence signal on temperature, and the photon-statistical noise-to-signal ratio have been compared with experiment. The results show that if the laser fluence is kept below values where multi-photon processes become significant and only contributions from absorption transitions which originate from the v"(0) and v"(1) vibrational levels of the O_2 ground electronic state are significant, the model is sufficiently accurate for the prediction of total fluorescence and its temperature dependence. Apparent inaccuracies in the model for contributions from higher vibrational levels currently limit its application to temperatures below 500 K. The spectral model was also used for predictions of the uncertainty with which temperature may be measured at the conditions in a hypersonic wind tunnel. The results show that uncertainties of less than 2% should be achievable for all temperatures above 60 K and densities above 0.01 amagat.

Finally, the technique has been successfully demonstrated at gas conditions which approach those in a hypersonic wind tunnel. Simultaneous measurements of temperature and density were made in a cell where temperature and pressure could be independently controlled. The minimum useful temperature which could be obtained in the cell was limited by the condensation of oxygen to 130 K. Moreover, only pressures down to 250 torr were tested. While these conditions are not as extreme as those in a Mach 10 flow, the results support the conclusion that the LIF technique will be a useful technique for the diagnostics of hypersonic wind tunnel flows at Mach numbers up to 10. As a result, a large scale, ultraviolet, optical system has been assembled for application in the NASA Ames 3.5-foot hypersonic wind tunnel.

1. Laufer,G., McKenzie, R., Fletcher, D., App. Opt.,29,4873-4883, 1990.
2. Fletcher, D, McKenzie, R., AIAA Paper 91-0458, Jan., 1991.

Tuesday

July 23, 1991

TuA.1 The Human Exploration Program: Technology Challenge

E.B. Pritchard, *NASA Langley Research Center, Hampton, VA*

The presentation will briefly describe the architecture being studied for the Lunar and Mars missions. Key technologies will then be discussed in terms of benefits, required readiness dates, technical issues, and near term focii.

TuA.2 Applications of Photonics in Space Automation and Robotics

Gary W. Sjolander *John A. Cuseo*
Martin Marietta Astronautics Group
Denver, Colorado USA

Although the key performance requirement for real time image processing manifests itself in terms of frame rates, space flight applications for image processing have additional requirements for minimizing volume, mass, and power. As space missions move from telerobotic operations to autonomous operations, the need for reliability, envisioned to be provided by optical correlators, also increases.

The acceptance of hybrid optical processing technology over exclusively digital techniques for systems application will be determined by the factor-of-ten rule. This rule basically means that if optical technology is not ten times better, smaller, lighter, or 1/10 th the cost, it is likely that a digital approach will be implemented within a given system. Thus, photonics development must not only be as good as digital technology, but it needs to be ten times better in some critical parameter before it is likely to purchased by the government.

Our overall objective is to provide photonic systems for space applications over the next two decades and beyond. The technology to be developed centers around the 4f and joint transform optical correlators for the purpose of pattern recognition and exploitation. There are three types of patterns that need to be recognized. The first is *precise patterns* such as the star field as viewed from space. The second is *fuzzy patterns* such as Martian or Lunar terrains where the pattern has been previously mapped but may vary due to weather or lighting conditions. The third type is the *unknown pattern* such as boulders, faults, and space debris that present hazards to a number of mission scenarios. The recognition of a variety of pattern categories not only includes development of optical correlators, but also the development of post correlation processing algorithms that include model based reasoning and neural networks.

Photonics, in general, is a rapidly growing technology with application to many space systems functions. A key advantage of a photonic correlator is that a single processor can provide the multiple functional processing for the variety of mission needs. A partial listing of NASA programs that could benefit from photonics technology and their corresponding applications is shown in Table 1.

Table 1 Photonics Applications to NASA Programs

Program	Application
Mars Rover/Sample Return	Autonomous Landing Site Selection Hazard Avoidance (planetary surface) Attitude Alignment Autonomous Docking
Space Transfer Vehicle	MRSR Applications + Hazard Avoidance (space operations) Near Space Station Operations Health Monitoring
The Earth Observing System/Data and Information System	Ground Processing

Martin Marietta Photonic Systems Center (Denver) and Martin Marietta Laboratories (Baltimore), in conjunction with the University of Colorado Optoelectronic Computing Systems Center and the University of Dayton Research Institute are conducting extensive research for the application and

transition of optical correlators into government systems. Key to this technology is the implementation of programmable spatial light modulators that allow target filter holograms to be correlated with an input scene at several thousand filters per second. The *binary phase only filter* and the *ternary phase amplitude filter* are two processing technologies currently being pursued. Scale and rotational invariance are being developed along with filter strategy (smart filters) to minimize the number of stored filters while maintaining a real-time, robust automatic pattern recognizer.

Advanced planetary missions like the Mars Rover/Sample Return (MRSR), planned for the late 1990s, provide the focus for solid, long ranged planning for photonic maturation. These plans include bench top testing with simulated Martian imagery, evaluation by integration with simulation hardware, followed by space flight experience.

Realistic simulation environments, incorporating a combination of hardware-in-the-loop and high-fidelity analytical modelling, are required in the development and evaluation of photonic systems for space applications. For example, simulation of the terminal descent phase of a planetary mission has been developed in our Space Operations Simulation Laboratory. Applications of photonics in this area are related to autonomous site selection (i.e., navigation update based on landmark correlation) and autonomous hazard avoidance. This real-time simulation architecture (Figure 1) incorporates a large amplitude 6 degree-of-freedom moving base carriage (MBC), with a multiple CCD camera sensor platform, controlled by an Encore computer. The subsystems and dynamics of the landing vehicle, as well as environmental effects, are modelled. Two 4.8 meter square terrain boards (180:1 and 60:1 scales) provide a model of the Martian surface.

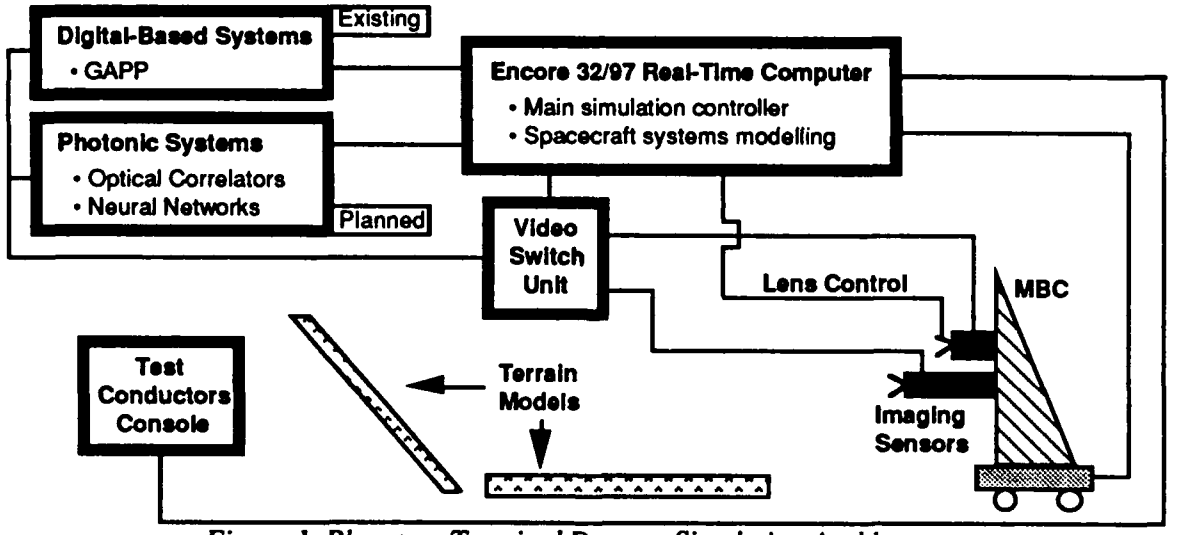

Figure 1 Planetary Terminal Descent Simulation Architecture

The simulation provides an ideal environment to compare the performance of photonic systems versus a purely digital approach. The simulation's existing digital capability uses a Geometric Arithmetic Parallel Processor (GAPP) for real-time image processing. Our GAPP workstation houses a 108x96 array of processors in a single instruction multiple data (SIMD) architecture controlled by a Motorola MC68000. The GAPP captures and processes video data at the RS-170 frame rate of 30 Hz. The simulation's photonics capability will involve integration of our portable optical correlator. Photonics correlators perform two dimensional Fourier transforms and cross correlations in the time it takes light to pass through the optics, and they are not restricted by the image resolution. Current speed limitations reside in the support hardware such as detectors, and frame rates of the spatial light modulators.

TuA.3 Electro-Optical Sensors for Docking of Space Vehicles

David J. Tubbs, Lynn O. Kesler, and Robert J. Sirko
Space Station Division
McDonnell Douglas Space Systems Company
5301 Bolsa Avenue
Huntington Beach, California 92647

Electro-optical sensors provide unique and critical functionality for space missions requiring rendezvous, docking, and berthing. In this paper orbital mechanics considerations, and the fundamental sensor performance requirements they impose, will be identified and parameterized. The analysis will take into account the highly sensitive interactions between (1) sensor requirements, (2) system performance cost functions, and (3) development cost, risk, and schedule.

This paper will present a brief historical review of principles of operation, development activities, and performance of electro-optical sensors at McDonnell Douglas (both internally and NASA funded) leading up to current capabilities. We will also describe current plans for a fully functional demonstration to address specific NASA mission needs.

TuA.4 Miniature Hybrid Optical Correlator for Space Applications

E. R. WASHWELL, G. O. GHEEN,
R. J. GEBELEIN, C. H. HUANG

LOCKHEED MISSILES & SPACE COMPANY, INC.
P.O. BOX 3504 - ORG. 62-61, BLDG. 589
SUNNYVALE, CA. 94088

SUMMARY

Hybrid optical correlators have considerable advantage over all-digital processors for a number of space-borne pattern recognition (image processing) applications. The advantages result from the inherent two-dimensional (parallel) processing of optics. Hybrid optical processors combine the speed of optical processing with the versatility and compatibility of digital techniques. In this paper we present a quantitative performance comparison of optical and all-digital correlators, the results of an optical design which miniaturizes the optical path length of an optical correlator, the requirements on the spatial light modulators (SLMs), a new algorithm for generating distortion invariant filters, and simulation results obtained with the algorithm.

In this paper, we compare the performance of an optical correlator to the Cray computer and two digital correlators; one uses the gray level input scene and is based on the FFT algorithm, and the other uses binarized input scene based on the direct time domain correlation. The performance measures used are throughput (correlations/sec) and a figure of merit defined as correlations/second/watt. The optical correlator performance capability is given for a commercially available SLM operating at a 300 Hz frame rate out to projected frame rates for ferro-electric liquid crystal SLMs (10kHz frame rates).

The raw throughput comparison shows that the optical correlator outperforms the Cray and FFT. The optical correlator also outperforms a variation of the next generation of systolic parallel array (SPAR) chip, currently being designed at Lockheed Missiles & Space Company, when the input field-of-view is 512 x 512 pixels or larger. The figure of merit comparison shows that the optical correlator enjoys a two to three order of magnitude advantage over the FFT-based correlator for both small and large field-of-views. For the case of the SPAR-based correlator, an optical correlator has a significant advantage when the input scene has a large field-of-view (i.e., space-bandwidth-product greater than 512 x 512 pixels).

An important aspect in the realization of a miniaturized optical correlator is the optical design which must not only provide a short optical path length (the order of inches) but also must utilize the full resolution capability of the SLMs used in the correlator. Results are given for an optical design having an optical path length of six inches, and optimized for 25 micron SLM pixels, and an input space-bandwidth-product (SBP) of 1024 x 1024.

The key elements required to make an optical correlator useful are the SLMs and the Fourier plane filters. The requirements on the filter plane SLM are more demanding, in many respects, than for the input plane. These requirements go hand-in-hand with the filter design algorithm. Requirements are presented for optical correlator SLMs in terms of frame rate, SBP, modulation characteristics, pixelation and pitch.

A new algorithm for generating distortion invariant quadratic filters is presented. This algorithm seeks to minimize the fluctuation of the response over the distortion range while maximizing the peak correlation value. Also, the filters are restricted to ternary modulation to accommodate current SLM limitations in optical correlators. The quadratic filters are implemented in an optical correlator by integrating the correlation response of a number of filters on the output detector array. The signal collected on the detector is then threshold-detected to classify possible targets in the input scene. This produces superior discrimination for distortion-invariant recognition because of the extra degrees of freedom permitted by the quadratic filters. Quadratic filters can also help alleviate the bottleneck in the output detector array of the correlator. Simulation results are presented for a six-dimensional quadratic filter invariant to out-of-plane rotation over 360 degrees.

TuA.5

Miniature Ruggedized Optical Correlator (MROC) Optimized for Space

W. E. ROSS

LITTON DATA SYSTEMS
8000 WOODLEY AVENUE
VAN NUYS, CA 91409

SUMMARY

Numerous computationally intensive tasks exist on spaceborne missions which need the 2 to 3 orders of magnitude throughput advantage of optical processing over digital. These applications include robotics, vision, docking, land, guidance, tracking and recognition systems.

An optical correlator design has been optimized to meet the requirements of space applications. The requirements of being highly rugged with minimum volume, weight, and power with high throughput capacity, will be achieved with a novel folded optics design which takes advantage of non-interference of optic beams and shares the same intersecting optic paths. This space sharing results in a palm-sized optical correlator which looks somewhat like a ring laser gyro (RLG) and can utilize the production tooling developed for mass production of ring laser gyros. The optical correlator has the inherent stability of an RLG but is much more forgiving in its requirements.

The Litton technology used in this device has been successfully tested in the form of a breadboard optical bench correlator both in the U.S. Army's ATR program, (NIFFTE 86) held at Eglin AFB and in a well-controlled experiment at the Army's Night Vision Electro-Optical Laboratory, Fort Belvoir, referred to as Optical Processing Identification (OPID). Results of the latter experiment indicated significant improvement with the optical correlator.

There has been an urgent need for a compact rugged optical processor correlator for Automatic Target Recognition (ATR).

Spatial pattern recognition compares the spatial (recognition classifier) of an unknown object with the spatial pattern of a known object. When they compare, or correlate, the target is then identified as the known object.

An enhanced version of Litton's patented Magneto-Optical Spatial Light Modulator (MOSLM) is being developed as part of this integrated design effort. It is the basic building block for various optical processing architectures. It is physically a small, solid state, array of picture elements (pixels), each of which can be electronically controlled to change the polarization properties of light passing through it to form an image. When coupled with a second spatial-frequency filter Light Mod(TM), via lenses, mirrors, and polarizers, the effect is to pass or block the transmission of light. Identification is made when the output light is at a maximum. Projected size is 16 in^3, 1 lb., and 30 watts power.

TuA.6

A Systems Approach to Robotic Vision using an Optical Correlator

Butler P. Hine III, John D. Downie, and Max B. Reid

Intelligent Systems Technology Branch
NASA Ames Research Center
Moffett Field, CA 94035

Summary

Currently planned and future NASA missions have a great need for semi-autonomous and autonomous robotic systems capable of performing tasks which are either too dangerous or too expensive for humans to perform. Examples of these tasks are the construction, inspection, and maintenance of structures both in space and on planetary surfaces. These robotic systems must be rugged and reliable, and must use as little precious volume and power as possible. Optical processing architectures, which rely on the speed and inherent parallel nature of light to perform computations, are attractive alternatives to digital electronics for performing some of the processing tasks required of an autonomous robotic system in space.

Vision processing is one of the most computationally intensive tasks required of an autonomous robot and can benefit greatly from novel processing architectures designed to accelerate computationally expensive functions. The data flow from a single typical imaging sensor is roughly 60 Mbits/sec, the processing of which can easily overload current onboard microprocessors. Many primitive operations required of vision feedback systems used in robotic control, such as object recognition, tracking, and orientation determination, can be performed using cross-correlation techniques. Cross correlation is well suited to analog optical implementation, using the Fourier transform ability of a lens, and can be performed at higher speeds than is possible with digital electronics at equivalent power levels. Incorporating an optical correlator as a special purpose coprocessor in a general hybrid vision processing system combines the speed of the optical processor with the generality of the digital one, resulting in a higher performance system than could be obtained with either alone.

We have developed at Ames Research Center a hybrid digital electronic/ analog optical robotic vision processing system designed to test concepts and algorithms for autonomous construction, inspection, and maintenance of space-based habitats. The benchmark task of the system is to allow a robot arm to identify, track, and grasp an arbitrary tool moving in space with all six degrees of freedom without using any kind of cooperative marking techniques for the vision system. This task is representative of one required from the Flight Telerobotic Servicer (FTS) or the EVA Retriever, both of which are robots designed to operate in a weightless environment. Figure one is a schematic of the hybrid vision system.

A common problem with correlator-based systems proposed for general vision processing is that the filter database required to account for all possible objects with all possible scales and orientations is prohibitively large and would take an unreasonable amount of time to search, even with the fastest possible optical devices. A technique which we use to decrease the filter database size and search time is to incorporate binary synthetic discriminant function filters (BSDF's) into the database [1,2]. These are composite filters designed to recognize objects over a range of distortions. As well as reducing the size of the database, they may be organized into structures which reduce the search time [3]. Even using BSDF's in this manner, however, the search time of filter databases for real world problems is prohibitive. Another technique to reduce the database size and search time is to use alternate sensors to determine some of the variables, such as an

object's scale, rather than relying on the correlator to provide them. In particular, stereo camera processing to calculate the range map or laser range finding to determine range directly, can be used to prescale images before the traversal of the correlation filter database. This requires using the correlator to define regions of interest, then the range map to estimate the scale of the object, and finally the filter database traversal to identify the object and determine its orientation.

In our tests of the system to date, we have demonstrated tracking and grasping capabilities at slow speeds (input image updates of 1 Hz excluding the range map determination time) in a two dimensional plane. The speed of the system is currently limited by the addressing time of the spatial light modulators and the digital image preprocessing stage. Both of these speed limitations can be minimized with faster devices and processors currently available. In comparing the performance of the system to more conventional all digital electronic ones developed concurrently, we have found that the hybrid system consistently performs better in terms of speed and robustness.

References

1) D.A. Jared and D.J. Ennis, 1989, Applied Optics **28**, 232.
2) M.B. Reid, P.W. Ma, J.D. Downie, and E. Ochoa, 1990, Applied Optics **29**, 1209.
3) M.B. Reid, P.W. Ma, and J.D. Downie, 1990, Japanese Journal of Appl. Physics **29**, L1284.

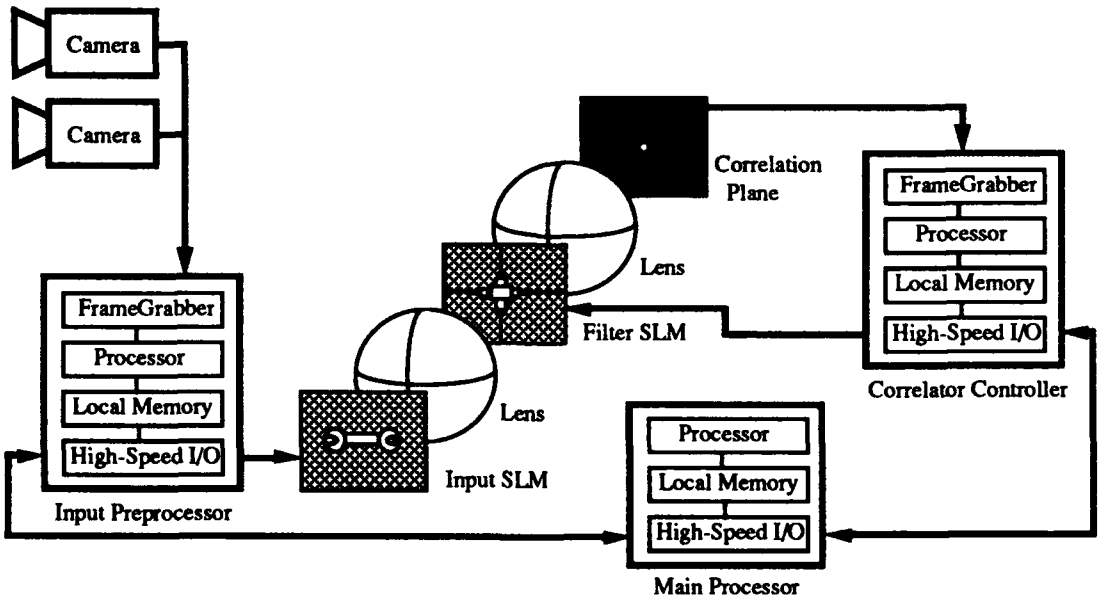

Figure 1: Schematic diagram of the hybrid correlator vision system. The camera data are digitized by a frame grabber and preprocessed by a DSP-based image processor (FGIP) before being displayed on a high speed input plane spatial light modulator (SLM). The correlation filters are sequenced through the filter plane SLM and the detected correlation plane grabbed and analyzed by a second FGIP.

TuB.1

Applications of Optical Communications in the Space Environment

V. Chan, *MIT Lincoln Lab, Lexington, MA*

Abstract not available at time of printing.

TuB.2 Optical Communications for Future Space

James R. Lesh
Jet Propulsion Laboratory
California Institute of Technology

Michael Fitzmaurice
NASA Goddard Space Flight Center

B. Seary
NASA Goddard Space flight Center

Ramon DePaula
NASA Headquarters

SUMMARY

NASA's plans for future space exploration will require reaching out to the extremes of the solar system and extending the touch of human life to at least the orbit of Mars. NASA also plans an extensive examination of our own planet to understand our natural processes on a global scale. To realize these objectives, a number of technological challenges must be overcome. One of these is to provide adequate communications capacity to relay space-acquired data between space-based resources, or between space vehicles and the ground.

Current radio-frequency communications systems have been optimized and extrapolated to the point that further significant increases in capacity will come at the expense of unacceptably large values of size and cost. For this reason NASA is developing optical (laser) communications technology for its future missions. Optical communications offers to provide 10-100 fold increases in data rate capacity of current rf systems. The applications time frame for this technology is the late 1990's and beyond, although technology flight verification experiments are expected in the mid-to-late 1990's.

With optical communications, the communications subsystem will become an attached assembly to the spacecraft bus, rather than becoming a major structural element of the spacecraft infrastructure. Telescopes (communications antennas) on the spacecraft that are only 50cm in diameter will be able to support data rates up to 60 Mbps from Mars and well into the Gbps range between Earth-orbiting satellites. Earth-vicinity telescopes for deep-space data reception will be sizeable (approximately 10 m diameter), but still substantially smaller than the current rf tracking stations (1/50th the area of the current 70 m rf antennas). Furthermore, the optical reception telescopes can be low-cost photon-bucket collectors for supporting directly-detected intensity-modulated optical signal modulations. Both space-based and ground-based reception systems are being studied.

Laser powers of less than 2-Watts will be adequate to provide most anticipated links of the future, with some Earth-orbiting links requiring as little as a few hundred milliwatts. Both semiconductor Laser diode transmitters and hybrid diode-pumped, solid-state crystalline lasers are being developed. Coherent (optical phase tracking) receiver structures utilizing frequency-stable laser sources are also under development. Such systems can permit communications against the solar background and, with the development of a spacecraft coherent transponder,will enable precise Doppler tracking of space vehicles as well as permit long-baseline (e.g. interplanetary) scientific investigations such as the search for gravitational waves.

This presentation will provide an overview of the integrated NASA program for the development, demonstration and eventual deployment of optical communications for future space scientific exploration. Activities planned or underway at both the Jet Propulsion Laboratory and at the Goddard Space Flight Center will be covered and will include space applications ranging from Earth-orbit intersatellite links to links with spacecraft at the edge of the solar system. Individual technology developments at the NASA centers, as well as the planning for a joint-center space flight experiment will be covered.

The research described in this paper was carried out, in part, by the Jet Propulsion Laboratory, California Institute of Technology, under contract with the National Aeronautics and Space Administration.

TuB.3

Optical Multiple Access Network (OMAN) for Advanced Processing Satellite Applications

Antonio J. Mendez
Mendez R&D Associates
El Segundo, CA 90245
(213) 640-0497

Robert M. Gagliardi
University of Southern California
Los Angeles, CA 90089-0272

and

William D.Ivancic
NASA Lewis Research Center
Cleveland, OH 44135

SUMMARY

Advanced Processing Satellites require a circuit switch which interconnects N uplink RF receivers with N downlink RF transmitters at a data rate D. Optical multiple access networks, in particular those based on code division multiple access (CDMA) techniques, are viable candidates because they are compatible with bursty, asynchronous, concurrent communication [1,2,3] and minimize scheduling delays [4]. We have designed a circuit switch based on temporal CDMA (see Figure 1). The encoders and decoders are based on optical delay lines because of the large data rate (>100 Mb/s) and number of users (>8) which results in very short chip times (<<1ns). In this paper we discuss the hardware design options and component trade offs. The hardware design options impact the network performance. One of the most critical network measures of performance is the mutual user interference (MUI) [5]. Figure 2 shows a computer simulation of the effects of MUI on signal and clutter as a function of number of concurrent users. Clearly, as the network is fully populated there is a potential degradation in the system's bit error rate (BER) due to the CDMA codes. For this reason we have been developing symbol encoding schemes which reduce this BER degradation. These symbol encoding schemes and their network performance enhancement will be described.

REFERENCES

[1] H.S. Hinton, "Photonic Switching Networks," IEEE Commun. Mag., Vol 20, p. 71 (1990).

[2] J. A. Salehi, "Code Division Multiple Access Techniques in Optical Fiber Networks - Part I: Fundamental Principles," IEEE Trans. Commun., Vol 37, p. 824 (1989).

[3] A.J. Mendez, S. Kuroda, R. Gagliardi, and E. Garmire, "Generalized Temporal Code Division Multiple Access (CDMA) for Optical Communications," SPIE Proc, Vol 1175, p. 208 (1989).

[4] M.A. Santoro and P.R. Prucnal, "Asynchronous Fiber Optical Local Area Networks Using CDMA and Optical Correlation," Proc IEEE, Vol 75, p. 1336 (1987).

[5] J.A. Salehi and C.A. Brackett, "Code Division Multiple Access Techniques in Optical Fiber Networks -Part II: Systems Performance Analysis," IEEE Trans Commun., Vol 37, p. 834 (1989).

Figure 1. Block Diagram of Advanced Satellite Circuit Switch

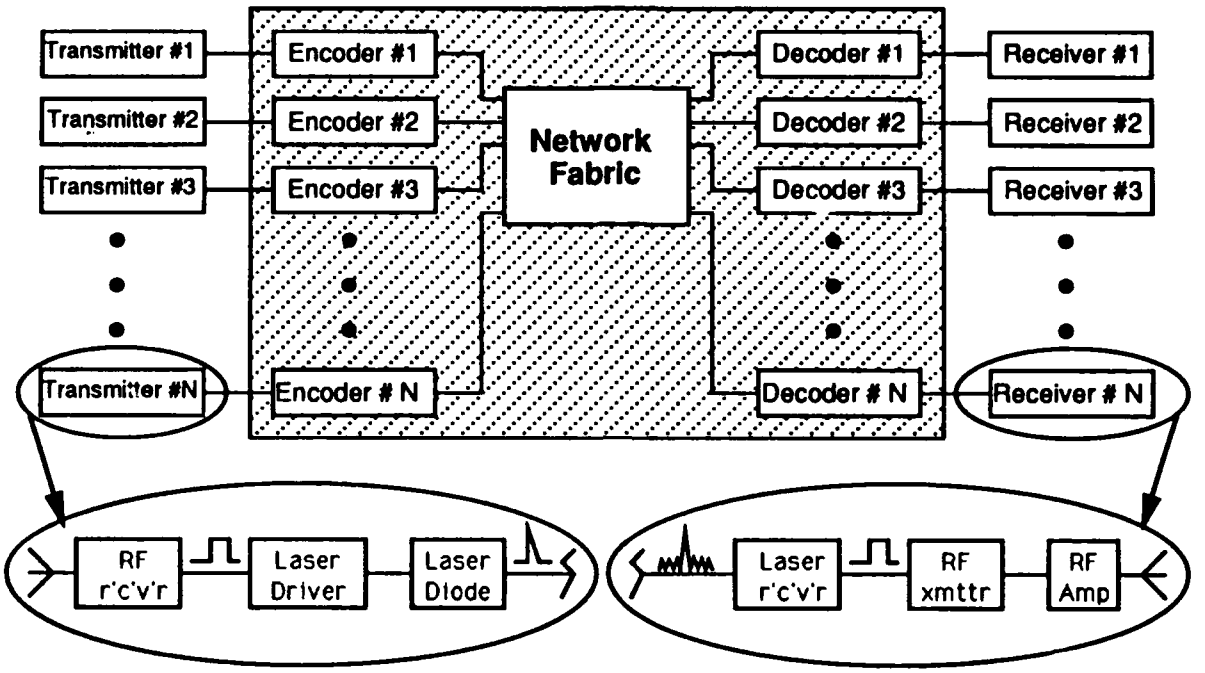

Figure 2. Temporal CDMA Network L(8,4)=49 3/19/91

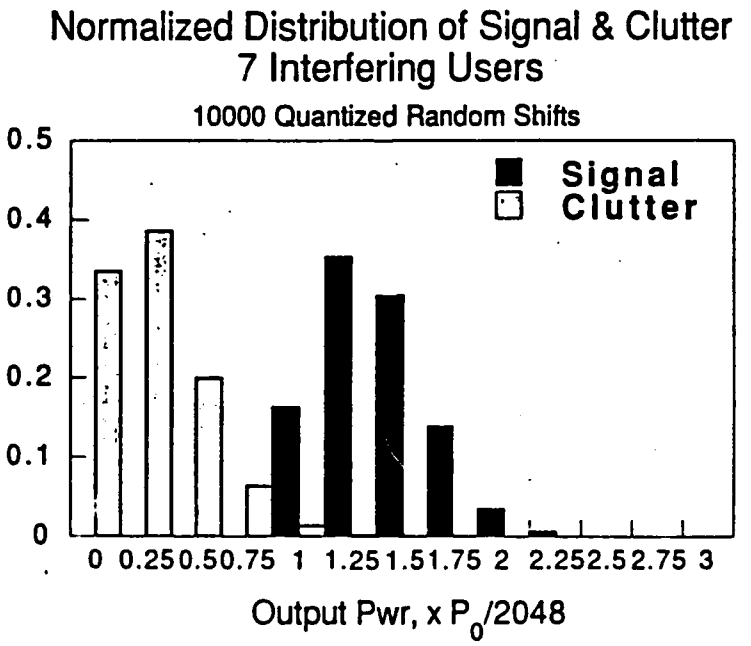

TuB.4 Architectural Issues of Photonic Networks

Nicholas D. Murray
NASA Langley Research Center
Hampton, VA 23665

The National Aeronautics and Space Administration, as part of its long range planning, has identified high performance data communication networks as a primary need for future agency needs. These networks must be capable of providing communication bandwidths and services well above what are projected for today's spacecraft, particularly for data systems that have an integrated form where video, graphics, voice, and data are to be simultaneously accommodated. The class of application is a confined environment in which there are a few well-defined network service connections (30 direct and one or two internet) and there are small distances (30 meters) that the network serves. Examples of these applications are launch vehicles, unmanned exploratory spacecraft (i.e., orbitors, landers, rovers), and transorbital lunar and Mars vehicles.

The objective of this research is an all photonic network that will provide maximum performance. The key to achieving an all photonic network is the implementation of an all photonic node, which is also the objective of this work. There are four requirements that these future network systems should meet:

- o High Performance
  - Data rate to meet quantity of information
  - Minimum data delay and delay variability for real-time data
- o Reliability/Fault Tolerance
  - Man rated and spacecraft rated safety
  - High cost of failed spacecraft operations
- o Extensibility//Modularity (Evolve Gracefully)
  - Spacecraft expands size and operations
  - Changed mission emphasis
- o Well Suited to Properties of Photonics
  - Connectivity that conforms to photonic limitations
  - Protocols that match photonic processing capabilities

A number of network architectures/topologies and protocols have been examined for meeting these requirements: i.e., linear buses, stars, rings, fully connected, and braided mesh, all with token passing and contention protocols. Each of these topologies and protocols was simulated to gain an insight into its relative performance. (Figure 1). The linear bus and the star bus perform similarly but are the least desirable from a performance comparison basis. The fully connected is the highest performing but requires the most complex implementation (number of ports/node equals number of nodes minus one) for large networks. The multiple token ring and the braided mesh are less complex and have acceptable performance.

The architectures/topologies were also examined for degree and method of achieving fault tolerance. (Figure 2). The linear bus, star, and ring achieve fault tolerance by duplicating the communications links, and fault tolerance is inherent in the braided mesh and fully connected thus leading to an integrated topology form which has advantages. The ring has the least potential for achieving higher degrees of fault tolerance.

A summary of the ability of each of these architectures/topologies to simultaneously meet all the requirements is given by Table 1. Each of the topologies, including the token ring, has the potential to enhance performance through the use of multiple and simultaneous data communications links. The preferred topologies for performance/complexity reasons are the ring and braided mesh. Each of the topologies, except the ring, has the ability for higher degrees (greater than

one) of fault tolerance. The braided mesh and fully connected have inherent fault tolerance properties which are desirable. Because of the multidrop loss problem, the linear bus has poor extensibility. Extensibility for the star must be accomplished at the level of duplicating an entire star and is considered poor. The fully connected requires a large number of ports per node and the complexity of making and breaking the port links for extensibility would be difficult. All topologies, except the linear bus, are well suited to photonic implementation The linear bus is again a poor candidate because of the multidrop loss problem.

The braided mesh is considered to be the top candidate to meet all the requirements simultaneously. Raghavendra, et. al., has shown how the braided mesh can be structured for maximum performance and good fault tolerance [1]. The best protocol for a photonic braided mesh has not been determined and is the subject of future research. Husain, et. al., has shown one form of how protocols could be processed in photonics [2].

1. Raghavendra, C. S., et .al.: "A Survey of Multi-Connected Loop Topologies for Local Computer Networks", in Computer Networks and ISDN Systems, Elsevier Science Publishers, North Holland, 1986.
2. Husain, A., et. al.: "Optical Processing For Future Computer Networks", SPIE Optical Engineering, Vol.25, No.1, Jan., 1986.

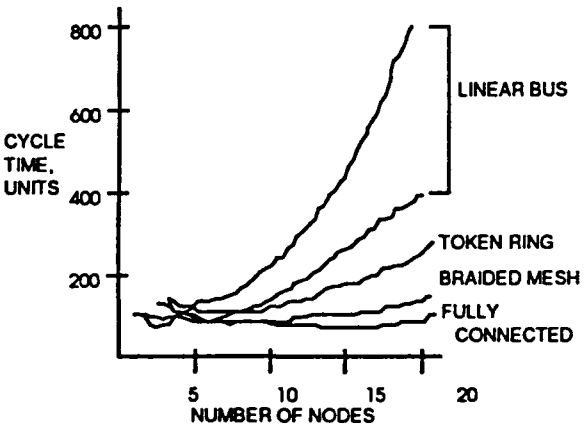

FIGURE 1: EFFECT OF DATA COMMUNICATIONS ON COMPUTATION CYCLE

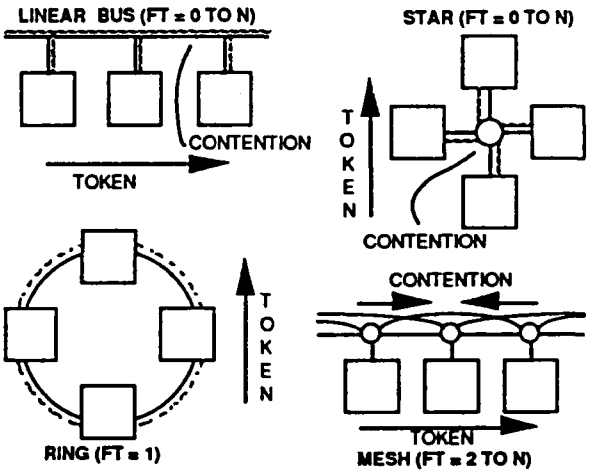

FIGURE 2: FAULT TOLERANCE OF NETWORKS

TABLE 1
NETWORK ARCHITECTURE SUMMARY

ARCHITECTURE	PERFORMANCE ENHANCING	FAULT TOLERANCE ENHANCING	EXTENSIBILITY	WELL SUITED TO PHOTONICS
LINEAR BUS - MULTIPLE	√	√	POOR	POOR
RING - SINGLE TOKEN	NO	LIMITED	√	√
- MULTIPLE TOKEN	√	LIMITED	√	√
STAR - MULTIPLE	√	√	POOR	√
BRAIDED MESH	√√	√√	√	√
FULLY CONNECTED	√√	√√	DIFFICULT	√

TuB.5 Photonic Switching Using Bistable Diode Laser Amplifiers

M. Dagenais and Z. Pan

Department of Electrical Engineering

and

Joint Program for Advanced Electronic Materials

University of Maryland
College Park, MD 20742

As data rates increase in networks such as broadband integrated services digital networks (B-ISDN) or distributed computing networks, it might be desirable to use highly functional optical devices to direct an optical signal from a particular node to its proper destination[1]. As optics progressively infiltrates our superfast computers for board-to-board and chip-to-chip communication and as the clock period gets shorter and progressively approaches a few nanoseconds, photonic switching devices might be required for relieving some of the present electronic bottlenecks. In future space missions, some of the same requirements, as can be found for terrestrial applications, might be encountered for the on-board optical local-area network, in terms of distributing signals between sensors and high-speed computers, and for optical interconnections within the on-board superfast computers. Bistable diode laser amplifiers are highly functional devices that might play an important role in photonic switching applications. These optical switches are amenable to integration. We will describe the properties of these devices in terms of switching energy, switching time, gain, cascadability, stability, and we will also present the potential application of these devices for the implementation of a generalized fully non-blocking optical crossbar switch, or for the implementation of different types of networks, including networks based on wavelength-division multiplexing.

The optical switch is based on a conventional semiconductor laser operated slightly below threshold. An input light beam is injected longitudinally in the active region of the diode laser. If the input light beam is tuned to the long wavelength side of the nonlinear Fabry-Perot resonance (within about 10 GHz), the output can exhibit optical bistability as the input intensity is varied. Thresholding and logic operations can be demonstrated with this device. A coupled optical power of order 10-20 μW is sufficient for switching the device between its two states. In a two-beam experiment, an optical switching power of less than 100 nW was demonstrated at 140 Mbit/s (return-to-zero). The device can be cycled in about 2 ns, limited by carrier lifetime. The total switching energy per unit gain of this device is the lowest that have been reported for an optical switching device and compares to the switching energy of the best electronic devices at room temperature[2]. A study of the switching power dependence and gain on detuning and current led to a new technique for accurately measuring the linewidth enhancement factor and the change of the refractive index versus carrier density[3]. A fully non-blocking optically addressable optical crossbar switch (1×2) was realized by assembling a small two- dimensional array of discrete bistable devices, each operated as an AND gate. This crossbar switch was operated at 140 Mbit/s. This crosssbar switch is capable of any interconnections of the input signals, from broadcasting, to multicasting, and wavelength division multiplexing.

An integrated two-dimensional array of bistable diode laser amplifiers, or more simply a two-dimensional array of electrically addressable traveling-wave semiconductor laser amplifiers, will find applications in future optical networks requiring photonic switching capability.

We are pleased to acknowledge the financial support from NSF (contract number: ECS-8818797) and DARPA (contract number: DAAH01-89-C-0067).

References

1. P.R. Prucnal and P.A. Perrier, IEEE LCS, May 1990, p.54.

2. M. Dagenais, Z. Pan, T.N. Ding, H.C. Lin, in "Digital Optical Computing", SPIE Critical Reviews of Optical Science and Technology, edited by R.A. Athale (SPIE, Bellingham, WA, 1990), p.126.

3. Z. Pan, H.C. Lin, and M. Dagenais, Appl. Phys. Lett. 58, 687 (1991).

TuC.1

Exploring Atmospheric Circulations Using the Laser Atmospheric Wind Sounder

G.D. Emmitt, *Simpson Weather Associates, Inc., Charlottesville, VA*

Of the three basic properties of the atmosphere, sensible heat, latent heat and momentum, the latter is the most poorly measured on a global basis. For most of the earth's atmosphere, the winds are inferred rather than measured directly. LAWS, however, will provide the first ever satellite-based direct measure of atmospheric circulations. Currently used inferences and assumptions will be challenged and replaced with a new knowledge base built with data from this new instrument.

TuC.2 The GLRS: A Laser System in Space for Geodynamics and Climate Measurements

B. E. Schutz
Center for Space Research
The University of Texas at Austin
Austin, TX 78712-1085
Tel: (512) 471-4267
FAX: (512) 471-3570

The Geoscience Laser Ranging System (GLRS) is an active laser remote sensing system designed to measure aspects of global change, particularly geodynamic, ice sheet, cloud and geological processes. The instrument is a facility instrument for the Earth Observing System and is under development at Goddard Space Flight Center.

The GLRS instrument consists of two modes: a ranging mode and an altimetric mode. The ranging mode is used to determine the precise positions of reflectors on the Earth surface; by making repeated measurements, the relative motion between reflectors can be inferred. Horizontal motions will be monitored to detect strain accumulation in seismic zones as well as velocities and strain rates of ice sheets, such as the Antarctic ice streams. Crustal deformations near tide gages will be measured in order to assess their contribution to apparent sea level. The inter-reflector distances will be measured to an accuracy of several millimeters over distances of several hundred kilometers. The GLRS altimeter will provide highly resolved observations of the distributions of ice on land and sea. Repeated measurements over the Greenland and Antarctic ice sheets will enable determination of ice sheet volume change from which mass balance can be inferred. In addition, the GLRS altimeter will have sufficient sensitivity to detect backscattering from atmospheric clouds and aerosols. Scattering from boundary layer aerosols and embedded clouds will enable GLRS detection of the planetary boundary layer, a key parameter in atmospheric models which provides information on latent and sensible heat flux across land and ocean surface both to and from the atmosphere.

This paper is presented on behalf of the GLRS Science Team.

TuC.3 Stratospheric Dynamics and Chemistry Using an Electro-Optic Phase Modulator

Daniel J. McCleese
Earth and Space Sciences Division
Jet Propulsion Laboratory
California Institute of Technology
Pasadena, California 91109 USA

INTRODUCTION

The Stratospheric Wind Infrared Limb Sounder (SWIRLS) on NASA's Earth Observing System (EOS B) will provide global measurements of stratospheric winds, temperature, and species abundances. These measurements are needed to develop an understanding of the complex coupling between chemistry and dynamics in the middle atmosphere. The SWIRLS investigation focuses on establishing the dynamical climatology of the stratosphere, emphasizing the climatologies of wind and temperature and their variations on diurnal and interannual time scales. In addition, the investigation will quantify the physical mechanisms responsible for stratospheric circulation, including the transport of ozone and other atmospheric constituents, as well as heat and momentum.

These objectives are addressed by SWIRLS through remote measurements of the horizontal wind field, the temperature field, and the concentrations of ozone and nitrous oxide. All measurements are made simultaneously in co-incident fields-of-view on both the day and night sides of earth, including the winter polar regions. By viewing the limb of the atmosphere SWIRLS provides 3 km vertical resolution (1/2 scale height) with a horizontal resolution of 350 km. Profiles of all observables are obtained over the altitude range 20 to 60 km.

MEASUREMENT APPROACH

The measurement of wind in the stratosphere is accomplished using a new technique developed at JPL - electro-optic phase modulation gas correlation spectroradiometry. The technique utilizes traditional gas correlation radiometry in which a static cell of gas provides a spectral reference, and electro-optic phase modulation which permits control of the frequency distribution of observed radiation. A schematic of one of the

SWIRLS wind sensing channels is shown in Fig. 1. Infrared radiation collected from the limb of the atmosphere by a telescope is imaged onto the front of a stack of CdTe crystals which exhibit the linear electro-optic effect. A change in the indices of refraction of the crystals is induced by an applied electric field. The radiation passes through this electro-optic phase modulator (EOPM), is subsequently directed through a gas cell which contains an atmospheric gas of interest (reference gas), and then is imaged onto a linear array of detectors.

The measurement of wind is accomplished by determining the wind induced Doppler shifts in atmospheric thermal emission from N_2O, as illustrated in Fig. 2. Band-pass spectral filters are used to select the $2\upsilon_2$ and υ_1 bands of N_2O - the Doppler shifts of approximately 100 spectral lines are observed simultaneously. The vector wind is determined by observing the limb with two telescopes oriented at 45 and 135 degrees with respect to the spacecraft velocity vector.

Measurements of atmospheric temperature and ozone concentration are made by SWIRLS using simple filter radiometry in the 15 and 9 μm spectral regions, respectively. The instrument utilizes cooled HdCdTe detectors for all of its measurements.

ACKNOWLEDGEMENTS

This research was carried out at the Jet Propulsion Laboratory, California Institute of Technology, under contract with the National Aeronautics and Space Administration.

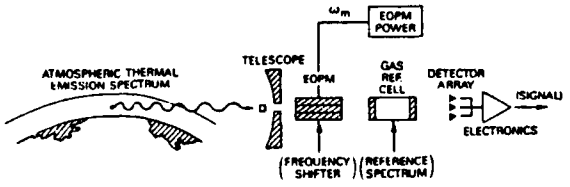

Fig. 1 Schematic diagram of a SWIRLS wind sensing channel.

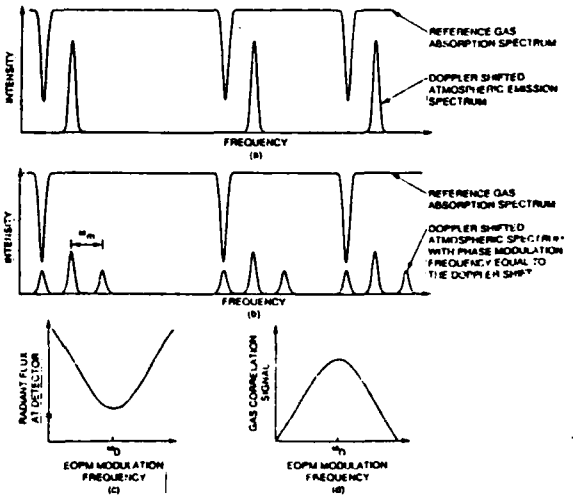

Fig. 2. Principles of EOPM gas correlation wind measurements.

TuC.4

Technical Challenges for High Spatial-Resolution Earth Remote Sensing From Geosynch

J. Breckinridge, *JPL, Pasadena, CA*

Abstract not available at time of printing.

TuD.1 Optical Neural Networks

K. Johnson, *University of Colorado, CO*

Abstract not available at time of printing.

TuD.2 Compact Acousto-optic Processor for Real-time Synthetic Aperture Radar Imaging

Michael W. Haney

BDM International, Inc.
7915 Jones Branch Drive
McLean, VA 22102

The high resolution microwave imaging technique known as Synthetic Aperture Radar (SAR) is now well established as an important tool for many remote sensing applications. Furthermore, since its inception over thirty years ago, the significance of SAR's role has continually risen as its application domain has expanded. As use of the SAR technique has expanded, the data processing techniques have, by necessity, become more sophisticated. Some proposed applications of SAR will require real time processing, aboard small radar platforms. The concomitant performance requirements of speed, flexibility, and compactness in some of these new applications are beyond the capabilities of existing processing techniques.

In the hybrid optical/electronic SAR processor the intrinsic processing abilities of optics and the programmability of electronics are combined in an architecture that is well matched to the programmable real time SAR applications in which size and power are constrained. The new approach is a generalization of an earlier time-and-space integrating (TSI) architecture.[1,2] It is based on a decomposition of the 2-D SAR problem into a cascade of two 1-D operations that are performed by temporal and spatial integrations of light respectively. In the new formulation, this problem decomposition is fully exploited by using 1-D acoustooptic cells as the electronic-to-light transducers for the radar return signals, as well as for the appropriate filter signals that are calculated and stored in an associated digital processor.[3,4,5,6] General SAR scenarios, such as spotlight mode, can be handled with this approach. The architecture interpolates the focused data in the optical domain to maintain high resolution without overburdening the associated electronic processor. Futhermore, due to the electronic programmability, the processor can compensate, on-the-fly, for the anomalous effects of range walk, range/azimuth coupling, and spurious or programmed changes in the parameters of the radar/target geometry.

1. D. Psaltis and K. Wagner, "Real-time Optical Synthetic Aperture Radar (SAR) Processor," Optical Engineering, Vol. 21, No. 5, Sept./Oct. 1982.

2. D. Psaltis, M. Haney, and K. Wagner, "Real-time Synthetic Aperture Radar Processing," Proceedings of the NASA Optical Information Processing Conference, Aug., 1983.

3. M. Haney and D. Psaltis, "Acoustooptic Techniques for Real-time SAR Processing," SPIE Proceedings, Vol. 545, April 1985.

4. D. Psaltis and M. Haney, Book Chapter: "Real-time Synthetic Aperture Radar Processors," in Optical Signal Processing, J. Horner ed., Academic Press, 1987.

5. M. Haney and D. Psaltis, "Real-time Programmable Acoustooptic Synthetic Aperture Radar Processor," Applied Optics, Vol. 27, No. 9, 1 May 1988.

6. M. Haney, "Real-time Acoustooptic Processor for Spotlight Mode Synthetic Aperture Radar," SPIE Proceedings, Vol. 1291, April 1990.

TuD.3 Semiconductor Laser Array Technology for the Space Optical Disk Recorder

Herbert D. Hendricks,
Anthony L. Cook
and
Thomas A. Shull
NASA Langley Research Center
Mail Stop 473
Hampton, Virginia 23665-5225

Summary

This presentation will discuss the development of individually addressed linear diode arrays for the NASA Space Optical Disk Recorder (SODR) for high-speed and high-capacity sensor data recording on the Earth Observing Satellite (EOS). Development and demonstration of the SODR will provide NASA a means on the EOS to make high-speed data recordings simultaneously of up to 8 different channels of data. The data rate for each channel of data will be 18.75 MBits/second for a total recording rate of all 8 channels up to at least 150 MBits/second per media side on a 14 inch disk. This then would provide for each SODR drive an 80 Gigabit capacity at a total recording rate of 300 MBits/second.

Independently addressable 9- and 10-element linear semiconductor laser diode arrays were developed in order to provide this recording capacity. In order to read, write and erase, a semiconductor laser with continuous wave operation at room temperature and a power output of 30 milliwatts was required to work with the newly demonstrated magneto-optical media and the prototype recording system optics. Two different Aluminum Gallium Arsenide (AlGaAs) semiconductor diode laser array designs were developed and demonstrated. The nine-element linear diode array technology demonstrated better performance with higher reliability and greater lifetime expectancy than the ten-element linear diode array.

The 10-element linear diode array utilzed an AlGaAs channeled substrate planar (CSP) laser structure grown by liquid phase (LPE). Results of the device performance in terms of its far field pattern, longitudinal mode structure, modulation characteristics, sensitivity to optical feedback in terms of relative intensity noise within the prototype optical recording system , lifetime and yield and other device characteristics will be presented.

The 9-element linear diode array utilized an AlGaAs stripe geometry quantum well structure grown by metal organic chemical vapor deposition (MOCVD). Results of the device performance in terms of its far field pattern, longitudinal mode structure, modulation characteristics, sensitivity to optical feedback in terms of relative intensity noise, lifetime and yield and other pertient device characteristics will also presented.

A discussion of the very-high-speed modulation of the linear diode arrays to force the operation of the lasers into multi-longitudinal mode operation in order to reduce sensitivity to optical feedback will be presented. The issue of linear diode array lifetime and redundancy in terms of the useful life of the SODR, and methods to achieve these characteristics in semiconductor lasers for optical recording will also be discussed.

TuD.4 High-Performance Optical Disk Systems for Tactical Applications

Mr. Fred Haritatos

United States Air Force, Rome Laboratory
RL/IRAP, Griffiss AFB, NY 13441

The Rome Laboratory (RL) has been actively pursuing the development and transition of optical disk storage technology from the laboratory into the real world environment. A considerable investment of R&D resources has been made by the Department of Defense with an emphasis on the development of high-capacity, high-performance systems.

Over several years, RL has conducted evaluations of candidate data storage technologies (semiconductor, magnetic and optical) for possible implementation in current and future military systems. Because of these reviews, optical data storage has been selected for additional development. The technology offers superior performance when a user needs to operate under severe environmental conditions and has a mass data storage and retrieval requirement.

Optical disk storage offers several advantages which are critical to tactical military applications. These advantages include: high data storage capacity, immunity to head crashes and data loss due to vibration and shock, fast random data access, removable recording media and reduced susceptibility to nuclear radiation effects.

In order to fully develop and demonstrate these inherent features, an R&D program was initiated entitled: Tactical Optical Disk System (TODS). Under this program, a suite of three Advanced Development Models (ADM) will be developed, flight tested and transitioned to the Air Force. A rewritable storage material, based on magneto-optics (M-O) technology, was selected since it provides a user with the ability to read, write and erase digital data. Currently, the TODS equipment suite will use both 5.25 and 14-inch diameter recording material on a glass substrate for better performance under military conditions.

The 5.25-inch TODS is designed to operate on-board tactical fighter aircraft. Some of the key environmental performance parameters include: high and low temperature, vibration, mechanical shock, acceleration, altitude and humidity.

An important design decision to insure in-flight operation was to reduce the mass of the optical head. This is accomplished by using a split optical design in which the laser diode and the majority of the optical components are removed from the moving head assembly. This enabled faster access times and exceptional vibration and shock performance.

A 5.25-inch TODS was fabricated which possesses the following features:

Storage capacity:	300 megabytes
Data transfer rates:	5 megabits per second (Sustained) 10 megabits per second (Burst)
Max access time:	100 milliseconds (inner to outer radius)
Size:	5.0 inches(W) x 6.5 inches(H)x 10.5 inches(D)
Weight:	16 pounds with disk cartridge

Although the equipment was subjected to a full array of laboratory environmental tests, only a single environmental parameter (e.g. temperature) could be evaluated at a time. In order to fully evaluate the design robustness under realistic environmental conditions, an operational flight test was conducted on-board an F-16 tactical fighter aircraft at Eglin AFB, FL from Jun-Jul 89. The equipment successfully completed a total of six (6) flights with the aircraft performing a series of aerobatic and combat maneuvers. Throughout the flights the 5.25-inch TODS was fully operational and demonstrated its ability to read, write and erase digital data. At the conclusion of each flight, collected data was analyzed which showed essentially no change in access time or raw bit error rate performance during the aircraft maneuvers.

As a result of the flight test, the 5.25-inch TODS has been transitioned to several Air Force and NASA programs. The first involves the Advanced Fighter Technology Integration (AFTI) program being sponsored by the Wright Laboratory, WPAFB, OH. Under the AFTI program, the 5.25-inch TODS will be installed on a specially configured F-16 tactical fighter aircraft which will demonstrate new Close Air Support concepts. Digital terrain map data, critical for low-altitude navigation, will be stored and retrieved from 5.25-inch TODS equipment. The second transition involves recording and playback of digital instrumentation data needed to support flight testing of the advanced Short Range Attack Missile (SRAM). In this application, the 5.25-inch TODS will be installed on-board a B-1B strategic bomber aircraft. The third transition is to the F-16 System Program Office (SPO) where the technology is capable of storing all mission related data for

in-flight use by fighter pilots. The final transition is to NASA-Goddard were the 5.25-inch TODS was launched by the space shuttle Discovery on 28 Apr 91 to demonstrate advanced robotics concepts. Minor equipment modifications were made to allow full system operation in the vacuum of space. TODS was interfaced to a DEC VAX minicomputer which will remotely control a robot at NASA. Information describing the robot's environment was stored on the optical disk. A rewritable optical disk was crucial to the success of the experiment since NASA ran several scenarios in which the robot's "world model" was changed.

The second ADM is designed to provide larger data storage capacity and higher data transfer rates. The equipment will operate in tactical environments found in larger aircraft and deployable ground processing facilities.

Digital data is recorded on a double-sided, 14-inch, rewritable M-O optical disk. A dual channel laser diode is used to provide higher data recording rates. The 14-inch TODS is under development which will possess the following features:

Storage capacity:	12 gigabytes
Data transfer rates:	25 megabits per second (Sustained) 50 megabits per second (Burst)
Max access time:	450 milliseconds
Size:	17.5 inches(W) x 21 inches(H) x 24 inches(D)
Weight:	150 pounds

The third ADM is designed to provide mass data storage and retrieval capabilities for ground-based, large data base requirements. Typical applications include: digital image exploitation, 3-D terrain map generation, weather prediction, intelligence data processing, etc. The Jukebox will store ten (10), double-sided, rewritable optical disk which provides a storage capacity of 120 gigabytes. Under computer control, individual optical disks can be located, transported and inserted into the 14-inch TODS equipment within 10 seconds.

In summary, optical disk storage technology has demonstrated its potential and is now ready for infusion into current and future military systems.

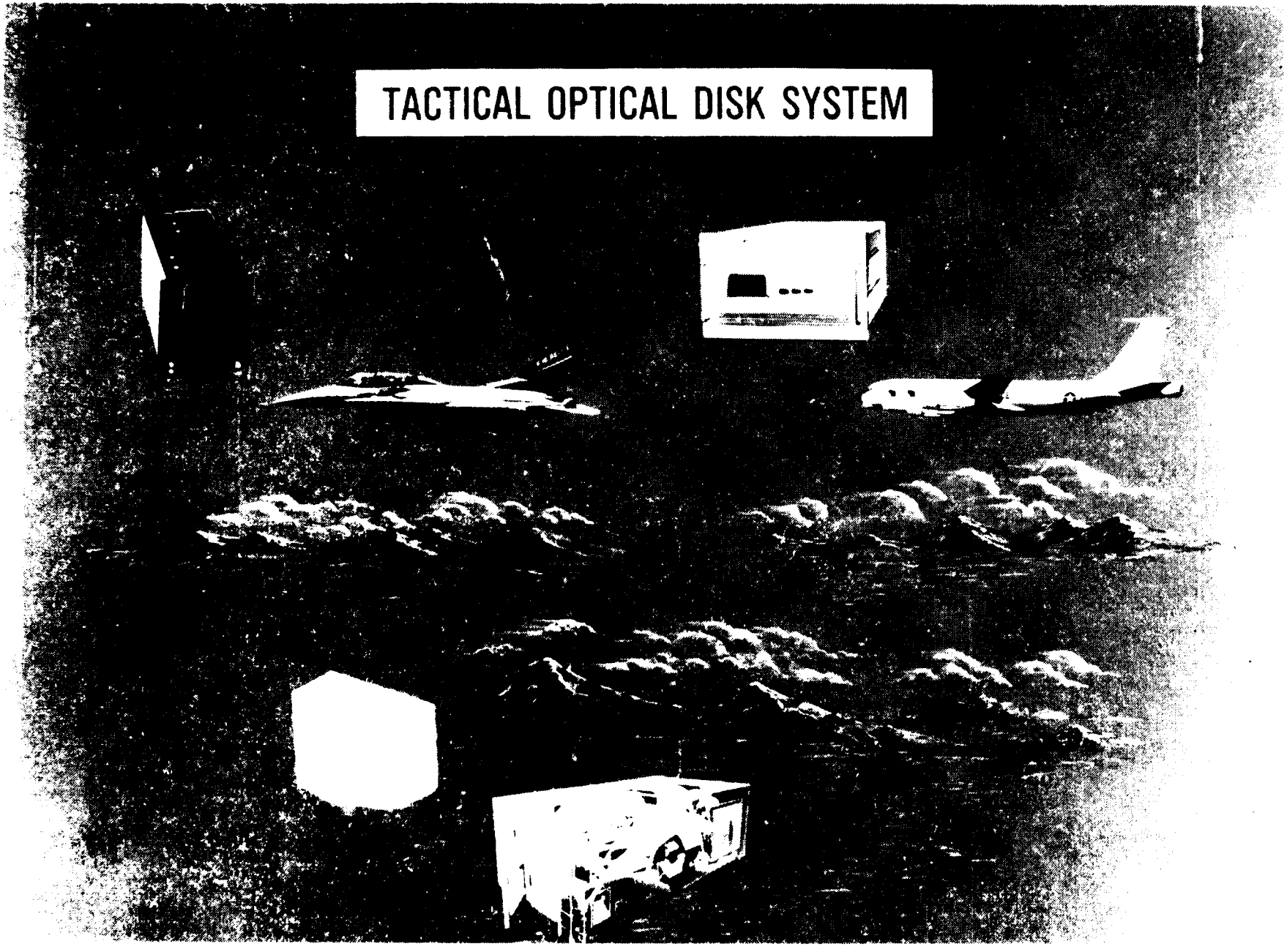
TACTICAL OPTICAL DISK SYSTEM

TuD.5

Two-photon 3-D Optical Memories

*Sadik Esener and P. M. Rentzepis**

Electrical and Computer Engineering Department
University of California, San Diego
La Jolla, CA 92093
and
*Chemistry Department
University of California, Irvine
Irvine, CA 92717

ABSTRACT

An optical volume memory based on two photon effect providing high storage density and memory bandwidth is described. Preliminary experimental data is presented.

1. Introduction

The advent of optoelectronic computers and highly parallel electronic processors has brought about a need for storage systems with with very large memory capacity and bandwidth. These demands cannot be met with current memory technologies (i.e. semiconductor, magnetic or optical disk) without having the memory system completely dominate the processors in terms of the overall cost, power consumption, volume, and weight.

To overcome the restrictions imposed by present memory devices, research has been seeking alternate means for storage, including three-dimensional (3-D) optical memory devices[1]. 3-D optical storage devices have higher theoretical storage capacity than present memory devices, because information is stored in volume. For example, the maximum theoretical storage density for an optical disk is $\rho_{2\text{-}D} = 1/\lambda^2 = 3.5 \times 10^8$ bits/cm^2 assuming that 0.5 μm wavelength of light is used to access the information. On the other hand, assuming the same wavelength of light, the maximum theoretical storage density of a 3-D memory device is $\rho_{3\text{-}D} = 1/\lambda^3 = 6.5 \times 10^{12}$ bits/cm^3. In addition, 3-D optical memory devices have the potential for parallel access, because an entire bit plane can be read or written in a single memory access operation. However, the difficulty in addressing the individual memory bits without data interaction and crosstalk with other bits has obstructed the development of 3-D optical memory devices.

In this paper, we describe two-photon optical materials and the device architecture for a bit-oriented two-photon 3-D optical memory device. Unlike other schemes which have been proposed for 3-D optical memories such as the photorefractive effect (for holographic storage),[2] spectral hole burning,[3] and optical echo,[4] the two-photon effect[5,6] provides a means of storing data into separate bit locations throughout the entire volume without affecting the neighboring bit locations. In addition, the two-photon process has the benefits of high sensitivity, high speed, and the ability to work near room temperature. A 3-D memory based on the two-photon effect can achieve very high capacity as well as parallel access of up to 10^6 bits per memory access operation. Finally, the two-photon 3-D memory can potentially have a low cost per bit because the material it uses can be made as an inexpensive polymer.

2. The Two-Photon Process

This section describes the nature of the two-photon effect and discusses how it can be incorporated into an optical volume memory due to the unique addressing capabilities. Experimental data are presented on the read and write cycles of the spirobenzopyran, a two-photon material.

Two-photon absorption refers to the excitation of a molecule to an electronic state of higher energy by the simultaneous absorption of two photons. The first photon excites the molecule to a virtual state, while the second photon further excites the molecule to a real excited state. The wavelength of the two beams are such that although neither beam is absorbed individually, the combination of the two wavelengths is in resonance with a molecular transition. Therefore, both beams must temporally and spatially overlap in order for two-photon absorption to result.

A prototype photochromic molecule has been used to demonstrate the feasibility of 3-D optical memory based on two-photon processes.[7] The photochromic molecule, a spirobenzopyran,[8] initially absorbs only in the UV region; on excitation it undergoes structural changes and it subsequently absorbs in the visible region. A schematic energy level diagram is presented

in Figure 1. The spirobenzopyran, embedded in a polymer matrix in the form of a 100μm film, has been irradiated simultaneously with two beams of 30ps pulses at 532nm and 1064nm, and a total energy density less than 10nJ/μm^2. Although initially the spirobenzopyran does not absorb in the visible or near infrared, two-photon absorption of the two beams resulted in coloration of the films. The absorption spectrum of the written colored molecule is shown in Figure 2.

The read process is also based on two-photon absorption of the laser light. The written form of the molecule was excited with two beams of 1064nm resulting in two-photon absorption of the IR photons and emission of fluorescence from the written form. The two-photon induced fluorescence spectrum of the written form is shown in Figure 3. Thus the read cycle, which can be as fast as few tens of picoseconds, is also based on a two-photon process allowing 3-D reading of the stored information. Since the read cycle is based on fluorescence rather than changes in absorbance, higher sensitivity is obtained. The written form persists at room temperature for several minutes. When the written form is placed in dry ice the written form persisted for several days. A complete discussion of the experimental results based on a spirobenzopyran molecule is presented elsewhere.[9]

3. Two-Photon 3-D Memory Device

The actual memory unit can be described as a multilayer storage system, with each layer composed of a large 2-D array of bits.[10] As shown in Figure 4, the desired memory layer is selected and illuminated with the addressing beam. At the same time, the data is sent into the memory on the information beam. Due to the two-photon nature of the material, the data can only be stored in the selected layer, as shown by the darkened regions in Figure 4. A very important characteristic of this system is the fact that as high performance spatial light modulator arrays become available and the two-photon materials are optimized for smaller writing energies, the entire array of bits in a single layer can be accessed simultaneously, allowing the memory system I/O to have a parallelism up to 10^6.

The complete two-photon 3-D memory device architecture is shown in Figure 5. The 3-D Memory Unit has been drawn to show the orientation of the individual memory layers. The connection between this memory system and the computer which is addressing the memory is via the Input and Output Arrays and the Address Manager. The optical components, such as the Dynamic Focusing Lens (DFL), polarizers, and retardation plate provide the necessary imaging between the input/output arrays and the selected memory layer. The system uses a Nd:Yag diode pumped solid state laser as the optical power supply.

Both the "write" and "read" cycles have been drawn to show the flow of information into and out of the 3-D memory unit. For the "write" cycle, it is desired to take the information which is contained on the input Spatial Light Modulator (SLM) and store it at a particular memory location. The first step of the "write" cycle is for the host computer to send the memory address to the Address Manager. The Address Manager then communicates with the Bit Plane Select (to illuminate the correct memory plane) and the DFL to establish a proper imaging system between the input array and the memory location. Next, the host computer puts the desired bit plane information onto the input array. The final step is for the "write" beam to enter through the Polarizing Beam Splitter (PBS) and be deflected towards the input SLM. The SLM will modulate the polarization of the optical field in direct correspondence with the desired information plane. On reflection back through the PBS, only the modulated parts are allowed to go straight through and will be imaged onto the selected memory layer.

For the "read" cycle, the Bit Plane Select array illuminates a particular layer of the Memory. This causes light to be generated by two-photon fluorescence at each of the written bits. This light is then polarized by P2 and imaged onto the Output Array using the DFL. To steer the information through the PBS and onto the output plane, the polarization must be rotated by 90°. This is achieved with the activation of the electro-optic $\lambda/2$ retardation plate during each "read" operation. The Address Manager controls all of the essential components (Dynamic Focusing Lens, Bit Plane Select, $\lambda/2$ retardation plate) to guarantee that the information is imaged onto the output detector array.

It is desirable for the memory system to have the highest possible access speed and parallelism. In the two-photon 3-D memory system, the speed and the parallelism are limited by the response time, size, and sensitivity of the Input and Output Arrays and the DFL, rather than by the very high inherent speed of the two-photon materials. Therefore, the design and characteristics of these components is critical for the overall performance of this memory system. During the presentation the expected characteristics of these components will be discussed and performance potentials for the two-photon 3-D memory will be evaluated.

4. Conclusion:

Two-photon 3-D memory stores information in volume and allows parallel access to a plane of information, thus allowing a potential increase in the memory bandwidth by orders of magnitude over present two-dimensional memory devices. In addition, because the data is stored in a volume, very high capacities can be achieved within a very small area. The fast access time and the expected low per megabyte cost can potentially make two-photon 3-D memory a competitor to magnetic and optical disk for mass storage applications.

Acknowledgements:

This work has been funded by RADC through Call/Recall Corp.

References:

1. D. Chen and J. D. Zook, "An Overview of Optical Data Storage Technology," Proceedings of the IEEE 63, 1207 (1975).
2. J. E. Weaver and T. K. Gaylord, "Evaluation Experiments on Holographic Storage of Binary Data in Electro-Optic Crystals," Optical Engineering 20, 404 (1981).
3. U. P. Wild, S. E.Bucher, and F. A. Burkhalter, "Hole Burning, Stark Effect, and Data Storage," Applied Optics 24, 1526 (1985).
4. N. W. Carlson, L. J. Rothberg, and A. G.Yodh, "Storage and Time Reversal of Light Pulses Using Photon Echoes," Optics Letters 8, 483 (1983).
5. *Multiphoton Processes*, P. Lambropoulos and S. J. Smith, Eds. (Springer-Verlag Berlin Heidelberg) (1984).
6. R. M. MacFarlane, Journal of Lumin. 38, 20 (1987).
7. P. M. Rentzepis, U.S. Patent Serial No. 07/342, 978 (1989).
8. R. C. Bertelson, in *Techniques of Chemistry: Photochromism*, vol. 3, G.M. Brown, Ed. (Wiley- Interscience, New York), 45 (1971).
9. D. A. Parthenopoulos and P. M. Rentzepis, "Three dimensional optical storage memory," Science, 245, 843 (1989).
10. S. Hunter, F. Kiamilev, S. Esener, D. Parthenopoulos and P.M. Rentzepis "Potentials of two-photon based #-D optical memories for high performance computing" Appl.Opt. 29 (14), 2058, May 1990.

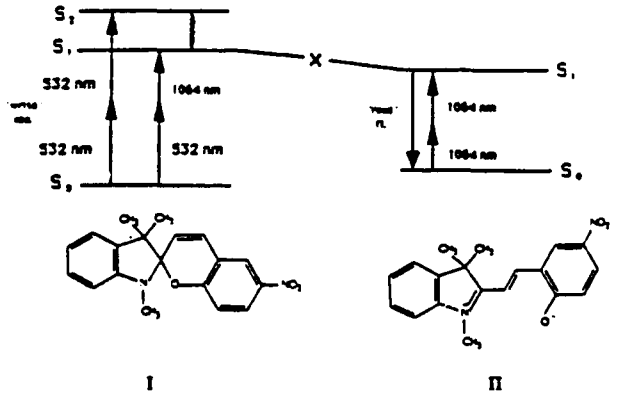

Fig. 1. Schematic energy level diagram of the write and read forms of the photochromic molecule. "X" is an intermediate to the isomerization of the spirobenzopyrans. The structures of the two forms of SP as well as the laser wavelengths used for writing and reading are shown also.

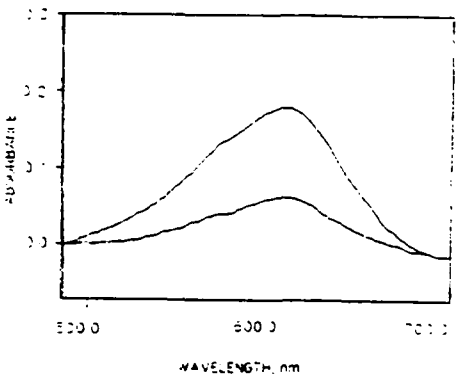

Fig. 2. Room temperature visible absorption spectrum of 1% SP in a PSt film. Upper curve: after irradiation for 5 s with 355 nm, pulse fluence, 4 mJ/cm². Lower curve: after irradiation for 60 s with 532 and 1064 nm; total pulse fluence, 20 mJ/cm²; beam diameter d = 1 cm.

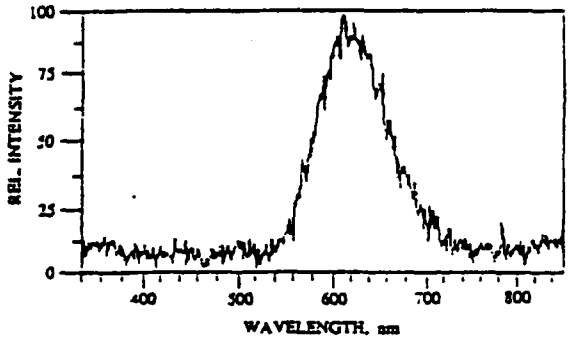

Fig. 3. Room temperature two-photon-induced fluorescence spectra of the colored merocyanine form of 1% SP in PMMA. Excitation wavelength, 1064 nm; pulse fluence, 1.5 mJ/cm^2; beam diameter d = 2 mm.

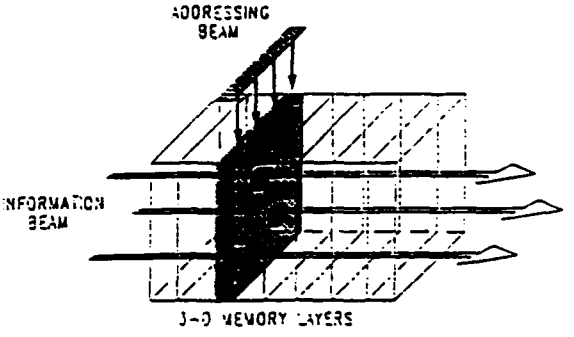

Fig. 4. Addressing a two-photon volume storage material. The dark regions indicate the written bits.

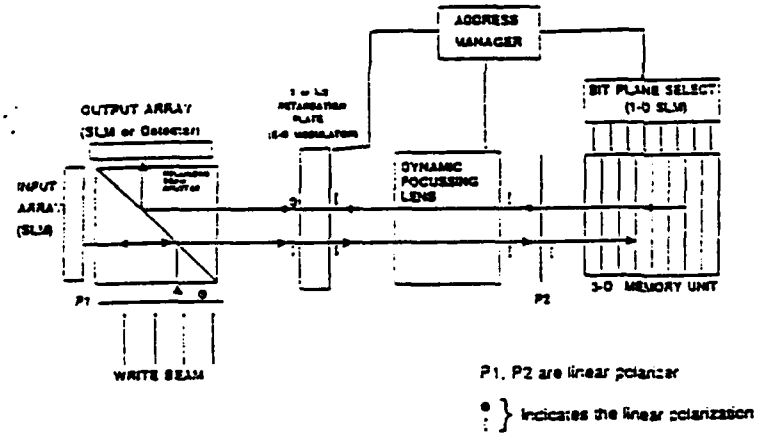

Fig. 5. Two-photon 3-D memory system. The memory I/O is achieved via the input and output SLMs. The address manager controls the internal components to assure proper imaging between the data arrays and the correct memory layer.

Wednesday

July 24, 1991

WA.1

Mars Observer Laser Altimiter

Jack L. Bufton
Laboratory for Terrestrial Physics
Goddard Space Flight Center
Greenbelt, MD

The Mars Observer Laser Altimeter (MOLA) is a pulsed laser ranging instrument developed for the 1992 Mars Observer Mission. The MOLA laser transmitter generates a pulse of ~ 10 nsec duration at 1064 nm wavelength. In operation on Mars Observer, MOLA will transmit this pulse toward the Martian surface from a 400 km polar mapping orbit and utilize a 0.5 m diameter reflector telescope to collect laser pulse backscatter from the surface for measurement of pulse time-of-flight and received pulse energy. The MOLA Instrument will produce a sensor footprint of 160-200 m diameter on the Martian surface and will be capable of making range measurements with a vertical precision of ~ 1-10 m. Each pulse is utilized without averaging for a continuous measure of the range to the surface at a rate of 10 pulses-per-sec along the nadir track of the spacecraft. This yields a horizontal along-track sampling resolution of ~ 330 m. Laser altimetry data derived from MOLA over the two-year mission lifetime of MARS Observer will be utilized to construct: (1) a gridded topographic map of the Martian surface with maximum grid spacings at the equator varying from 0.2° to 1°; (2) high-resolution topographic profiles along the spacecraft nadir track for studies of geology, geophysics, and atmospheric circulation; and (3) laser backscatter profiles related to surface reflectivity and atmospheric transmission at the1064 nm wavelength. Range precision, the MOLA contribution to surface measurement accuracy, is primarily dependent on receiver signal-to-noise in the measurement of backscattered laser pulses that are broadened by surface slope. Accuracy in determination of Martian surface elevation is also a function of Mars Observer pointing knowledge (~ 3 mrad) and orbit determination from radio beacon tracking. The overall measurement goal is 30 m surface elevation accuracy.

The MOLA instrument was designed and developed between August 1988 and June 1991 by a government and industry team centered at the Goddard Space Flight Center. Design and development choices were tightly constrained from the outset. Foremost among the constraints was instrument cost, which was capped at $10M. This was a result of the laser altimeter's role as a replacement for an earlier radar altimeter design that was canceled for cost considerations. The MOLA instrument inherited the mass allocation (26.18 kg) and electrical power allocation (28.3 Watt) of the original radar altimeter design. Other principal constraints were the launch vibration levels (16.5 g rms random & 6 g sine) of the Titan III vehicle and the in-space thermal environment of Mars Observer for cruise to Mars (-30°C to + 40°C) and operation in Martian orbit (-20°C to +30°C). A tight instrument build schedule was necessary to meet the September 1992 launch window.

The cost and schedule constraints permitted only the use of existing laser, telescope, detector, and electronics technology (circa FY1989). This requirement and the low mass and electrical power available resulted in the choice of a space-qualified diode-pumped Nd:YAG laser transmitter design from McDonnell Douglas Electronic Systems Company

(MDESC). The MDESC design was successfully implemented within all the interface constraints, with performance close to the stated goals, and was delivered to NASA in November 1990. Recent diode array laser tests at MDESC suggest that this laser should also be capable of meeting the operational lifetime of $6X10^8$ pulses. Details of the laser transmitter are reported by Gaither et al[1] and performance specifications are summarized in Table 1. Note that laser output parameters vary as a function of the laser interface temperature due primarily to the temperature-dependent optical pumping of the Nd:YAG laser slab by the GaAlAs laser diode arrays.

The overall design and configuration of the MOLA instrument is illustrated in Fig. 1. The core of the instrument is an all-beryllium optical assembly composed of the laser transmitter, optical bench, and receiver telescope. This assembly weighs only 10 kg, due in large part to the ultra-lightweight telescope (3 kg) built by Texas Instruments and American Beryllium Company in 1975 as a spare for the Infrared Spectrometer instrument on the Voyager spacecraft. The laser transmitter and receiver telescope are co-boresighted with dual-axis Risley prisms which are mounted in the extension of the laser cavity at the periphery of the telescope primary mirror. The backscattered laser light collected by the telescope is collimated, bandpass filtered at 1064 nm, and focused on to a silicon avalanche photodiode detector (APD). This APD is a special-order low-noise hybrid device constructed in 1986 by EG&G (formerly RCA) Canada. Details of the MOLA optical assembly were reported by Ramos-Izquierdo & Bufton[2]. An essentially passive thermal design for the laser transmitter and optical assembly is achieved by thermal control coatings on the beryllium solar shield and the isolation of the optical assembly from the Mars Observer Spacecraft by a titanium support tube and thermal blankets. Some supplementary heat is provided to reduce the thermal extremes.

The altimetry electronics, consisting of a four-channel matched-filter receiver and single-channel time-interval-unit, are housed in the electronics assembly together with the payload computer and power supplies. Details of the MOLA altimetry electronics are provided by Abshire et al[3] and McGarry et al[4]. All the electronics and the laser operate from a +28 vdc prime power input. Both the electronics and optics assemblies are mounted on a triangular aluminum honeycomb panel and three magnesium piramidal feet which together provide the stiffness and low mass required for the MOLA support structure. In operation the MOLA instrument collects range and pulse energy data, formats them together with temperature, start pulse, and status bit data into 1 4 sec duration packets, and sends these packets to the Mars Observer Payload Data System for telemetry transmission.

1. G. Gaither et al., "Design of the Mars Observer Laser Altimeter Laser Transmitter", Paper CFI2, Proc. of the Conf. on Lasers & Electro-Optics, Baltimore, MD, May 12-17, 1991, p. 520.
2. L. Ramos-Izquierdo and J. Bufton, "Optical System Design of the Mars Observer Laser Altimeter", Paper CThR31, op. cit., p. 448.
3. J. Abshire et al., "Design and Performance of the Receiver for the Mars Observer Laser Altimeter', Paper CFI4, op. cit., p. 520.
4. J. McGarry et al, "Design and Performance of an Autonomous Tracking System for the Mars Observer Laser Altimeter Receiver", Paper CThR27, op. cit., p. 446.

WA.2 High-Power Coherent Diode Lasers for Space Applications

D. Botez

TRW Research Center
One Space Park, D1/2519
Redondo Beach, CA 90278

SUMMARY

Phase-locked arrays of GaAs/AlGaAs diode lasers without active phase control are sought as reliable sources of high coherent powers (>100 mW diffraction limited) for applications such as space communications, second harmonic generation, and output fanout for optical interconnects. Conventional narrow stripe (2-4 micron width) lasers which operate single mode are generally limited to below 100 mW reliable operation, as limited by the optical power density at the laser facet. For reliable operation at higher output power levels, a larger aperture source is necessary in order to reduce the optical power density at the laser facet. The challenge has been to maintain a coherent single spatial mode at high power levels from a large aperture device. For this reason, multi-element phase-locked arrays have been under development for over a decade as a means of obtaining a mode stabilized device which can operate reliably at power levels in the range 0.5-1.0 W.

Monolithic (linear) arrays consisting of phase-locked gain-guided or index-guided lasers have proved useful tools in understanding the complex modal behavior of arrays. Gain-guided devices have inherent limitations as a result of mode instabilities with drive current and junction temperature. Positive-index guided devices designed to operate in-phase generally oscillate in several array modes in excess of 50% laser threshold or 50 mW.[1,2] None of the positive-index-guided arrays reported to date have demonstrated diffraction-limited-beam operation beyond 50 mW because of either weak coupling or confinement (see Table 1). The real problem is that researchers have taken for granted that strong nearest neighbor coupling implies strong overall coupling. In reality, nearest-neighbor coupling is "series coupling" and makes for weak overall coherence. Strong overall coupling happens only when each element couples to all others, so called "parallel coupling"[3], which implies full coherence.

A new class of phase-locked arrays, consisting of closely spaced negative-index waveguides has renewed interest in the possibility of obtaining high-output-power, single-mode operation from a monolithic source.[4] The unique feature of these devices is the fact that they have both strong and optical mode confinement (within each element) and strong overall interelement coupling (i.e. parallel coupling via leaky waves).[5] Such arrays called ROW arrays[5] have allowed the first demonstration of diffraction-limited beam operation (uniphase mode) to output powers in excess of 1 W from monolithic diode lasers.

Typical results for 20-element ROW arrays are shown in Figure 1 : 0.5 W CW diffraction-

Table 1
Instrument Paramaters for the Mars Observer Laser Altimeter

LASER TRANSMITTER

Operating Temperature Range: 5°C ± 15°C
Pulse Energy: 30-45 mJ
Pulsewidth: 7.6-10 nsec
Divergence: 0.4-0.5 mrad
Overall Efficiency: 2% to 3% (ratio of optical power out to electrical power in @ 28 vdc)

RECEIVER

Telescope: 0.5 m diam. all-beryllium f/6 Cassegrain, f/1.85 focusing optics
Image Quality: 260 μrad blur circle
Optical Bandpass: 2.25 nm FWHM
Detector: 0.8 mm diam. silicon avalanche photodiode, 30% quantum efficiency @ 25°C
Receiver Sensitivity: ~ 0.1 nanowatt
Field-of-view: 0.85 mrad
Matched Filter Channels: 20, 60, 180, 540 nsec
Time-interval-resolution: 10 nsec

INTERFACE

Mass: 26.18 kg
Power: 28.3 Watt total: 13.5 Watt (laser); 13.3 Watt (altimetry electronics)
Size: 0.6 m triangular cross-section, 0.8 m high
Data Rate: 617 bps

Figure 1. The Mars Observer Laser Altimeter Instrument

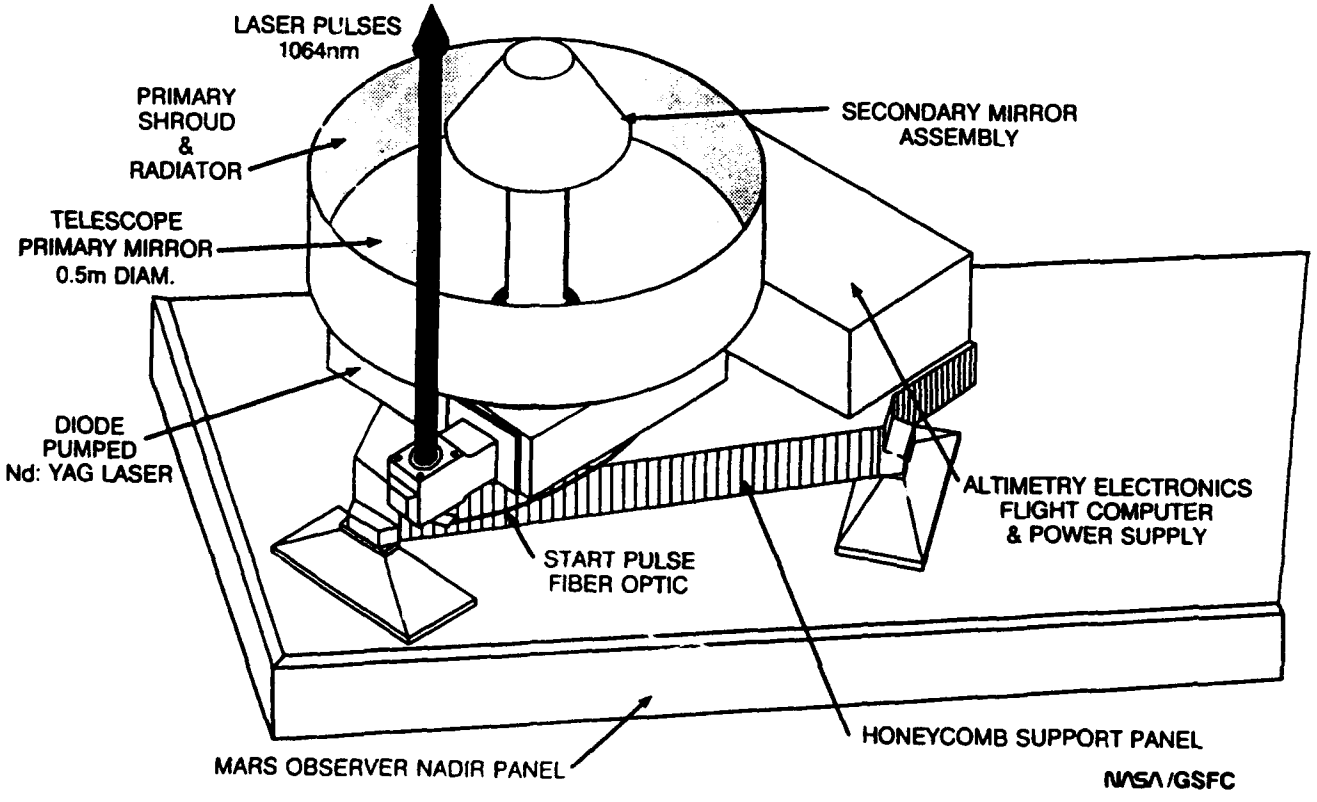

limited operation; 1.5 W pulsed diffraction-limited operation; and 5 W in a beam 3 x diffraction-limit. Such devices could be used for direct-detection space communications.

For coherent communications one needs to use single frequency high-power devices: injection-locked broad-area devices[6], injection-locked ROW arrays [7], or monolithic master-oscillator power amplifier (MOPA) devices [8-10]. M-MOPA devices in particular have shown up to 1 W coherent pulsed power in a single longitudinal mode[8], and 0.38 W pulsed diffraction-limited power[10].

REFERENCES

1. S. Mukai et al, Appl. Phys. Lett., 45, 834, (1984).
2. D. Botez, T. Pham, and D. Tran, Electron. Lett., 23, 416 (1987).
3. W. J. Fader and G. E. Palma, Opt. Lett., 10, 28 (1985).
4. D. Botez et al, Appl. Phys. Lett. 53, 464 (1988).
5. D. Botez, L. J. Mawst, G. Peterson, and T. J. Roth, Appl. Phys. Lett. 54 2183 (1989).
6. L. Goldberg and M. K. Chun, Appl. Phys. Lett., 53, 1900 (1988).
7. M. Jansen et al, unpublished.
8. D. F. Welch et al, Appl. Phys. Lett., 57, 2054 (1990).
9. N. W. Carlson et al, Photon. Tech. Lett. 2, 708 (1990).
10. D. Mehuys et al, Electron. Lett., 27, 492 (1991).

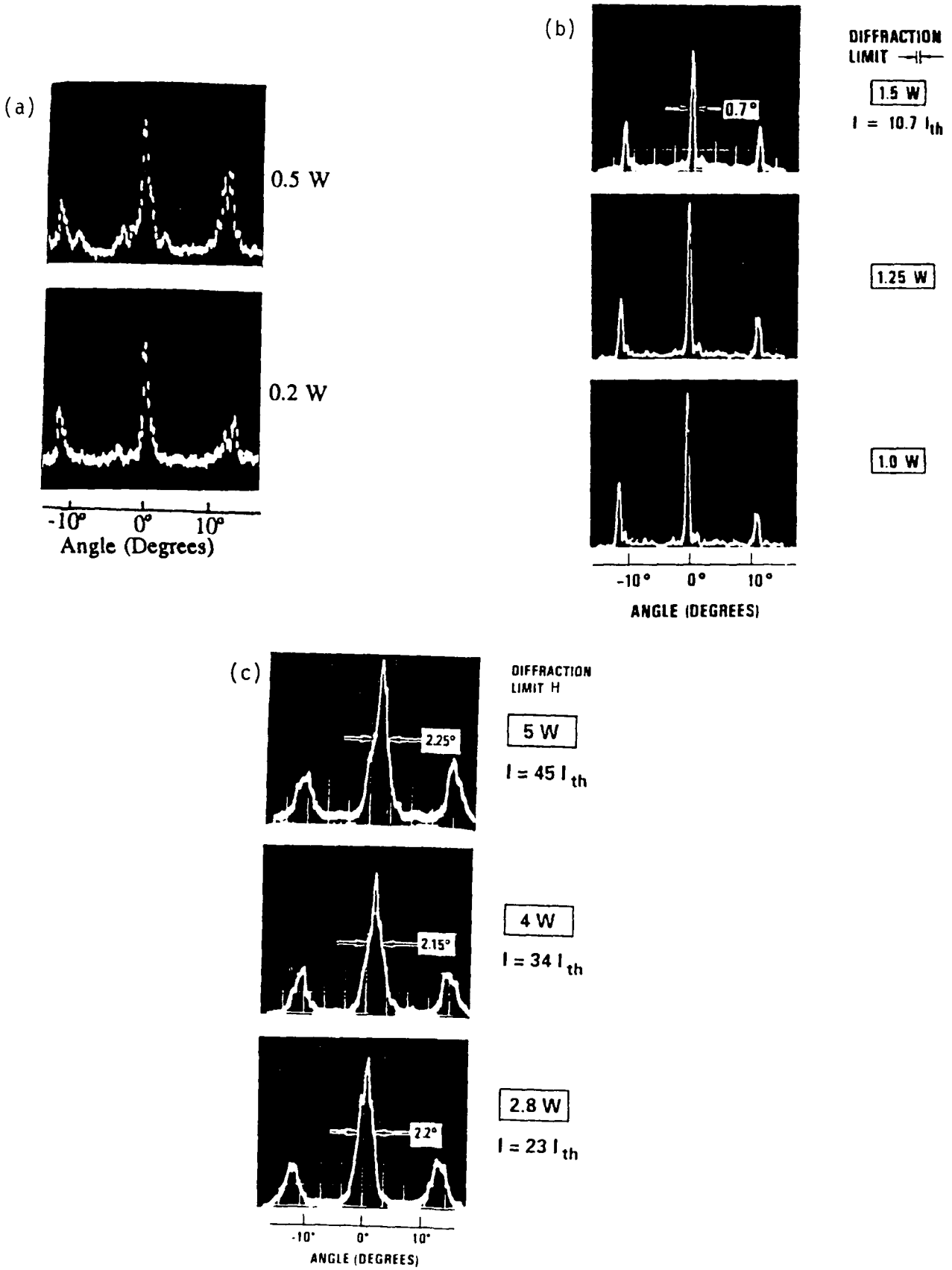

Figure 1. Far-field patterns of ROW arrays: (a) CW operation; (b) and (c) pulsed operation.

WA.3 High-Power Optically-Pumped Surface-emitting Semiconductor Lasers for Free-space Communication and Sensing

John G. McInerney and Cunkai Wu
Optoelectronic Device Physics Group
Center for High Technology Materials
University of New Mexico
Albuquerque, NM 87131-6081.

Cheryl J. White
Mission Research Corporation
1720 Randolph Avenue SE
Albuquerque, NM 87106-4245

SUMMARY

Vertical-cavity surface-emitting semiconductor lasers (VCSELs) are potentially useful for fast optical interconnection between wafers, free-space communication or remote sensing, and formation of coherent 2-D laser arrays. The use of resonant-periodic-gain (RPG) media, in which a series of gain regions (single quantum wells or closely-spaced groups of quantum wells) with half-wave optical periodicity is aligned with the antinodes of the optical standing-wave in the laser cavity, provides enhanced gain along the cavity axis and at the designed lasing wavelength. The result is a considerable reduction of the laser threshold [1]. Moreover, it should be possible to pump large active areas because of reduced parasitic transverse amplified spontaneous emission.

Despite long experience with edge-emitting semiconductor lasers, it is not obvious that electrical pumping is most appropriate for high-power VCSELs. Transverse electrical injection of VCSELs has been successfully demonstrated but with very low efficiency [2]. Longitudinal electrical injection has been somewhat more successful, but there are still severe problems with electrode placement and large series resistances ($\sim 100\ \Omega$ per 20 μm spot). Here we demonstrate that optical pumping - ultimately diode laser pumping [3] - can be feasible for high-power VCSELs.

In this paper we describe experiments using tunable (730-760 nm) pulsed dye lasers to pump GaAs/GaAlAs and InGaAs/GaAlAs VCSELs. In the first detailed experiments, short (7 ns) pump pulses were used to avoid thermal effects, and the lasing properties of VCSELs were measured for various spot sizes from 10 to 100 μm, the latter dimension being limited by available pump power. Of particular

interest are the threshold optical fluence and slope efficiency, which do not depend on the spot size in the range of values considered. These data indicate that transverse ASE is not playing a significant role. Spectral measurements indicate multi-transverse-mode operation with overall envelopes ~1 nm wide.

Another indication of ASE suppression by the RPG structure is the ability to pump large (cm^2) spots efficiently. In these experiments, a high-power flash-pumped dye laser (500 ns pulse width) was used, generating peak output powers of up to 20 kW from 1 cm^2 GaAs/AlGaAs samples, and 50 kW from 0.1 cm^2 InGaAs/GaAlAs samples, limited by available pump power and occasionally by sample damage at "hot spots" in the pump beams.

Our results augur well for compact, rugged and efficient kilowatt pulsed VCSELs using incoherent rack-and-stack diode arrays as pump sources. Suitable external cavities or other transverse mode selection schemes will be required for optimum coherence properties. The primary advantage of the diode-pumped VCSEL over traditional edge- and surface-emitting high-power diode lasers is enhanced spatial and temporal coherence: as in the diode-pumped Nd:YAG laser, the second gain medium acts as a "coherence converter". The diode-pumped Nd:YAG is itself a serious contender for free-space communication, but operates at fixed wavelengths, needs careful choice of pump diode lasers and requires external modulation. The diode-pumped VCSEL, by contrast, has a very broad pumping band, permits multi-gigabit direct modulation of the electrical or optical bias, and can be designed and optimized across a broad range of wavelengths, which may (for example) be chosen to match atomic line filter receivers. Finally, since semiconductor lasers are extremely sensitive to external reflections, they may conveniently be used to observe backscatter from distant objects to determine target positions, velocities and possibly configurations.

REFERENCES

1 M. Y. A. Raja, S. R. J. Brueck, M. Osinski, C. F. Schaus, J. G. McInerney, T. M. Brennan and B. E. Hammons, "RESONANT PERIODIC GAIN SURFACE-EMITTING SEMICONDUCTOR LASERS", *IEEE J. Quantum Electron.* **QE-25**, 1500 (1989).

2 C. F. Schaus, A. J. Torres, J. Cheng, S. Sun, C. Hains, K. J. Malloy, H. E. Schaus, E. A. Armour and K. Zheng, "TRANSVERSE JUNCTION VERTICAL-CAVITY SURFACE-EMITTING LASER", to be published in Appl. Phys. Lett., April 1991.

3 D. L. McDaniel Jr., J. G. McInerney, M. Y. A. Raja, C. F. Schaus and S. R. J. Brueck, "VERTICAL CAVITY SURFACE-EMITTING SEMICONDUCTOR LASER WITH CW INJECTION LASER PUMPING", *IEEE Photonics Technol. Lett.* **2**, 156 (1990).

WA.4 Twin Pulse Nd:YAG Laser System

Julie A. Williams-Byrd
Norman P. Barnes
Keith E. Murray
Charles D. Nichols*
C. Duane Armstrong
Waverly D. Marsh*

NASA Langley Research Center
Mail Stop 474
Hampton, Virginia 23665
(804) 864-1629

*STX Corporation
28 Research Drive
Hampton, Virginia 23666

ABSTRACT

A frequency doubled Nd:YAG laser was constructed which produces two closely spaced, or twin pulses. With this described design the temporal separation of the pulses could be varied from the length of the flashlamp pulse to the time interval between twin pulses. Consequences of this temporal variation of the efficiency are discussed.

SUMMARY

Many applications would benefit by having a laser system capable of producing twin pulses, two pulses with a temporal separation varying from about 100μ sec to 10 m sec, especially if the output were in the visible. An obvious application would be stop frame photography. Another application would involve remote sensing, particularly DIAL remote sensors where two closely spaced laser pulses are required. By utilizing the twin pulse concept, both pulses can be produced with single laser system; thereby minimizing cost, size, and weight. However, the characteristics of the laser, particularly the second pulse, will depend on the temporal separation. Specifically, the laser output energy and beam quality of the twin pulse laser was investigated.

A twin pulse laser was designed by utilizing two parallel pulse forming networks to produce each of the two pulses. Thus, a separate pulse forming network was used to

provide electrical energy to a single flashlamp. Pulse separation was controlled by triggering the separate SCR at the desired time. If needed, this concept could be extended to produce three or more pulses. For short time intervals between the pulses, the design of the parallel pulse forming networks must account for the temporal characteristics of both the flashlamp and the upper laser level. As not all of the energy is extracted from the laser rod by the first pulse, some on the energy remains available for the second pulse if the pulse separation time interval is less than a few times the upper laser level lifetime. In addition, the flashlamp may be expected to operate differently after having been warmed up by the first pulse. Both of these factors can contribute to the efficiency of the second pulse in varying degrees, depending on the pulse separation of the twin pulse. Thus the design of the second pulse forming network depends of the pulse separation.

Fluorescence from the upper laser manifold and current characteristics of the flashlamp were monitored to determine the extent of these effects. Fluorescence was monitored by observing radiation at 0.94 μm with a photomultiplier tube while the current was monitored with a current transformer. For the pulse separation germane to the NASA application, 400 μ sec, considerable energy from the first pulse was available for the second pulse. Energy remaining in the laser rod could be measured by observing the level of fluorescence. Measurements of the fluorescence were then used to determine the required energy for the second pulse. Because of this effect, the design of the second pulse forming network reflected a lower electrical energy stored on the capacitor. In order to utilize a single power supply, the size on the capacitor was decreased in the second pulse forming network from 32 μF to 26.5 μF. Further details of the pulse forming network and the warm up effects of the first pulse will be presented.

WA.5 Characterization of the Shuttle Flight Qualified NASA Lite LTM Three Color Nd:YAG Output Beams

Marc C. Cimolino, Mulugeta Petros and John Chang
TITAN/SPECTRON
3535 Hyland Ave., Suite 102
Costa Mesa, CA 92626-1439

The LITE Laser Transmitter Module contains two 10 Hz three color Nd:YAG lasers which are fully optically redundant with only one operational at a time. Each output beam is composed of the 532 nm second harmonic, the 355 nm third harmonic and the 1064 nm fundamental remaining after nonlinear conversion.

Complete optical characterization of the two lasers is not only important in verifying that the laser meets specification at delivery, but it is crucial in measurements required to flight qualify the whole transmitter. The necessary optical diagnostics for ground testing have been designed to fit a 2'x 2' breadboard which is rigidly mounted with respect to the LTM. The only beam diagnostics inside the nitrogen purged canister are pyroelectric laser energy sensors for each color of each laser. The external diagnostics are used to calibrate the energy sensors inside the canister which are used during ground environmental testing as well as during flight. These recorded shot to shot energies are used to correct the lidar data.

The measurement requirements and methods for the full optical characterization are summarized in Table I. The key parameter of pulse energy is measured first using an averaging thermal detector which is internally calibrated with traceability to NIST. Measurements taken simultaneously with the thermal and pyroelectric sensors calibrates the shot to shot energy. The Labtech Notebook data acquisition software allows calculation of the shot to shot energy stability.

Beam divergence, pointing stability and beam quality measurements are made at the focal point of a 2 meter mirror using a CCD array camera and Beamcode software. The beam divergence of the IR beam is set using a telescope. The lower limit of 0.5 mrad is set by the eye safety limit for the green beam and the 1.5 mrad limit is to keep all the energy in the field of view of the receiver. The pointing stability over the short term is limited by shot to shot oscillator fluctuations.

Final acceptance test data will be presented for both lasers. This baseline data will be used to assess the affects of subsequent aging, vibration testing, thermal cycling and space flight.

TABLE I. MEASUREMENT REQUIREMENTS AND METHODS

MEASUREMENT	REQUIREMENT	METHOD
Pulse Width	< 100 ns	100 ps photodiode and 1 GHz oscilloscope
Pulse Energy	> 200 mJ 1064 nm > 400 mJ 532 nm > 150 mJ 355 nm	thermal power meters to calibrate pyro-electric sensors
Pulse Energy Stability	> 90% of all pulses within 5% of 1 hour avg.	record shot to shot energy for 1 hour
Beam Divergence	0.5 to 1.5 mrad full angle	far field CCD camera system-86.5% energy diameter
Pointing Stability	< ± 0.25 mrad	far field CCD camera system-energy centroids
Beam Quality	Times the diffraction limit	far field CCD camera system-minimum spot size
Beam Diameter	< 10 mm at 86.5% energy	near field CCD camera system-beam diameter
Linewidth	< .15 nm	Fabry-Perot etalon and CCD camera system

WA.6 Self-Injection Locked, High Power Laser Diode Arrays For Space Applications

R.E.Stone, S.C.Wang
Lockheed Palo Alto Research Laboratories
3251 Hanover Street, B202,97-30, Palo Alto, California 94304
(415) 424-2800

SUMMARY

Both multiple-stripe phased-array laser diodes and broad area laser diodes can generate high power output that make these lasers very attractive for space applications. However, these lasers typically have multiple oscillation frequencies and produce a multi-lobed beam pattern which are not desirable for certain applications. We have reported previously single frequency and single lobe output of up to 500mW from high-power laser diode arrays using a self-injection locking technique .[1,2,3] Here we report the results of extending this technique to higher power laser diode arrays now available. We also discuss on the modulation characteristics and their application to space communications and lidar.

The basic principle of this technique is to inject the multimode laser diode array with one of its own oscillation modes thus locking the oscillation of the laser array to that particular mode. In practice this is accomplished by a setup shown in Fig. 1. A small amount of the laser output power is tapped off by a beam splitter and passed through an etalon. The multiple oscillation modes of the laser are filtered by the etalon to allow only one particular mode corresponding to the etalon transmission mode to pass, while all other modes are blocked. This particular mode is then fed back into the laser array, thus forcing the laser array to oscillate in this particular mode. This technique has following key advantages: (1) It requires no additional external master oscillator as injection source, thus the frequency selection and tuning become easier; (2) No modification of existing laser diode is necessary using this scheme, therefore it is applicable to any commercial laser diode sources; (3) Since only a small portion of laser output power is used in injection-locking the laser diode itself, the output power of the laser suffers little loss; (4) The oscillation frequency of the laser can be tuned over the oscillation bandwidth of the laser by the adjustment of the etalon, making a tunable single frequency source possible; (5) The output beam is nearly colinear with the laser diode emission, making follow-on beam shaping optics easy to attach.

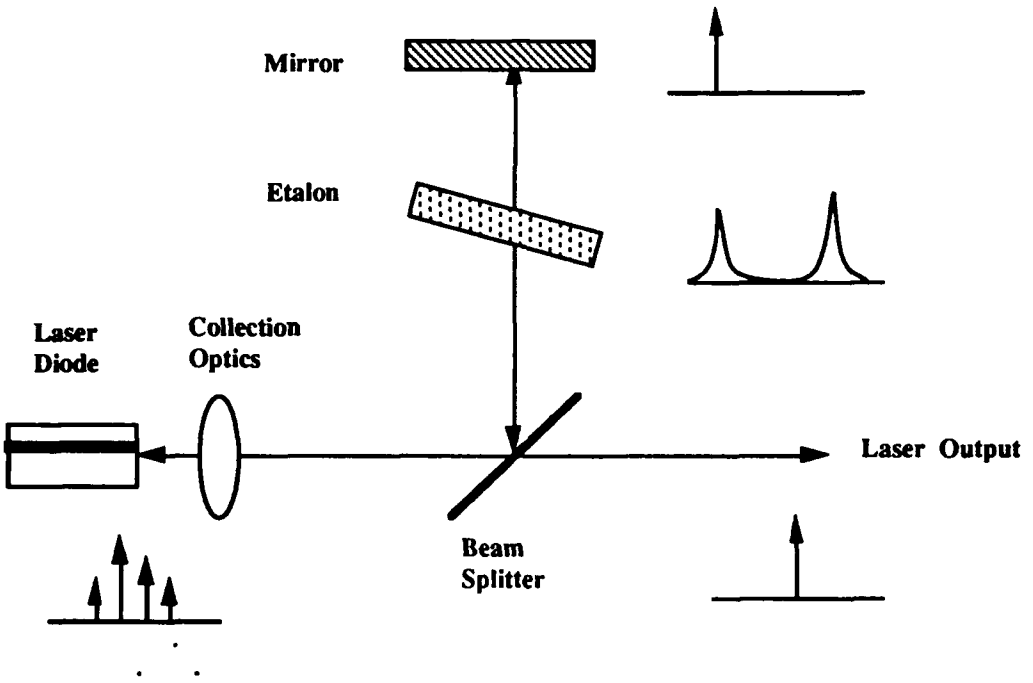

Fig 1. Schematic diagram of a self-injection locking scheme

Using a commercially available high power laser diode array we obtained more than one watt of narrow linewidth CW output tunable over the gain width of the laser array. The self injection locked laser array, under direct current modulation, also shows high frequency modulation response with high modulation depth and low distortion.The typical modulation response of the array shows a 3 db bandwidth of about 2.2 GHz. The harmonic distortions are at 30 db and 35 db down from the fundamental for the second harmonic and third harmonic respectively. We believe such a self injection-locked laser diode array producing high power output and narrow spectral linewidth should make a suitable candidate for airborne, free space, optical communication applications.

REFERENCES

1. S.C. Wang, R.E. Stone, and L.Z. Gacusan, "Self-injection locking of high power gain-guided laser diode arrays," Technical Digest, Conference on Lasers and Electro-Optics (CLEO), paper WM8, pp. 212 - 213, April 1988.

2. S.C. Wang , R.E. Stone and L.Z. Gacusan, " High power diode laser array with diffraction - limited output, " Technical Digest, CLEO, paper THK 22, pp. 298 -299, April 1989.

3. S. C. Wang and R. E. Stone, "Spectral control of high-power laser diode arrays by self-injection locking," Technical Digest, International Conference on Lasers'89, paper HD.4, p.28, Dec. 1989.

WA.7

2 Micron Lasers for Coherent Lidar

Mark E. Storm
ST Systems Corporation
28 Research Drive, Hampton, Va.,23666
804 -864-1635

2-Micron lasers are seriously being considered in the LAWS application for measuring global winds using coherent lidar. 2-micron lasers are rare-earth doped crystals similiar to Nd:YAG, however, they are more complex because they are quasi-3 level lasers with populated lower laser levels. They are pumped at 785 nm using highly efficient and reliable GaAs laser diodes and 5 year lifetimes are expected for the all-solid-state lasers presently envisioned. This paper will discuss recent progress in developing coherent 2-micron lasers and their prospect for space missions.

Significant spectral refinement, in addition to generating high laser power, will be required for lidar applications of 2 micron laser sources. The control of both absolute wavelength and lasing bandwidth is necessary for both DIAL and coherent lidar applications. Laser diode pumped monolithic crystals are simple devices that can be made compact , reliable and tunable over small ranges using temperature or stress.[1] These narrow bandwidth, CW sources will be used as master oscillators to control both the wavelength and bandwidth of Q-switched lidar transmitters. Continuous frequency tuning over 5 Angstroms and heterodyne detection have been demonstrated using these monolithic crystals[2]. The basic principle in this monolithic laser design is to increase the resonator free spectral range (FSR) such that the next longitudinal mode away from the fluorescence peak will not successfully compete for stimulated emission.

Single longitudinal mode lasing was achieved using a flat/flat cavity which was 1 mm thick with 2.1 micron laser mirrors coated directly onto the crystal. These lasers operated at 2 distinct wavelength at 2.091 and 2.122 microns. The wavelengths are chosen by selecting the output coupling reflectivity. An output coupler reflectivity of 99.8R was used to generate the 2.122 micron line. This crystal operated up to a temperature of 40C. Single mode output powers of 12 mW were demonstrated. The 2.091 micron line was

selected using an output coupler reflectivity of 99.0% R and the crystal was cooled to -15C to achieve threshold. Single mode output power of 13 mW was demonstrated using this crystal.

The FSR for the 1mm crystal length is 12.5 Angstroms. The flat/flat resonator was chosen because spacial modes other than the Temoo are effectivily discriminated against they experience higher diffraction losses. The longitudinal mode spacing of 12.5 Angstroms was easily resolved using the monochromator. The crystal was pumped by a SONY 303V laser diode which was circularized and focused to a 60 micron beam radius. The single mode lasing spectrum and the fluorescence spectrum for the Ho:Tm:YAG crystal is displayed in figure 1. Continuous tunability of the holmium laser has been demonstrated using and external cavity, diode-pumped laser[4]. Monolithic resonators have been customized to lase on several of the laser peaks by choosing the right output coupler reflectivities and temperature. Special mirror coatings on the crystal might also be used to offer discrimination between the various fluorescence peaks. The actual lasing bandwidth is almost certainly less than the 0.8 angstroms presented here. The ultimate bandwidth of the laser is unknown pending further investigation using Fabry-Perot and heterodyne measurement techniques.

Demonstration of compact, tunabe, single mode laser represents a significant first step toward development of a space-based coherent laser transmitter. Laser efficiencies of 10% must be demonstrated for Q-switched lasers for space applications. This work has been supported by the NASA/Langley Research Center in Hampton,Va.

REFERENCES:

1. M.E. Storm and W.W. Rohrbach, " Single-longitudinal-mode lasing of Ho:Tm:YAG at 2.091 microns," Appl. Opt. 28,23,4965,1989.
2.0 Mark E.Storm, Grady J. Koch and Wayne W. Rohrbach, "Single-Mode Lasing of Ho:Tm:YAG at 2.091 Microns in a Monolithic Crystal," published in the OSA Proceedings on Advanced Solid State Lasers, Optical Society of America, Utah, 1990.
3.0. Mark E. Storm, "Spectral Performance of Monolithic Holmium and Thulium Lasers," Technical Digest on Advanced Solid State Lasers, Optical Society of America, Hilton Head SC., March 1991.
4.0 S.W. Henderson,C.P. Hale,"Tunable single-longitudinal-mode diode laser pumped Tm:Ho:YAG laser, Appl. Opt. 29,12,1716,1990.

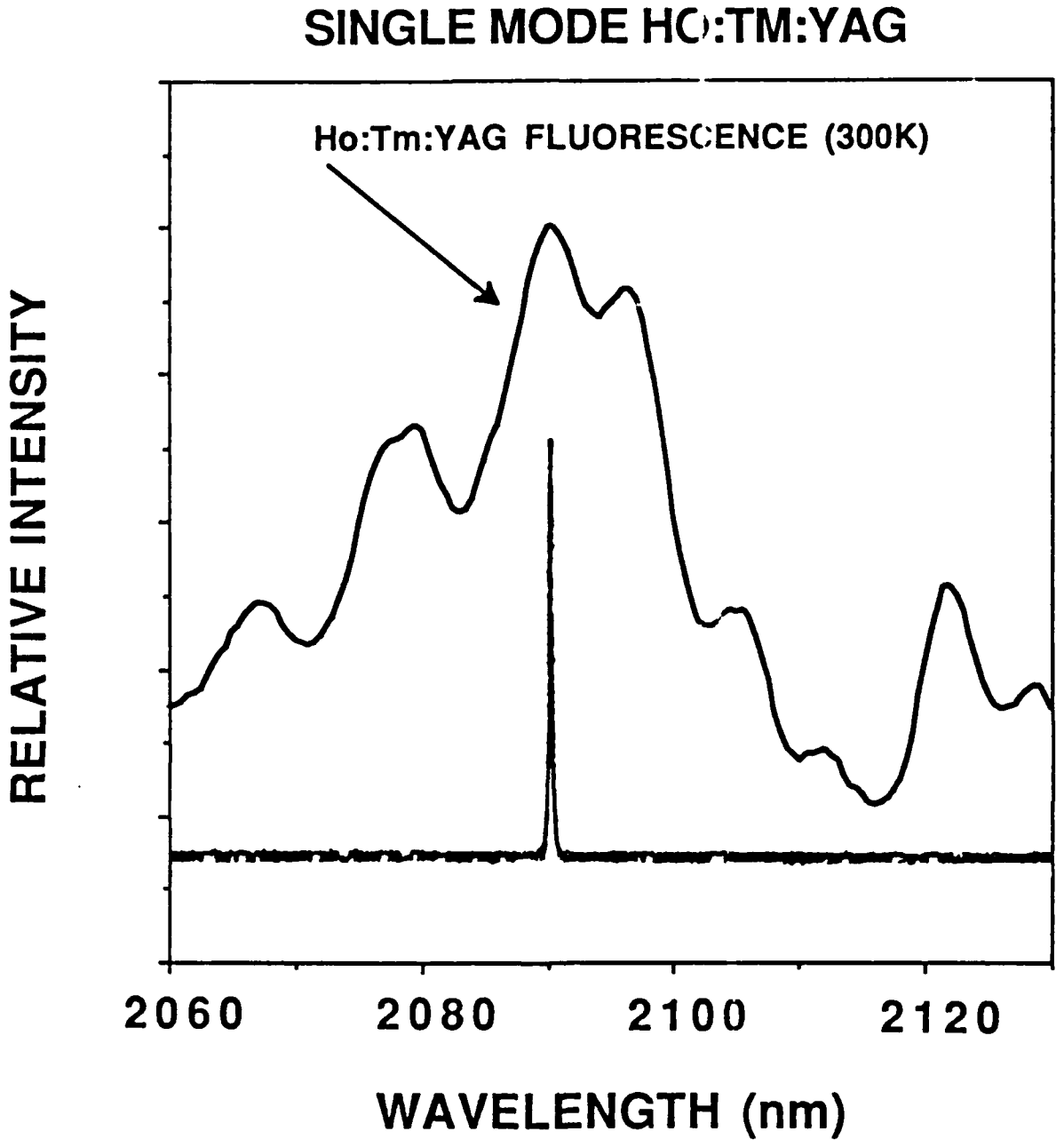

Figure 1: Fluorescence and Lasing Spectrum of Single-Frequency Ho:Tm:YAG laser.

WA.8

AlGaAs-GaAs Quantum-Well Lasers for Direct Solar Photopumping

Sreenath Unnikrishnan and Neal G. Anderson

Department of Electrical and Computer Engineering
University of Massachusetts at Amherst
Amherst, MA 01003

Semiconductor lasers are well suited for space applications because of their small size, light weight, and low power consumption. Solar powering of spaceborne current injection lasers is possible using photovoltaic cells, but the efficiency of such a configuration may be limited by optical-to-electrical and electrical-to-optical energy conversion losses at the cell and laser, respectively. We are investigating an alternative solar pumping scheme in which a semiconductor laser would be *directly* photoexcited by focused sunlight. As part of a more comprehensive feasibility study of direct solar pumped semiconductor lasers, we have first considered lasers fabricated from the most common laser materials: AlGaAs and GaAs. Output from such lasers could be used directly, and would also be at wavelengths suitable for efficient pumping of Nd:YAG lasers.

We have specifically considered separate-confinement quantum-well-heterostructure (SCQWH) lasers since these lasers operate at low threshold excitation levels, and limited power is available in the usable portion of the solar spectrum. The SCQWH geometry we have examined is shown schematically below. This structure consists of high-gap $Al_yGa_{1-y}As$ cladding layers surrounding a medium-gap $Al_xGa_{1-x}As$ waveguide (or optical confinement) region, the center of which is punctuated by a single GaAs quantum well layer. Unique design considerations arise for such a structure when solar photoexcitation is considered, as compositions and thicknesses which would yield minimum threshold operation in a diode structure can not be expected to minimize photoexcitation power requirements for solar pumping. For example, high-composition cladding regions and thin waveguide regions increase optical confinement, thus lowering threshold currents in injection lasers. In a solar pumped laser, however, absorption of sunlight would be maximized both by decreasing cladding layer compositions (thus band gaps) and increasing waveguide thicknesses. Hence, a trade off exists between absorption and optical confinement. In order to investigate this and other trade offs and to identify structures suitable for direct solar pumping, we have developed a model of SCQWH lasers which explicitly treats the case of photoexcitation by a broadband source.

Our model combines a straightforward treatment of gain and loss in the laser active region with explicit treatment of position- and wavelength-dependent light absorption and carrier transport through the structure. The gain spectrum of the quantum well is calculated assuming parabolic energy bands and a lineshape function which reflects both homogeneous and inhomogeneous broadening contributions. In calculating the gain and other properties, quasi-fermi levels are assumed constant throughout the waveguide region (including quantum well) and this

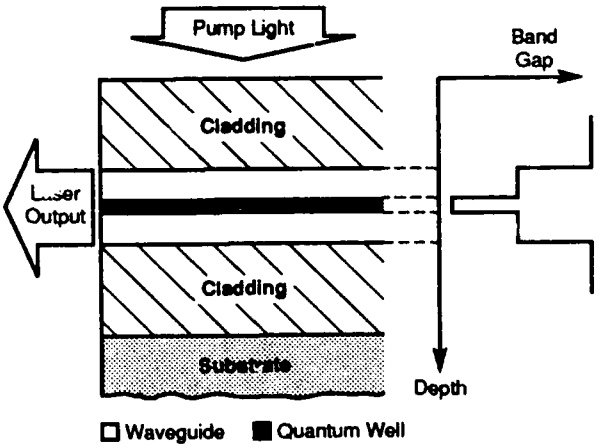

region is assumed to be charge neutral. Optical loss mechanisms include free-carrier absorption and a uniformly distributed scattering loss (assumed $5cm^{-1}$) in addition to mirror losses. A standard dielectric slab model is used to treat optical confinement in the active region. Absorption of sunlight is treated using experimentally determined wavelength-dependent absorption coefficients and a 5800K blackbody approximation to the solar spectrum normalized to a total AM0 power density of $137mW/cm^2$. Transport of carriers to the active region from the top cladding layer, where photogeneration may be significant, is treated using a one-dimensional drift-diffusion model and typical values for recombination lifetimes and surface recombination velocity at the semiconductor/air interface. The waveguide region is assumed to collect all carriers incident on it from the cladding region, and the well is assumed to collect all carriers which enter or are generated within the waveguide region. Non-radiative recombination involving indirect conduction-band minima and Auger recombination are also considered. Cavity lengths of 800μm are assumed for our calculations. Suitably modified and applied to broad-area AlGaAs-GaAs SCQWH injection lasers of similar cavity lengths, this model overestimates recently measured threshold currents (*J. Appl. Phys.* **68**, 1964 (1990)) by a factor of ~1.3 with no parameter adjustment. Absolute errors in prediction of thresholds, while very modest here, should not obscure identification of optimum structures as trends are more accurately predicted than absolute threshold currents.

In our initial investigations of the feasibility of direct solar pumping of these lasers, we have used our model to identify structures which operate at the lowest solar photoexcitation levels. While we have not yet rigorously identified an optimum structure, lowest thresholds seem to occur for lasers with ~55Å quantum wells, ~0.18μm waveguide layers with compositions near x~0.32, and ~0.9μm cladding layers with compositions near y~0.70. Significantly thinner wells and lower composition waveguide layers increase thresholds by reducing carrier confinement in the quantum well. Significantly thicker confining layers increase thresholds by increasing the number of carriers photogenerated in the top confining layer which are lost to recombination before diffusing to the waveguide and well. Cladding-layer composition and waveguide thickness roughly trade off, with increases in one allowing increases in the other for a given threshold magnification. For a structure using the parameters listed above (identically), our model predicts a solar threshold required for lasing of 9300 suns. Further reduction should be possible using a multiple-quantum-well active region and/or graded-gap waveguide layers, but lower bounds will be set by the minimum band gaps practical for the materials used. Use of lower gap materials can be expected to significantly reduce solar pumping requirements, even though reductions from enhanced absorption will be opposed by increasing Auger losses in some cases. Indeed, initial results for strained-layer $Al_{.70}Ga_{.30}As$-$Al_{.20}Ga_{.80}As$-$In_{.20}Ga_{.80}As$ SCQWH lasers with structural dimensions identical to those described above suggest that laser operation should be possible at solar photoexcitation levels of <5000 suns for such a structure.

To summarize, we have theoretically examined the solar power requirements for low-threshold AlGaAs-GaAs quantum-well lasers *directly* photopumped by focused sunlight. Using a laser model which explicitly treats absorption and transport phenomena relevant to solar pumping, and which yields threshold current predictions for injection lasers, we have identified separate-confinement single-quantum-well laser structures which should operate at photoexcitation intensities of less than 10000 suns. We expect that further optimization of structural parameters, modification of structural configuration, and use of lower-gap semiconductors will reduce pumping requirements to less than 3000 suns. Reduction of pumping requirements will be a focus of our future studies, and optical-to-optical power efficiencies for optimum structures will be compared with those expected from injection lasers driven by photovoltaic cells.

This work is supported by NASA (Grant NAG-1-1148).

WB.1 Strategic Applications for Space-Based Lidar Systems

W.W. Simmons, *LLNL, Livermore, CA*

Let us explore the unique demands placed upon space-based laser systems intended for simultaneous ranging and imaging over a three-decade range of regard; and how modern technology is rising to this challenge.

WB.2 Aerospace Applications of Lidar for DOD

P. McManamon, *WL/AARI, Wright-Patterson Air Force Base, OH*

SDI, air to air, and air to ground DOD Lidar applications will be discussed. SDI and air to air Lidar will be viewed as an adjunct to passive sensors. Air to ground Lidar will pursue target detection and recognition, with emphasis on non-imaging, non-conventional Lidar technologies.

WB.4 Enabling Space Optics Through Phase Conjugation

Richard H. Moyer
R1/1078
TRW Applied Technology Division
Redondo Beach, CA

Future space-based optical systems will require diffraction-limited performance from very large apertures. Conventional approaches using adaptive optics or stringent optical tolerances are difficult to implement, due to complex control mechanisms and inevitable mechanical deformation. Nonlinear optics can automatically correct optical systems aberrations, including those caused by large optics figure error, segmented optics misregistration, inhomogeneous laser gain media, and optical train jitter. This automatic aberration correction property of nonlinear optics allows the use of looser (10 to 100-fold) tolerances than would be required in conventional systems. Configurations employing processes such as stimulated Brillouin scattering or four-wave mixing phase conjugation have been developed for high-energy laser systems, passive and active imaging systems and for large aperture collimators, producing diffraction-limited performance and automatically correcting aberrations without the need for high-bandwidth adaptive optics.

These concepts generally use a multi-pass approach: a plane wave reference beam samples optical aberrations on an initial pass through the system; then the phase conjugator inverts the phase so that during the beam's second pass, the aberrations are canceled. One objective in implementing this approach is to minimize the differences between the two passes (subject to other design constraints, such as system compactness and reference beam isolation) so that the cancellation of the aberrations is maximized.

WB.3

Short-wavelength Imaging Laser Radar

S. C. Hiser, G. L. Trusty, J. A. Blodgett, J. A. Welch
Naval Research Laboratory
Washington, D. C. 20375

M. G. Roe*, T. H. Cosden
University of Maryland, University Research Foundation
Greenbelt, Maryland 20770

G. Benedict-Hall, R. Ginaven, M. Khazra, E. Odeen,
J. Page, N. Swanberg, and F. Feiock
Science Applications International Corporation
San Diego, California 92121

SDIO has several requirements that lead toward the development of a long-range laser radar. Among these requirements are discrimination between real deployed threats and decoys, acquisition of track files of threats, and targeting and aim-point selection for DEW. Key issues are precision three-dimensional position measurement, agile access over an extended field of regard, and high resolution at each target. This paper describes a rapid-retargeting 0.53-μm imaging laser radar that is a result of an SDIO technology development program that addresses these issues.

This short-wavelength laser radar experiment uses a gated Digicon receiver[1] to detect seven targets dispersed along a 60-m light tunnel. The system provides 8 x 8 - pixel range and intensity images along with three-dimensional target locations for each target within a wide field of regard. Figure 1 illustrates the Digicon receiver comprised of optics and the magnetically focused Digicon tube. In the image plane the 8 x 8 - array of 100-μm pixels can be directed to target anywhere over the 30-mm surface of the photocathode. This direction is achieved by magnetic electron-beam deflection with settling times of 1 msec. The range resolution for each pixel is less than 1 m. The photocathode's field of regard is determined by the focal length of the preceding optics.

The block diagram of Figure 2 shows the laser radar experimental set-up. The Digicon Receiver Head is connected via 64 cables (for the 8 x 8 array) to the processing electronics which includes an 80286 computer. In addition to processing the return signals from the targets, this AT controls the current for Digicon's electron-beam deflection coils, the timing of the laser trigger, the gating circuit, and the pointing of the beam director. At present, the AT uses established target lists to control the Digicon deflection and the beam director. A video camera connected to a frame-grabber in a Sun Workstation provides a means of developing an acquisition and hand-off capability.

The computer monitor displays pseudo-color range-per-pixel and intensity-per-pixel images for each shot of the laser. Figure 3 illustrates two targets at dramatically different ranges

*Now with Rockwell International, Rocketdyne Division, Canoga Park, CA.

in a single field of view display. Rapid multiple retargeting is visualized on the full photocathode display of Figure 4. Nine distinct range images are visible within seven fields of view scattered across the field of regard. These images are magnified 3 times for ease of interpretation. Likewise, gray-scale intensity images can be displayed. Multiple retargeting at 15 Hz is easily achieved with an off-the-shelf AT at 10 MHz; thus, the SDIO requirement of 50 targets/second could be obtained with a dedicated machine.

Future directions of interest for this short-wavelength laser radar include: 1) completion of the acquisition and hand-off capability, 2) tracking, 3) long-range demonstrations (1 km), and 4) completed development of a 16 x 16 array Digicon tube with magnification.

---

[1]R. Ginaven, E. Odeen, M. Urbach, and F. Feiock, "Laser Radar Receiver Using a Digicon Detector," SPIE Laser Radar IV 1103, 61 (1989).

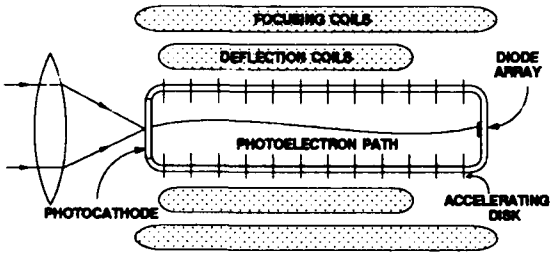

Figure 1. Digicon receiver comprised of optics and magnetically focused Digicon tube with electron image deflection.

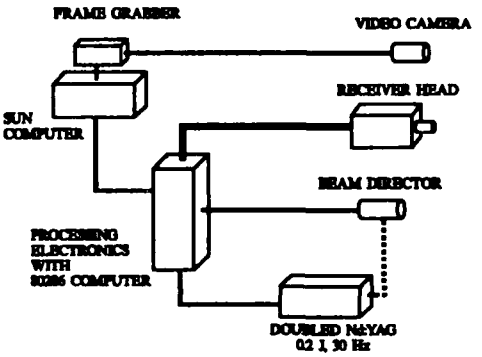

Figure 2. Block diagram of the short-wavelength laser radar experiment.

Figure 3. Single field of view display with a range-per-pixel image, and intensity-per-pixel image, and three-dimensional position measurement.

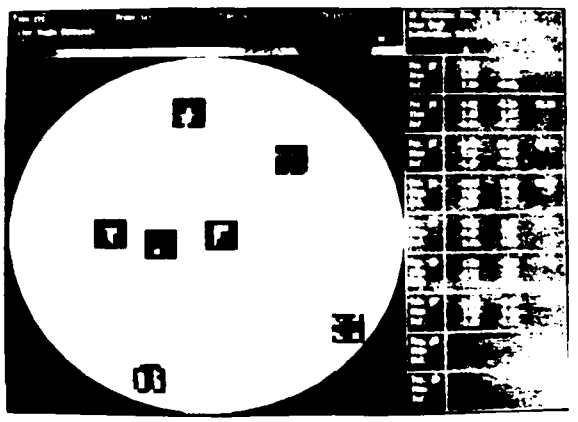

Figure 4. Multiple range images across the photocathode field of regard. These fields of view are magnified 3 times for ease of viewing.

Spaceborne Photonics
AUTHOR INDEX

Optical Millimeter-Wave Interactions: Measurements, Generation, Transmission and Control

July 24-26, 1991

Sheraton Newport Beach
Newport Beach, California

Support provided by:
Air Force Office of Scientific Research

IEEE# 91TH0345-9

Library of Congress #: 90-85245

The papers in this book comprise the digest of the meeting mentioned on the cover and title page. They reflect the authors' opinions and are published as presented and without change, in the interest of timely dissemination. Their inclusion in this publication does not necessarily constitute endorsement by the editors, the Institute of Electrical and Electronics Engineers, Inc.

IEEE#: 91TH0345-9
Library of Congress #: 90-85245
ISBN: 0-87942-618-7 Softbound
0-87942-619-5 Microfiche

F O R E W O R D

Welcome to the Summer Sopical Meeting on Optical Millimeter-Wave Interactions which is sponsored by the IEEE Lasers and Electro-Optics Society in co-operation with the IEEE Microwave Theory and Techniques Society and the Optical Society of America.

This meeting will focus on the expanding role of lasers and electro-optics in millimeter-wave applications. Laser-based picosecond testing has become the major technique for the characterization of the newest advances in high-frequency semiconducting devices including FETs, HEMTs and HBTs. Recently, these techniques have been extended to the generation of millimeter wave and open up new forms of spectroscopy. At the same time, continuous-wave lasers in conjunction with mixing and high-frequency modulators, have established an important role in the transmission and control of millimeter-wave signals.

The meeting has been organized into six sessions including picosecond testing, electro-optic techniques, millimeter-wave generation, novel structures, and applications. Each session has been structured to include invited papers which will review the state of the art, and contributed papers which will present the newest advances in the field. In all, 11 invited and 19 contributed talks are to be presented. In addition, a panel has been invited to discuss the present status and future directions of this exciting technical area.

The co-chairs would like to thank all those who have contributed to the success of this meeting, including the speakers, the panelists, and the technical program committee. Help provided by the LEOS staff is gratefully acknowledged. This meeting is partially supported by the US Air Force Offices of Scientific Research.

G. Arjavalingam
IBM Thomas J. Watson Research Center

H. Fetterman
University of California, Los Angeles

TECHNICAL COMMITTEE

General Co-Chairmen

Harold Fetterman
University of California

G. Arjavalingam
IBM T.J. Watson Research Center

Program Committee

David Auston
Columbia University
Kul Bhasin
NASA Lewis Research Center
T. Itoh
University of Texas at Austin
Chi-Hsiang Lee
University of Maryland
George Simonis
Harry Diamond Laboratory

TABLE OF CONTENTS

WEDNESDAY, July 24, 1991

THURSDAY, JULY 25, 1991

FRIDAY, JULY 26, 1991

Wednesday

July 24, 1991

WA.1

Picosecond Optics for Millimeter-Wave Device Characterization and Control

Chi H. Lee and M.G. Li
Department of Electrical Engineering
University of Maryland
College Park, MD 20742

Hing-Loi A. Hung
COMSAT Laboratories
Clarksburg, MD 20871

Abstract

Progress in the application of ultrafast optics to microwave and millimeter-wave technology is reviewed. Generation, control and characterization of cw high frequency waves are presented. A time-domain network analyzer which uses optoelectronic techniques for on-wafer monolithic microwave and millimeter-wave integrated circuit (MMIC) measurements is described. An optical microwave intermixing technique has been applied to the picosecond laser pulses. Thus complete coherence between the microwaves and picosecond optical pulses is established. Application of such technique for two-dimensional field mapping of MMIC circuits and waveform displays of microwaves will also be presented.

Summary

In this talk we will review the progress in the application of ultrafast optics to microwave and millimeter-wave technology. A time domain broad band method based on photoconductive sampling has been applied to characterize a monolithic microwave integrated circuit (MMIC). The S-parameters of the MMIC measured by the optical technique are compared directly to those obtained by the standard network analyzer measurements. In order to integrate monolithically the photoconductive sampling gaps and the device under test, the gaps have to be fabricated with a technology compatible with the GaAs MMIC's fabrication technology. For this purpose 0^+ implanted photoconductive switch has been developed. With careful calibrations a good agreement between the optoelectronic and network analyzer measurement results are achieved with up to a 40 db dynamic range for a three stage MMIC amplifier.

An on-wafer optical microwave intermixing technique has been developed in GaAs MMIC's using either the electrooptic effect of the GaAs microstrip line on a picosecond photoconductor as the mixer. Once the wide-band mixer is chosen, the mixing is between the high frequency microwave and the mode-locked laser pulses. The output of the mode-locked laser consists of a train of ultrashort optical pulses equally spaced in time. Thus it can be regarded as an ideal electronic comb generator with the optical carrier frequency stripped-off. The Fourier component of such a pulse train consists of equally spaced spectral lines extending to the frequency corresponding to the reciprocal of the optical pulse width. Thus a mode-locked pulse train consisting of 2 picosecond duration pulses with interpulse spacing of 10 nanoseconds will have spectral components extending from DC

to 500 GHZ spaced by 100 MHZ, the repetition rate of the laser pulses. When such an optical signal is mixed with a high frequency microwave source in an optoelectronic mixer it does not suffer bandwidth degradation caused by electronic circuit parasitic, and thus preserve the bandwidth capability. The mixing condition is

$$f_m = N f_L \pm f_{IF}$$

where f_m is the frequency of the microwave signals, f_L the laser repetition frequency; N an integer; and f_{IF}, the intermediate frequency. The corresponding description in the time domain can be understood as follows: The intermixing of microwave with ultrashort optical pulses in a pulse train is represented by equivalent time sampling where the IF waveform is a replica of the high frequency waveform with the time axis expanded. Thus the phase information of the original RF is carried over to the IF waveform. Actually most of the RF information is imprinted on the IF waveform. Therefore by examing the IF with a spectrum analyzer after the modulated laser pulse train is demodulated one obtains most of the vital information relating to the RF.

Phase locking of the microwave to the laser pulses can be achieved based on optical microwave intermixing. To phase lock the original RF to the laser pulses one simply needs to compare the IF with the reference signal derived from the driver of the laser mode-locker. This driver signal is usually in the same frequency range as the IF. The resultant error signal is then used to control the original RF oscillator (e.g. VCO) through a loop filter. We have successfully used this principle to demonstrate the phase-locking of several VCO's and also measure the temporal waveforms after they are locked by an optical equivalent time sampling technique in a separate sampler (same as the mixer) using exactly the same principle.

In conclusion with the technique described above one can: (1) pull the information of the microwave sources out of the chip by optical mean alone without any high frequency electrical contact, (2) phase lock the free running high frequency oscillator to the ultrashort optical pulses, (3) measure the frequency of oscillation, spectral line shape, power and noise of the signal, (4) display the temperal waveform of the high frequency microwave (to the high gigahertz range) on an ordinary oscilloscope via a low frequency replica, (5) coherently modulate the high frequency microwave for ultrawide-band waveform generation, (6) characterizing nonlinear microwave circuits, and (7) device a true time delay phased array beam forming network by optical control. The potential shown by this new technique is unlimited. This work was supported by the Maryland Industrial Partnership Program.

WA.2 Comparison of the Invasiveness of 1.05 μm Laser Probe on InP-versus GaAs-based HBT's

Ruth Ann Mullen, Peggy F. Lou, and Joseph F. Jensen
Hughes Research Laboratories, Malibu, CA 90265

SUMMARY

While mode-locked solid-state lasers are an excellent, non-invasive probe of high-speed GaAs-based circuits[1], their 1.2 eV photon energy is strongly absorbed in the 0.75 eV band-gap GaInAs material usually used in the fabrication of circuits on InP substrates. Without taking special measurement precautions, the 1.2 eV laser photon energies can affect circuit operation by generating stray photocurrents within the circuit, by modifying the IV characteristics of the circuit's devices, and/or by destroying the circuit via photo-induced resistive heating of individual devices.

An example of the effect of a 1.05 μm laser probe on the common-emitter IV characteristics of an AlInAs/GaInAs HBT on an InP substrate[2] is shown in Figure 1. The collector current (for several values of I_B and for V_{CE} = 1 volt) was found to vary linearly with intensity, as shown in Figure 2. The effect of the proximity of the laser probe (30 mW of power incident on the bottomside of the InP wafer, beam diameter a few microns) to the HBT (10 X 10 μm^2; transverse collector dimension of about 22 μm) was quantified by measuring collector photocurrent (of an unbiased HBT) with a spectrum analyzer tuned to the 250 MHz repetition rate of the mode-locked laser probe. The results, plotted in Figure 3, show that the rf photocurrent drops by nearly four orders of magnitude to about -70 dBm (into 50 Ω) when the laser beam is positioned just outside the collector region. The width of the peak in Figure 3 may be influenced by the following factors: laser spatial noise, optical scattering within the integrated circuit, and waveguiding in the substrate or polyimide. At these rf photocurrent levels, the influence of the laser probe on the IV characteristics of the HBT was not discernible. The results of the same measurements on an AlGaAs/GaAs HBT are included in Figure 3, demonstrating the fact that the YLF laser probe is between three and four orders of magnitude less invasive in the AlGaAs/GaAs device as compared to the AlInAs/GaInAs device. This is likely ascribable to the fact that the photocarriers in the AlInAs/GaInAs device are efficiently generated by band-to-band absorption in the GaInAs layer, while the photocarriers in the AlGaAs/GaAs device are generated at a

much lower rate, probably from mid-gap traps. Potential applications of these results to the design and characterization of integrated photoreceivers will be discussed.

In conclusion, we suggest that the following measurement precautions be taken when using mode-locked solid-state lasers for substrate-probing measurements of circuits based on AlInAs/GaInAs HBT's: (i) avoid positioning the unattenuated laser probe directly on any transistors when the circuit is biased, and (ii) avoid measurements involving optical probing of any GaInAs collector materials.

1. K.J. Weingarten, M.J.W. Rodwell, and D.M. Bloom, IEEE Jour. Quantum Electronics, vol. 24, pp. 198-220, 1988.

2. J.F. Jensen et al., IEEE J. Solid-State Circuits, vol. 26, pp. 415-421, 1991.

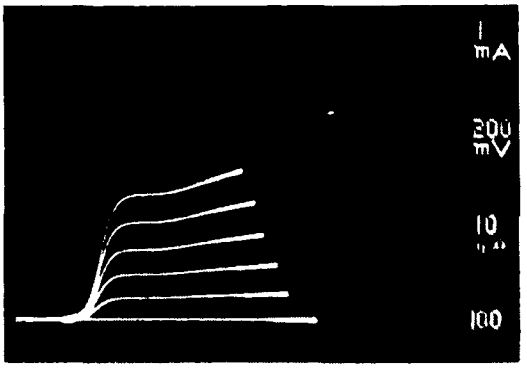

LASER POWER = 0 mW

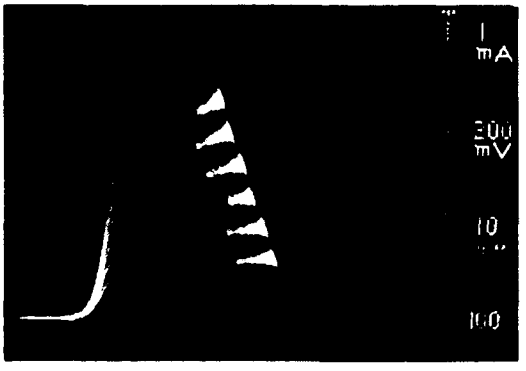

LASER POWER = 0.3 mW

Figure 1. Illuminated and unilluminated HBT common-emitter characteristics

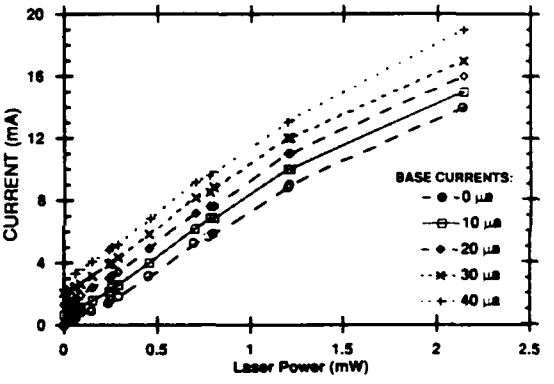

Figure 2. Collector current (for V_{CE} = 1 volt and for several values of I_B) as a function of laser power

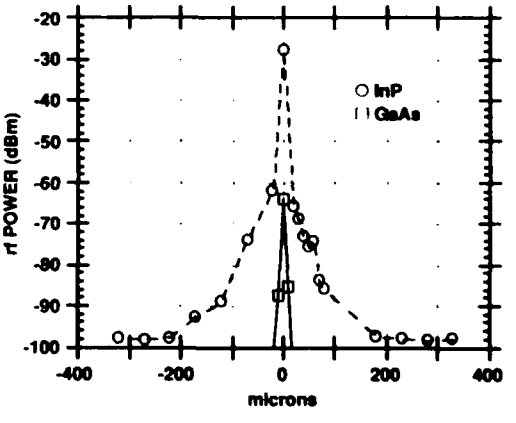

Figure 3. rf power at 250 MHz (into 50 Ω) due to induced collector photocurrent as a function of beam/HBT separation

WA.3 Time Window Limited Dynamic Range of Photoconductive Sampling

Sheng-lung L. Huang†, *Laurence P. Golob*†, *Eve A. Chauchard*†, *Chi H. Lee*†
Thane Smith‡, *Timothy T. Lee*‡ ,*and Thomas R. Joseph*♮
† *Electrical Engineering Dept., University of Maryland, College Park, MD 20742*
‡ *COMSAT Laboratories, Clarksburg, MD 20871*
♮ *TRW Electronic System Group, Redondo Beach, CA 90278*

I. Introduction

Optoelectronic techniques, such as photoconductive (PC) sampling and electrooptic (EO) sampling, are used for the characterization of modern semiconductor devices. This technology is needed to test devices with a frequency bandwidth larger than that of the conventional electronic network analyzers. Additionally, optical sampling permits on-wafer characterization, a feature advantageous to the microwave device manufacturer.

In this work, we measure the S_{21} parameter of a 3 stage 12 GHz MMIC amplifier using the PC sampling technique. The switches are fabricated with a technology compatible with MMIC's fabrication technology,[1] and have shown to be very effective for PC sampling because of their nonlinear response to the bias voltage.[1] One important issue which has been overlooked is the limitation of the dynamic range of optoelectronic sampling technique. In this work, we achieve a good agreement with network analyzer measurements up to 40 db dynamic range and use a simple model to explain the dynamic range limitation.

II. Experiment

Using the standard photoconductive sampling technique,[1] we could obtain an output waveform with a 1 ns time window. In order to study the effects of time windowing, we lengthened the delay line and extended the temporal range by combining several data sets together resulting in an output time window of 2 ns. The S parameter is then obtained from the ratio of the Fourier transform of output waveform and that of input waveform.[2]

III. Results

The measured S_{21} parameter with different output time windows is shown in Fig. 1. A good agreement with network analyzer measurement is obtained up to 40 db dynamic range in the case of the 2 ns time window. Two distinct features of the PC sampling measurements are evident. First, the separation of the peaks of the ripples is approximately equal to the inverse of the length of the time window. Second, the matching dynamic range increases as the time window increases. These observations can be explained by the following simple model. Let's consider a sine wave with period t_0 measured by PC sampling with a time window of T. The measured waveform and the magnitude of its Fourier transform can be expressed as follows :

$$A(t) = \begin{cases} sin\frac{2\pi t}{t_0} & ; -\frac{T}{2} < t < \frac{T}{2} \\ 0 & ; eleswhere. \end{cases} \qquad |A(f)| = \left| \frac{sin(\pi f T)}{\pi} \frac{t_o}{1 - f^2 {t_o}^2} \right|$$

First, it is clear from Fig. 2 that time windowing generates ripples which limits the dynamic range. Second, the distance between two minima is $\frac{1}{T}$ and independent of t_0. A computer simulation, using a 7 GHz bandwidth waveform with a center frequency of 12 GHz and 2 ns time window, shows that the dynamic range at 6 GHz is 38 db which is in excellent agreement with our experimental data. A more detailed study showed that the next most imporant limitation on the experimental dynamic range comes from the windowing of the input temporary waveform.

IV. Conclusion

A simple model has been used to explain the limitation on dynamic range of S parameter measurements. This model and the experimental data show that the limitation is primarily on the length of time windows, not the noise created by laser fluctuations. We also demonstrate the S parameter measurement by PC sampling with all the switches fabricated by a technology compatible with MMIC fabrication technique. This work was supported by the DARPA MIMIC phase III program, monitored by the U.S. Army Labcom.

References

(1) S. L. Huang, E. A. Chauchard, C. H. Lee, T. Smith, T. T. Lee, and T. R. Joseph, "Picosecond Electronics and Optoelectronics" meeting, OSA/IEEE, March 1991.

(2) H-L. A. Hung, P. polak-dingels, K. J. Webb, T. Smith. H. C. Huang, and C. H. Lee, "Millimeter-wave Monolithic Integrated Circuit Characterization by a Picosecond Optoelectronic Technique," IEEE MTT-37, p. 1223-1231, 1989.

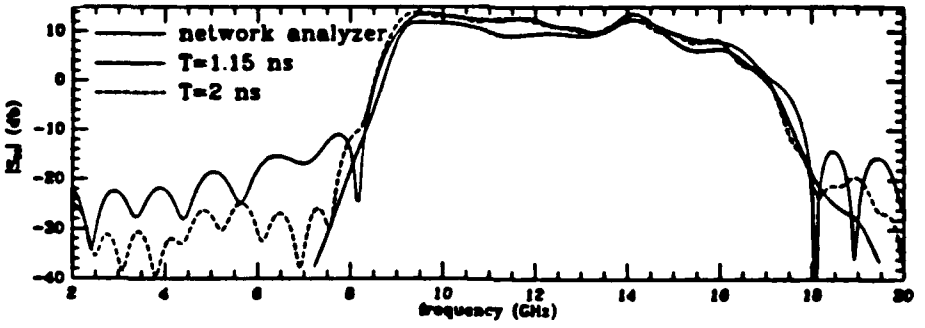

Fig. 1 The magnitude of S_{21}

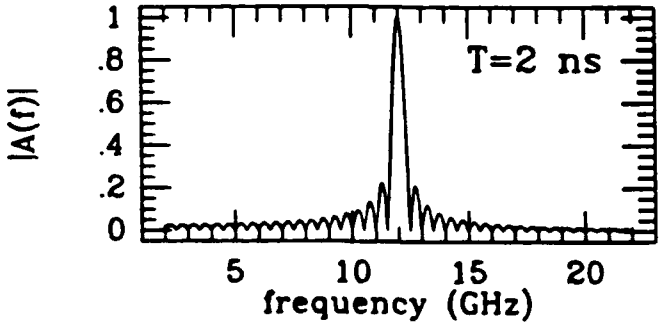

Fig. 2 The magnitude of A(f)

WA.4 Effect of Line Resistance on Picosecond Optoelectronic Probes and Device Characterization

M. Scheuermann
IBM Research Division, T. J. Watson Research Center
PO Box 218, Yorktown Heights, NY 10598

The dc resistance of the transmission lines on high bandwidth probes, and in particular on optoelectronic probes,[1] can have a large effect on the measured response of a device. This resistance manifests itself as a resistive tail having an amplitude which scales with the width of the intrinsic device response. Many mechanisms which generate tails on picosecond pulses have been observed and are well understood. These include intrinsic effects such as dispersion and slow wave propagation as well as extrinsic effects such as carrier lifetime and thermal effects in the pulse sources. The dispersive effect of the dc resistance on pulse propagation which has been reported for communication lines[2] and normal superconductor lines,[3] also plays an important role in the design of optoelectronic probes for device characterization. In general, it is desirable to keep the dc line resistance as low as possible. However, this is difficult to do in cases where the probe is integrated on the same chip as the device or the probe is fabricated using thin films. Therefore it is useful to develop criteria to determine what resistance can be tolerated and how the resistance impacts device characterization. Simulations illustrating the significance of the dc resistance on device characterization and measured examples will be presented.

A simple model using an ideal current source driving a balanced coplanar transmission line having a dc resistance illustrates the effect. The transmission line used in this model is defined by an impedance $Z_0 = 120\ \Omega$ and a dc resistance $r_{dc} = 270\ \Omega/cm$. The current source drives the line with gaussian current pulses of various widths. Figure 1a shows the normalized response on the transmission line at the generation point for several different pulse widths. For the shorter pulse widths, the resistive tail is visible but has a low amplitude. However, as the pulse width increases, the amplitude of the tail increased dramatically. To first order the amplitude of the tail[4] is $\simeq R_s/(Z_0 + R_s)$ where R_s is an effective series resistance related to the resistance of the line segment the current pulse overlays during its generation. Thus $R_s \simeq r_{dc}\lambda_p$ where λ_p is the spatial extent of the pulse. The amplitude of the tail is small when $r_{dc}\lambda_p < Z_0$. Note this

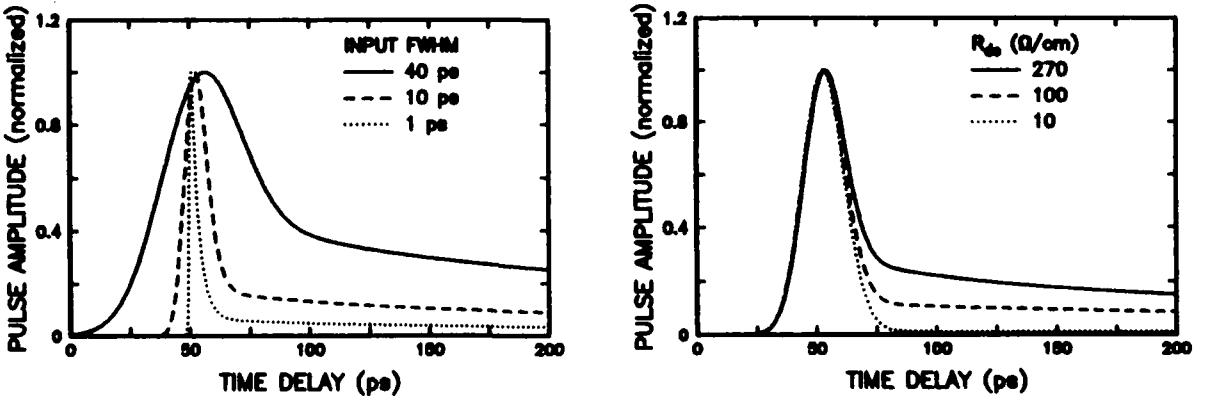

Figure 1. Simulation of pulse on transmission with dc resistance: a) line response with gaussian inputs having a FWHM of 1 ps, 10 ps, and 40 ps. b) line response with dc resistances of 270 Ω/cm, 100 Ω/cm and 10 Ω/cm.

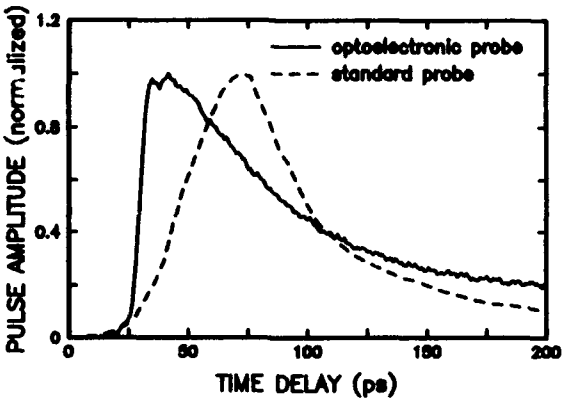

Figure 2. Response of photodetector using: a) optoelectronic probe with lossy lines (solid line). b) conventional high-speed low resistance probe (dashed line).

condition can be met if λ_p is short enough. A similar tail is observed when the ideal current source is replaced by a photoconducting switch (variable conductance in parallel with a capacitance) in the simulation. It is clear from the above analysis that a probe with lossy lines may appear to have a high bandwidth when characterizing devices with a response of several picoseconds, however the same probe will have a low bandwidth when probing slower devices. Figure 1b shows the effect that varying the dc resistance has on the amplitude of the tail.

An example showing the difference between a lossy probe and non-lossy probe is shown in Fig. 2. Here the response of a photodetector under identical bias and illumination are compared. Curve (a) shows the response as measured with an optoelectronic probe having lossy lines. The optoelectronic probe can detect pulses having a FWHM as short as 2 ps, so is appears to have a high bandwidth. The rising edge of the response shown is under 10 ps, however the trailing edge has a significant tail[5] with a long time constant due to the dc resistance of the probe. To verify that the tail is not due to the intrinsic response of the device, a second measurement was preformed (curve (b)) with a fast conventional probe having a lower dc resistance and narrower bandwidth. Although the rising edge of the pulse is much slower the long tail is no longer present.

The author would like to acknowledge helpful discussions with J.-M. Halbout, R. Matick, C.-C. Chi and W. Gallagher.

References

1. M. Scheuermann, R. Sprik, J.-M. Halbout, P.A. Moskowitz, and M.B. Ketchen, in **OSA Proceedings on Picosecond Electronics and Optoelectronics**, Vol. 4, p. 22, OSA Proceedings Series, 1989.
2. O. Heaviside, Electrician **19**, 295 (1887), reprinted in **Electrical Papers**, (Chelsea, New York, 1970), Vol.2, pp. 137-141.
3. W.J. Gallagher, C.-C. Chi, J.N. Duling III, D. Grischkowsky, N.J. Halas, M.B. Ketchen and A.W. Kleinsasser, Appl. Phys. Lett. **50**, 350 (1987).
4. R. Matick, **Transmission Lines for Digital and Communication Networks** (U. Michigan Microfilm International, Ann Arbor, 1969), pp.153-210.
5. M. Lambsdorff, M. Klingenstein, J. Kuhl, C. Moglestue, J. Rosenzweig, A. Axmann, Jo. Schneider, A. Hulsmann, H. Leier and A. Forchel, Appl. Phys. Lett. **58**, 1410 (1991).

WA.5 Picosecond Testing and Evaluation of Three Terminal Devices

H.R. FETTERMAN, M. MATLOUBIAN*, D.V. PLANT,
M. MARTIN AND F. OSHITA
Department of Electrical Engineering
University of California, Los Angeles
Los Angeles, California 90024

We report the use of picosecond measurement techniques to characterize three terminal devices to frequencies above 100 GHz. Our measurements determine the S parameters of the device under test directly with no adjustable parameters. In developing this approach we have used electrical techniques to validate our measurements whenever possible. Now with HEMTs and MMIC circuits showing capabilities well above all electric network analyzers this technique becomes extremely important.

The basic approach that we use incorporates Auston switches to both inject and sample the device performance in both reflection and transmission. The structure we currently use is based upon microstrip on silicon on sapphire. Ion implantation was used to creat sufficient damage to generate 2 picosecond pulses. Newer switches using coplanar lines and low temperature GaAs materials are now being fabricated for the next generation of measurements.

The measurements that will be presented will range from the S parameters of InGaAs/AlInAs HEMTs shown in figure 1 to the measurements of MMIC circuits shown in figure 2. In both cases the fundamental limitation was the bonding of the device to the test circuit using wirebonds. Direct injection of the optical pulse into the device can help characterize these parasitic effects. This is shown for the case of a high frequency HEMT in figure 3.

Finally the same concepts for directly generating millimeter waves using pulsed excitation will of course work for these three terminal devices. In fact, since the impedance is driven lower than the two terminal switches, it is possible to generate more power. Output using an integrated antenna system is shown in figure 4. The combination of picoseconds and three terminal devices has opened an entirely new area of testing and evaluation.

* M.Matloubian is now with the Hughes aircraft company
Research Laboratories, Malibu, Ca 90265

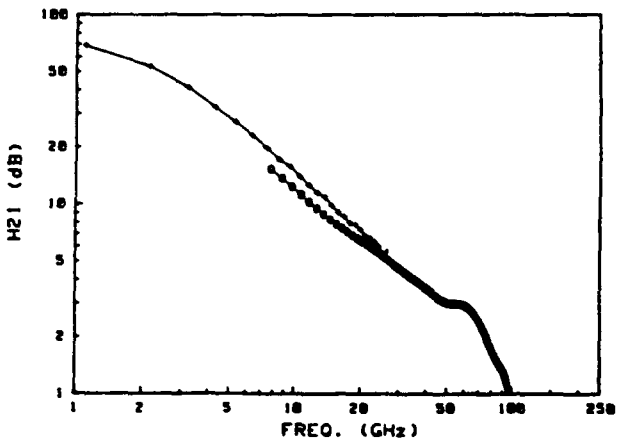

Figure 1. Current gain vs. frequency
for AlInAs/GaInAs HEMT
o = optoelectronic system
+ = network analyzer

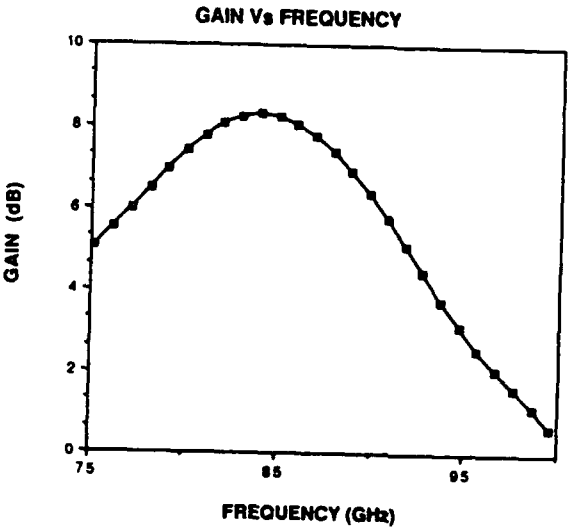

Figure 2. Gain from monolithic InGaAs
HEMT single stage LNA

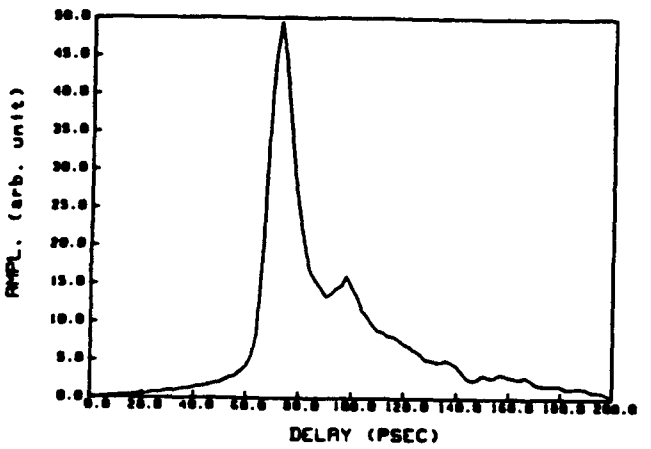

Figure 3. Optical reponse of AlGaAs/GaAs HEMT

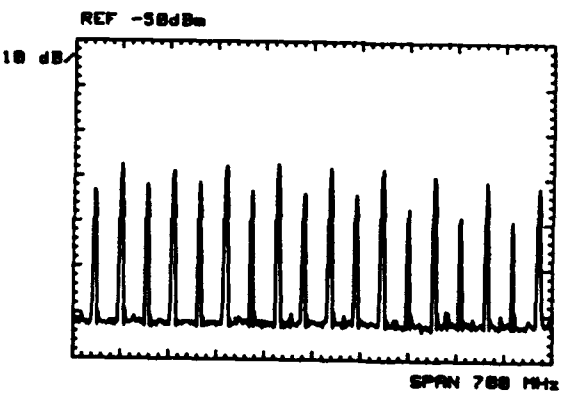

Figure 4. 60 GHz. output from picosecond
excitation of HEMT displayed on
Spectrum Analyzer

WB.1 Progress in High Speed Modulators

S.Y. Wang, *Hewlett-Packard Laboratories, Palo Alto, CA*

Lithium niobate travelling wave modulators have made great strides in increasing their modulation bandwidth from under 10 GHz to 30-40 GHz. III-V modulators have also demonstrated 30-40 GHz bandwidth for both the electro-optic and electro-absorption structures. III-V modulators can potentially attain bandwidth approaching 60 GHz with $V\pi$ under 10 V and monolithic integration with laser diodes to reduce the switching voltage to 1 V. A review of the recent developments in high speed modulators in the various material systems will be given and their potential for higher speed will be discussed.

WB.2 Efficient Optical Phase Modulation Using a Semiconductor Optical Amplifier

U. Gliese, T.N. Nielsen, B. Mikkelsen and K.E. Stubkjaer

Center for Broadband Telecommunications
Electromagnetics Institute, Technical University of Denmark
Building 348, DK-2800 Lyngby, Denmark

Advanced modulation formats such as PSK and QPSK are of high interest in optical microwave links. To obtain these modulation formats, it is necessary to use external modulators. Unfortunately, most of the external modulators available have the drawbacks of insertion loss and high power consumption. This is a problem especially in spaceborne systems, e.g. optical beam forming networks [1]. Recently, various experiments have demonstrated the feasibility of using optical amplifiers as phase modulators in optical communication systems [2]-[4]. These phase modulators provide the advantages of gain and low modulation power requirements.

Measured values of the modulation power necessary to obtain the PSK phase shift of π is depicted in Fig. 1 and the necessary power for obtaining the QPSK phase shift of $\frac{3\pi}{2}$ is easily found by adding 3.5 dB to these values. The 3 dB bandwidth is given at the point where the required modulation power has increased by 3 dB and is found to be 600 MHz. This bandwidth is determined by the carrier lifetime and can be increased by using higher bias currents although current heating would prevent a bandwidth greater than 1 GHz. It should be noticed, however, that the modulator presented here has sufficient bandwidth since the bit rates under consideration for microwave transmission links are normally lower than 500 Mbit/s. It is expected that the bandwidth of 600 MHz will allow for PSK modulation speeds of up to approximately 900 Mbit/s and QPSK modulation speeds of approximately twice this bit rate. Non-linearities may, however, limit the QPSK modulation speed to 900-1500 Mbit/s. The required modulation power was found to be as low as 5 dBm which corresponds to a V_π of 1,1 V. This is comparable to or better than what can be expected for Lithium Niobate modulators with the same bandwidth. Finally, it should be noted that the measurements were performed for an optical input power of -7 dBm, a bias current of 70 mA and a fibre to fibre gain of 10 dB, resulting in an optical output power of 3 dBm.

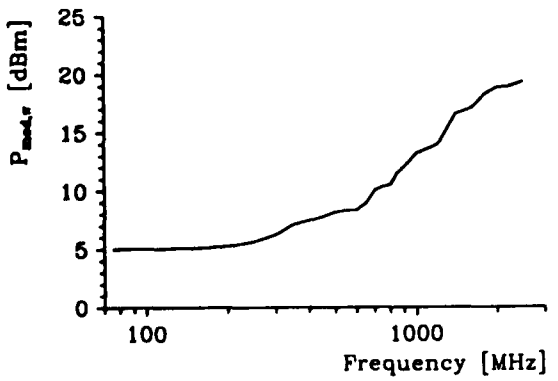

Figure 1: Required modulation power to obtain a phase shift of π radians.

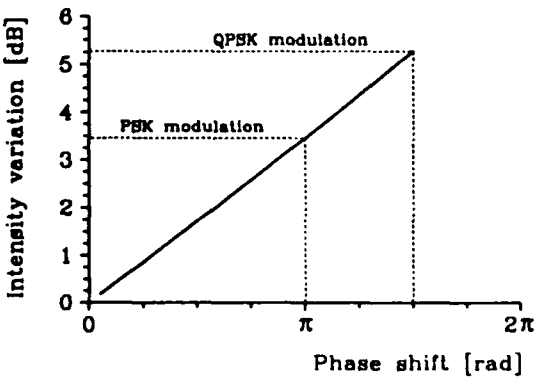

Figure 2: Intensity variation due to amplitude modulation versus the required phase shift.

The major drawback of using the optical amplifier as a phase modulator is the inevitable amplitude modulation induced by the amplifier. As seen in Fig. 2, the intensity variation introduced by the amplitude modulation is rather large and for QPSK modulation variations of up to 5 dB can be expected. This is not tolerable in practical systems.

A novel method for reducing the amplitude modulation is the use of a two-electrode amplifier as illustrated in Fig. 3. It is possible to reduce the amplitude modulation by modulating the two electrodes in anti-phase. The modulation powers are adjusted so that the two sections will introduce the same amount of amplitude modulation. This will result in a cancellation of the amplitude modulation since the modulation is π radians out of phase in the two sections. In order to avoid an associated reduction of the phase modulation, the phase response per mA of modulation current has to be different in the two sections. The ratio between the phase and amplitude modulation is governed by the so called linewidth enhancement factor α [5] which for a fixed wavelength increases with the electron concentration [5]. To obtain a good overall phase response, the electron concentration in the two sections of the amplifier must therefore be different. This is easily achieved by saturating the amplifier with a high power optical input signal (above -10 dBm) and by lowering the bias current in the output section.

A multi-section numerical model has been used to calculate the intensity variation due to amplitude modulation in the two-electrode amplifier. The predicted intensity variation is shown in Fig. 4 as a function of the anti-phase modulation index, i.e. the ratio of the modulation current in the input section and the modulation current in the output section. It is seen that the intensity variation can be reduced from 3.5 dB to 0.8 dB (77 % reduction) for the PSK modulation format.

The results show that the optical amplifier may be an attractive solution for phase modulation even in spaceborne systems. Furthermore, the semiconductor optical amplifiers have the great advantage of potential optoelectronic integration in future systems.

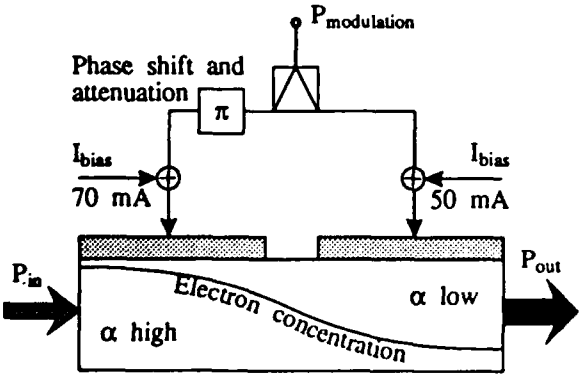

Figure 3: Two-electrode amplifier with anti-phase modulation concept.

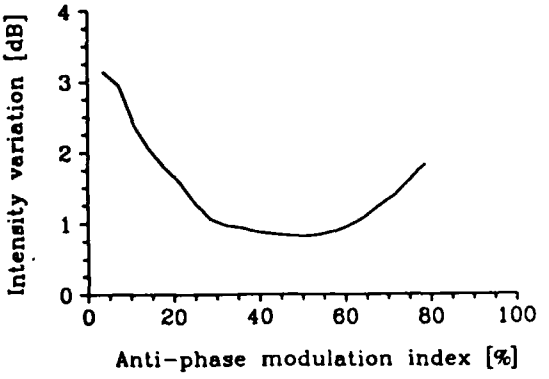

Figure 4: Intensity variation versus anti-phase modulation index for a phase shift of π radians.

References

[1] U. Gliese et al.: In Proceedings of CLEO, 1991, paper CWM5.

[2] J. Mellis et al.: Electronics Letters, vol. 25, no. 10, pp. 679-682, 1989.

[3] G. Großkopf et al.: In Proceedings of IOOC, 1989, paper 21B4-2.

[4] D. Hui Bon Hoa et al.: Journal of Ligthwave Technology, vol. 9, no. 2, pp. 266-270, 1991.

[5] N. Storkfelt et al.: Submitted for publication in Photonics Technology Letters, 1991.

WB.3 Antenna-Coupled Millimeter-Wave $LiNbO_3$ Electro-Optic Modulator*

William B. Bridges and Finbar T. Sheehy
California Institute of Technology

and

James H. Schaffner
Hughes Research Laboratories

The phase-velocity mismatch due to material dispersion in traveling-wave $LiNbO_3$ optical waveguide modulators may be greatly reduced by breaking the modulation transmission line into short segments and connecting each segment to its own surface antenna. The array of antennas is then illuminated by the modulation signal at an angle which produces a delay from antenna to antenna to match the optical waveguide's delay.

A phase modulator, 25 mm long with 5 dipole antenna/transmission-line elements, was operated from 4.3 to 13 GHz with a maximum phase modulation sensitivity of about 100 degrees/$\sqrt{\text{Watt}}$ (Figure 1). The optical wavelength was 633 nm. The expected variation of response with illumination angle was confirmed. A simple theory of antenna and transmission-line modulator behavior has been developed and matches the measured frequency response. This work was reported previously[1,2].

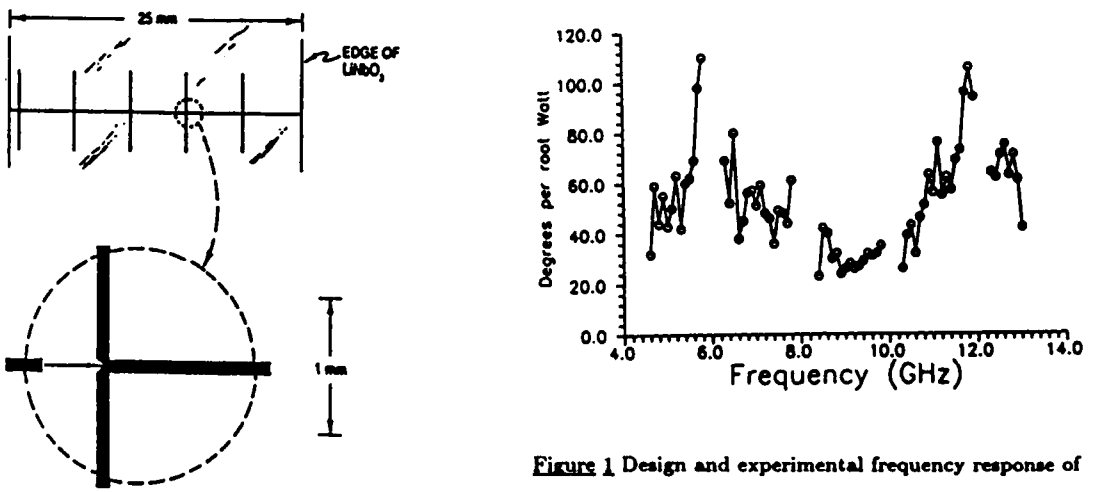

Figure 1 Design and experimental frequency response of the X-band prototype antenna-coupled modulator.

---

* This work was supported by a grant from the Caltech President's Fund and a grant from Rome Air Development Center.

A second phase modulator, 18 mm long with 20 antenna/transmission-line elements was operated at V-band and had a maximum phase modulation sensitivity of approximately 80 degrees/$\sqrt{\text{Watt}}$. This showed that the modulator design can be scaled for mm-wave operation quite successfully (Figure 2). This second modulator was designed simply by scaling the antenna/transmission-line elements of the X-band modulator by a factor of six. Of course, many more elements were needed to cover the interaction length.

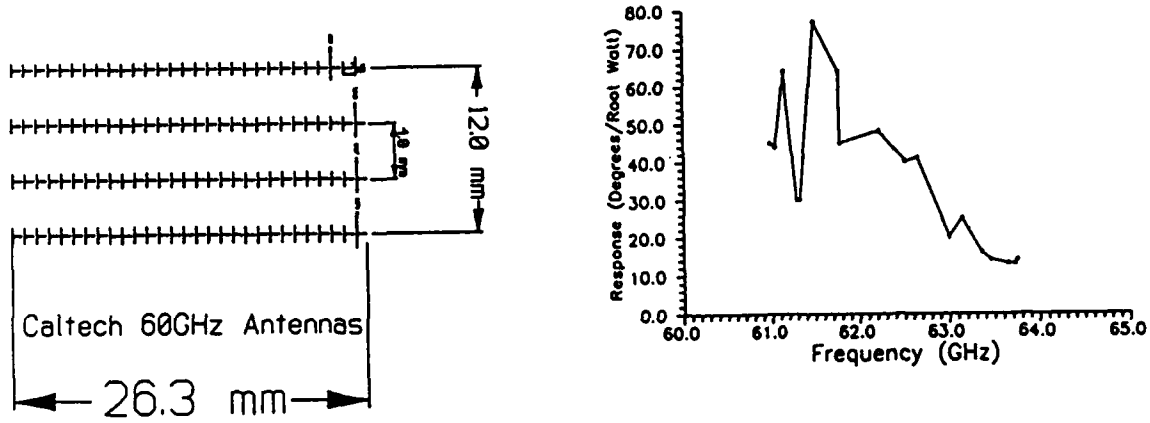

Figure 2 **Mask design and experimental results of the *V-band prototype phase modulator.***

A third modulator, using broad-band bow-tie antennas and designed for W-band operation, is being fabricated at the time of writing. This modulator is to be operated as a Mach-Zehnder amplitude modulator. A Mach-Zehnder modulator requires use of dc bias to set the unmodulated phase-difference between the optical paths to $\pi/2$. This cannot be done with dipole antennas, but bow-tie antennas are insensitive to dc connections made to the ends of the antennas. Results obtained with this modulator will be presented.

References

[1] William B. Bridges, Finbar T. Sheehy and James H. Schaffner, "Wave-Coupled $LiNbO_3$ Electro-Optic Modulator for Microwave and Millimeter-Wave Modulation,": to be published in Photonics Technology Letters, Feb. 1991

[2] –, "Velocity-Matched Electro-Optic Modulator," SPIE Vol. 1371 High Frequency Analog Fiber Optic Systems (1990) pp. 68-77, San Jose, California, September 1990

WB.4 Electro-Optic Mixers

Brian H. Kolner
Electrical Engineering Department
University of California, Los Angeles
Los Angeles, CA 90024-1594

The classic electro-optic amplitude modulator uses the Pockels effect to convert a voltage-controlled linear change in the optical index of refraction to a periodic change in the output light intensity.[1] Although used predominantly for linear optical communications, in conjunction with a photodetector, they can also be used to multiply or mix electrical signals. There are two fundamental mechanisms inherent to electro-optic modulators that make them suitable as mixers. The first is that amplitude modulation is a multiplicative process. That is, the output optical power is proportional to the input power times some function f(v) of the driving voltage. Thus, $I_{out}=I_{in}f(v(t))$. If the output of one modulator is fed into the input of a second modulator (Fig. 1), then the final output contains the product of the two modulation functions: $I_{out}=I_{in}f(v_1(t))f(v_2(t))$. Clearly, if f(v) contains a linear term, the direct product $v_1(t)\,v_2(t)$ will be available. In the case of Pockels effect electro-optic modulators, f(v) is periodic and, depending on the static bias point, all orders $v^n(t)$ are available. Therefore, a pair of modulators can act as a mixer for the input signals $v_1(t)$ and $v_2(t)$.

The second mechanism that can produce mixing is the nonlinear nature of the function f(v) and occurs in a single modulator. When two signals are present at the modulator input, the output is proportonal to $f(v_1+v_2)$. Any nonlinearity in f(v) will then provide for multiplication between $v_1(t)$ and $v_2(t)$. In general, higher order terms $v_1^n(t)$ and $v_2^m(t)$ will also be present.

Electro-optic mixers possess certain advantages (and some disadvantages) that make them attractive for special applications where, for example, negligible local oscillator (LO) reradiation or high RF input damage thresholds are important. Also, because of their continuing evolution for applications in fiber optic communications systems, integrated optical modulators have achieved very low switching voltages (<5v) and very high bandwidths (>40GHz).

It is interesting to evaluate the performance of electro-optic mixers in conventional terms such as noise figure, conversion loss (gain), 1 dB compression point, third order intercept, and so on.[2] All of these characteristics can be calculated directly from knowledge of the transfer function f(v) and surrounding circuit parameters. In general, due to the sinusoidal nature of f(v), the mixing products for two input voltages produce a detected photocurrent of the form

$$i(t) \propto \cos\Gamma_o\, J_n\left(\frac{\pi v_1}{V_\pi}\right) J_m\left(\frac{\pi v_2}{V_\pi}\right) \cos(n\omega_1 \pm m\omega_2)t$$

where Γ_o is the static bias point, J_n and J_m are Bessel functions of the first kind and ω_1 and ω_2 are the angular frequencies of the two input voltage signals $v_1\cos(\omega_1 t)$ and $v_2\cos(\omega_2 t)$. V_π is the half-wave switching voltage. The third-order intercept and -1 dB compression voltages for a single modulator are readily calculated to be

$$v_{toi} = 2\sqrt{2}\,\frac{V_\pi}{\pi} \qquad v_{-1dB} = \frac{V_\pi}{\pi}$$

the latter of which sets a realistic upper limit on input signal amplitude (see Fig. 2).

The spurious free dynamic range is bounded at the lower end by the minimum detectable voltage and at the upper end by the emergence of the first odd-order distortion products from the noise floor and is given by

$$SFDR = \left[\frac{2i_{avg}}{qB}\right]^{1/3}$$

For an average detected photocurrent of 1 mA and $V_\pi = 7$ volts, we calculate the following:

$$v_{toi} = 6.3\text{volts} \quad v_{-1dB} = 2.2\text{volts} \quad \text{SFDR} = 107\ \text{dB Hz}$$

Experimentally, the third order intercept and -1 dB compression points were confirmed on a modulator with 25 Ω electrodes.[3] The corresponding input powers were +30 dBm and +21.4 dBm, respectively. These values are comparable with conventional diode mixers, but in other respects, electro-optic mixers do not compare well. For example, since there is a tradeoff between bandwidth and output voltage in the detector circuit, the conversion loss can be greater than 25 dB for a broadband network. On the other hand, if the photodetector circuit was limited to very low frequency operation, conversion gain is possible. Note that this limitation does not restrict the input bandwidth to the electro-optic modulator, which could still provide mixing over many tens of GHz.

Finally, since it is not possible for a modulation signal to propagate backwards on an optical beam, the tandem modulator mixer arrangement provides infinite port-to-port isolation in the reverse direction and thus reradiation of the local oscillator will not occur.

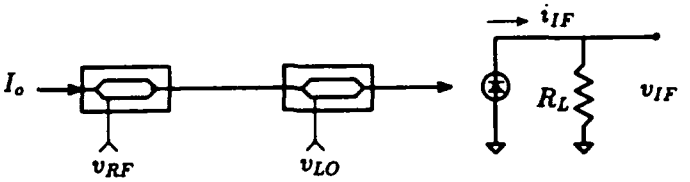

Fig. 1. Electro-optic mixer comprised of two electro-optic mixers in series. IF output is derived from the detected photocurrent. A single modulator will also produce mixing due to the nonlinear modulator transfer function.

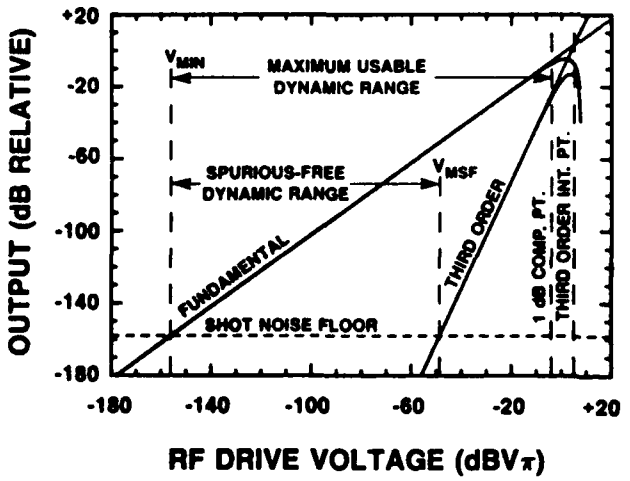

Fig. 2. Input-output relationship for an electro-optic mixer showing fundamental and third order distortion products. Dynamic range is defined in terms of the minimum detectable voltage V_{min} and the appearance of the third order term or the 1 dB compression point. Third order intercept point is also shown.

References

1. I.P. Kaminow, *An Introduction to Electro-optic Devices*, Academic Press, New York, NY, 1974.
2. Mixer Application Information, *RF Signal Processing Components*, (Watkins-Johnson Co., Palo Alto, CA, 1985).
3. B.H. Kolner and D.W. Dolfi, "Intermodulation Distortion and Compression in an Integrated Electro-optic Modulator," *Applied Optics*, vol. 26, 3676 (1987).

WB.5 External Electro-Optic Sampling for High-Frequency Electrical Network Analysis

John F. Whitaker, Michael Y. Frankel,
Janis A. Valdmanis, and Gerard A. Mourou

University of Michigan
Department of Electrical Engineering and Computer Science
Ultrafast Science Laboratory
2200 Bonisteel Blvd., Rm. 1006
Ann Arbor, Michigan 48109-2099

Optically-based sampling techniques have gained regard for their ability to provide unprecedented resolution in the measurement of temporal characteristics of electronic signals. External electro-optic sampling possesses a sub-0.5-ps temporal resolution,[1] which translates into a measurement capability in the frequency domain that extends in bandwidth past one terahertz. This technique has been applied to the investigation of transmission-line,[2] semiconductor-device,[3] and integrated-circuit behavior.[4] When utilized with a suitable test fixture, an electro-optic crystal may be employed in a sampling system that effectively becomes an extremely high-frequency network analysis instrument.[3]

In an example of the use of such an external electro-optic instrument, time-domain waveforms at the gate and drain of a 0.15-mm-gate-length pseudomorphic heterojunction FET[5] have been measured (Fig. 1a) and the two-port small-signal *S*-parameters of the device extracted from the transient input, reflected, and transmitted signals.[3] Figure 1b displays the forward transmission coefficient of the device, experimentally determined without extrapolation up to a frequency of 100 GHz. A fully characterized, high-bandwidth coplanar-stripline test fixture was employed in order to propagate signals at such a high frequency. The ultrashort electrical input transient was generated using a dc-biased photoconductive switch, and the various signals were measured using a 20-μm-thick lithium tantalate electro-optic crystal which required no electrical contact to the circuit.

This and other optically-based measurement techniques have demonstrated that modern ultrafast electronic devices may be accurately characterized without extrapolation up to frequencies that cannot be easily reached through other means.

The HEMT device reported here was characterized via rf network analysis and then provided to us by P.M. Smith of the Electronics Laboratory at General Electric in Syracuse, NY. This work was supported by the Air Force Office of Scientific Research, University Research Initiative under contract number AFOSR-90-0214, by NASA under contract number NCC3-130, and by Siemens, Munich.

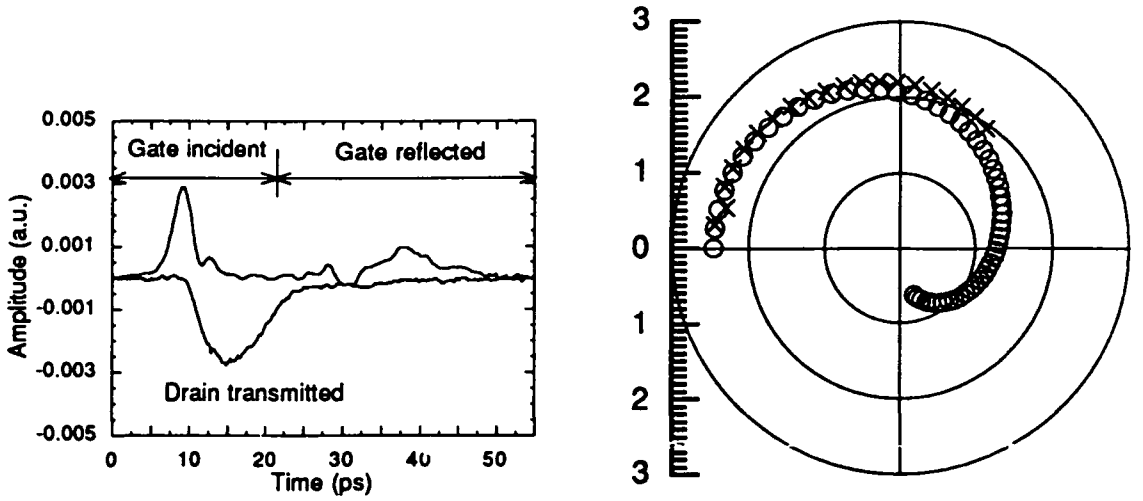

(a) (b)

Fig. 1 (a) *Electrical transients input to and reflected from the gate and output from the drain of a HEMT device, as measured on a coplanar-stripline test fixture via external electro-optic sampling. These are the waveforms necessary to determine both forward S-parameters of the device. Similar waveforms have been measured in order to acquire the reverse characteristics.* (b) *A polar plot of the* S_{21} *transmission coefficient for the HEMT, extracted from electro-optic data to 100 GHz* (O) *and conventional rf network analysis to 40 GHz* (X). *Without extrapolation, one can observe from the electro-optic network analysis the point where the transmission coefficient crosses the unity circle and becomes less than one.*

---

[1]Valdmanis, J.A. and G. Mourou, "Subpicosecond electro-optic sampling: principles and applications," *IEEE J. Quantum Electron.*, vol. 22, pp. 69-78 (Jan. 1986).

[2]S. Gupta, J.F. Whitaker, and G.A. Mourou, "Subpicosecond pulse propagation on coplanar waveguides: experiment and simulation," to appear in *IEEE Microwave and Guided Wave Lett.* vol. 1, no. 7 (July 1991).

[3]M.Y. Frankel, J.F. Whitaker, G.A. Mourou, J.A. Valdmanis, and P.M. Smith, "100-GHz Electro-optic *S*-parameter characterization of high electron mobility transistors," accepted for *Picosecond Optics and Electronics VI*, Berlin: Springer-Verlag, 1991.

[4]Valdmanis, J.A. and S.S. Pei, "A non-contact electro-optic prober for high speed integrated circuits," *Picosecond Electronics and Optoelectronics II*, Mourou, Leonberger, F.J., C.H. Lee, F. Capasso, and H. Morkoc (eds.), Berlin: Springer-Verlag, 1987, pp. 4-10.

[5]P.M. Smith, L.F. Lester, P.-C. Chao, P. Ho, R.P. Smith, J.M. Ballingall, and M.-Y Kao, "A 0.25-μm gate-length pseudomorphic HFET with 32-mW output power at 94 GHz," *IEEE Electron Dev. Letters*, vol. 10, pp. 437-439 (Oct. 1989).

Thursday

July 25, 1991

ThA.1 Tunable High Frequency Radiation Source Utilizing a Relativistically Propagating Ionization Front

C. Joshi, R. L. Savage Jr., and W. B. Mori
Electrical Engineering Department
University of California at Los Angeles

We have experimentally demonstrated a new type of tunable, high power radiation source capably of producing very short pulses in the millimeter wave range. This technique utilizes a laser-produced ionization front which passes through a pulse of microwave radiation and in doing so causes the frequency of the radiation to upshift dramatically. By controlling the density of the plasma in the ionization front, we can continuously vary the degree of upshift. Using this technique, source radiation at 35 GHz has been upshifted to more than 116 GHz.

The source radiation is provided by a pulsed magnetron that gives 300 nsec long, 10 kW peak power pulses at 35 GHz. This radiation is fed via rectangular waveguide through the side wall of a cylindrical cooper cylinder that is closed by quartz windows at each end. The TE_{01} mode is excited and resonates in the cavity which is evacuated and filled with azulene vapor, which is chosen because it is easily ionized by ultraviolet radiation. A short (50 psec), intense (40mJ) ultraviolet (266 nm) laser pulse is introduced through one of the quartz windows and propagates down the axis of the cavity. As the laser ionizes the azulene vapor, a sharp boundary is formed between the neutral gas and the newly created plasma. It is this boundary, which propagates at the group velocity of the laser radiation in the plasma-filled guide, that we refer to as an ionization front.

As the front propagates down the cavity, it encounters both the co-propagating and the counter-propagating radiation that make up the standing wave of source radiation in the cavity. Theory predicts that the frequencies of these two waves will be upshifted by different amounts, but that in both cases the degree of upshift will be proportional to the plasma density in the front. This density is varied by adjusting the neutral azulene pressure in the cavity.

The upshifted radiation is detected by a series of diode detectors preceeded by sections of rectangular waveguides in various sizes that form a set of high-pass filters.

A 1 GHz bandwidth oscilloscope is used to display the upshifted radiation which appears in a single sub-nsec pulse. The detectors are rotated in the plane of the laser table about the output of the cavity in order to measure the antenna pattern of the radiation. This information is then used to estimate the amount of power in the upshifted pulses.

This experiment has shown that the frequency of source radiation can be upshifted in a continuously tunable fashion to greater than a factor of three times the source frequency. With slight modifications, this technique should be capable of producing short, high power pulses of radiation well into the terahertz frequency regime.

This work was supported by DOE grant no. DE-FG03-91-ER12114 and DOE contract no. DE-AS03-83-ER40120.

ThA.2

Laser-Induced Microwave Index Gratings in Thin-Film Superconductors

By

N. Glass and D. Rogovin
Rockwell Science Center
Thousand Oaks, CA

Optical index gratings are radiation-induced periodic spatial variations in an active medium's dielectric constant. These structures are responsible for numerous active optical processes and are of central interest to nonlinear optics. Here, we extend this concept to superconducting thin films and discuss some of the consequences this has on the millimeter electrodynamics of thin-film superconductors.

Theory asserts that an optical index grating can be induced in a thin film superconductor by irradiating it with two degenerate, noncollinear laser beams. These beams form an optical interference pattern which splits pairs and generates quasiparticle (qp) population gratings. These qp gratings establish conductivity gratings within the thin-film superconductor, that are active for frequencies below the pair-splitting frequency. Since the conductivity has both real and imaginary parts, both phase and amplitude gratings are established in the superconducting thin film. The existence of these optical index gratings modifies the superconductor's millimeter characteristics, which can be verified by measuring the angle-resolved transmittance and reflectance of millimeter waves. In particular, theory asserts that well-defined off-specular peaks, corresponding to grating diffraction orders, appear.

ThA.3: Enhancement and Stabilization of a Self-Pulsating Laser Diode for Microwave Oscillator Application

Yaron Simler, John Gamelin and Shyh Wang

University Of California at Berkeley
Department of Electrical Engineering and Computer Science
Cory Hall
Berkeley, California 94720.
Tel: (415)643-9862, FAX: (415)643-8426

Self-pulsating lasers are commercially used in compact-disc players and have also been considered for use in optical storage and in multi-mode fiber computer data links[1]. In this paper we explore another important potential application for this mass produced, low-cost laser: a widely tunable stable microwave oscillator. Using a simple optoelectronic feedback loop, timing jitter and phase noise of a self-pulsating laser were reduced as evidenced by a considerable reduction in the pulsation linewidth and enhancement (> 10 dB) of the pulsation strength (Figure 2). The fact that the oscillations are in the optical domain is especially attractive since they can be distributed long distances via an optical fiber and can also serve as an optical local oscillator signal.

Self-pulsating lasers typically consist of a two-section cavity with separate DC bias contacts[2]. Control of the pulse repetition rate is accomplished by varying the bias to each of the sections[3]. The fundamental tuning range spans from about 300 MHz to a few GHz with harmonics of the strongly nonlinear pulsation extending the range to X-band. Open loop operation of self-pulsating lasers exhibits two dominant noise mechanisms. One is a slow drift in the pulsation frequency which results from thermal effects, DC bias power supplies drifts, etc. The other noise source results from timing jitter and phase noise inherent to the physical mechanisms involved in the pulsation phenomenon.

In order to stabilize the laser pulsation frequency we have applied a simple feedback scheme as illustrated in Figure 1. The laser we had used had its absorber section grounded with a threshold current of 42 mA. Its pulsation frequency varied from 500 MHz to 1.5 GHz with a visible frequency drift of 10-15 MHz. The laser output was coupled into a 14%-86% fiber coupler with the 14% branch monitored with an RMS detector and the 86% branch coupled into a 16 GHz PIN detector biased at -4V. The detected current was amplified with half diverted to a spectrum analyzer and the remaining half used in the feedback loop. The feedback loop consisted of a bandpass (shaping) filter, RF amplifier, and tunable delay line (for phase control).

This feedback method improved the signal-to-noise ratio by more than 15 dB by both reducing the noise floor and enhancing the pulsation strength. In particular, the phase noise and timing jitter have been suppressed resulting in improved short and long term stability and a much cleaner spectrum. Figure 2 shows the spectrum of the laser with and without feedback for an injection level of 10% of the DC bias above the laser threshold. Similar behavior has been observed for operating points throughout the tuning range. While these results are promising, further exploration is needed in order to make this method practical and competitive. Experiments and theoretical analysis are underway to determine the optimal feedback conditions and improve the feedback scheme and the results will be reported.

References

1. R. J. S. Bates and S.D. Walker, "A 450Mb/s Throughput SubCarrier Multiple-Access Network using 790nm Self-Pulsating Laser Transmitters", European Conf. on Optical Communications, September 16-20, 1990, Amsterdam.
2. T. P. Lee and R. H. R. Roldan, "Repetitively Q-switched Light Pulses from GaAs with Tandem Double-section Stripe Geometry," *IEEE J. Quantum Electron.*, Vol. QE-4, p. 855, 1968.
3. M. Honsberg, "Controlled Generation of Optical Pulse Trains by Double-contacted GaAs Laser Diodes," *Electron. Lett.*, Vol. 20, p. 844, 1984.

EXPERIMENTAL SETUP

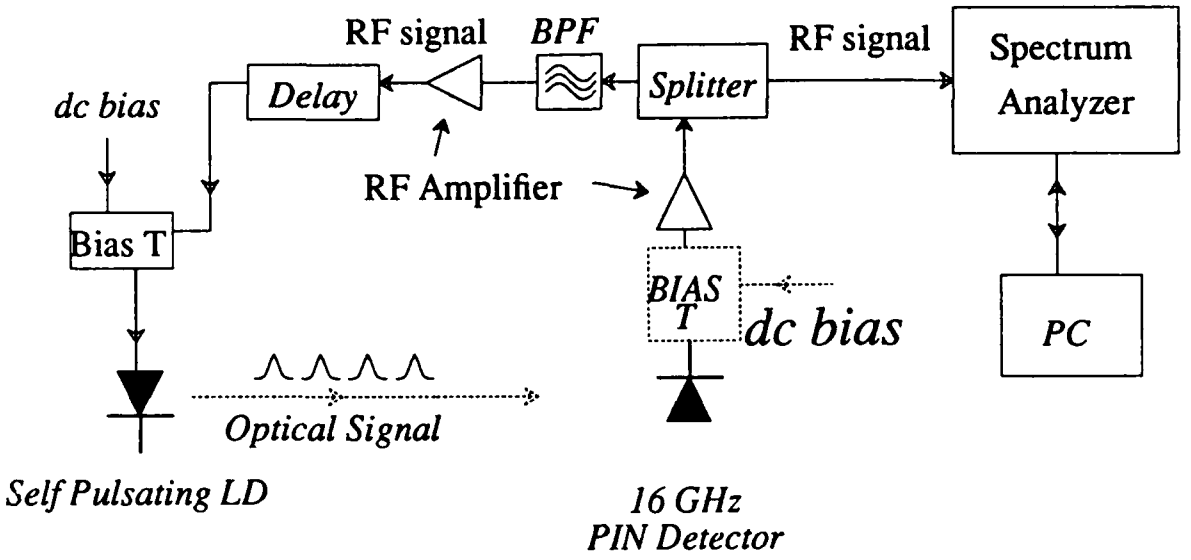

Figure 1.

Schematic of experimental setup for providing current feedback to the self-pulsating laser diode.

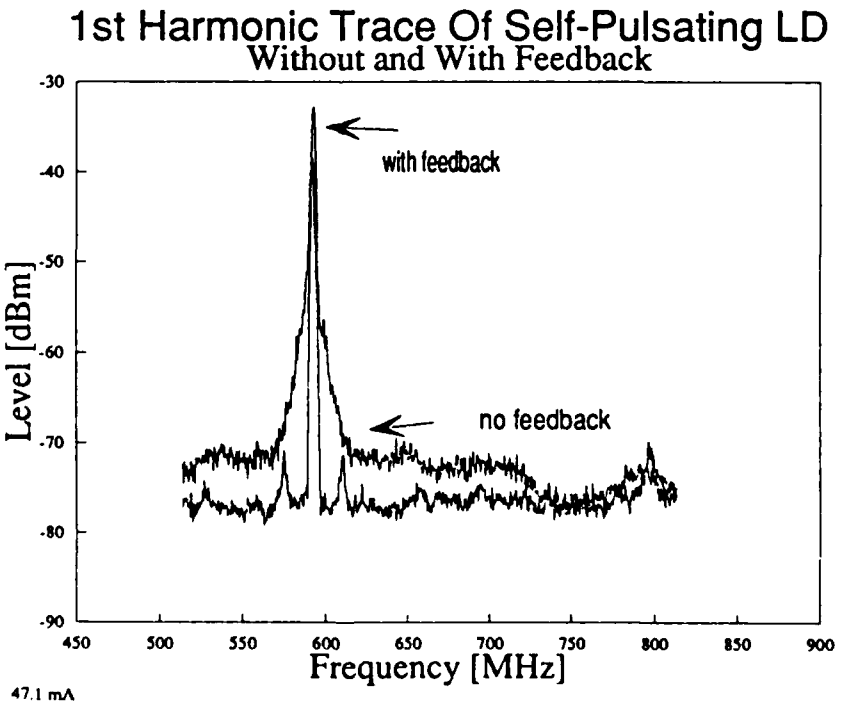

Figure 2.

Spectrum analyzer trace of the self-pulsating laser output without and with feedback for 5mA above threshold.

ThA.4 Modelocked Pulses From Semiconductor Lasers at Greater Than 100 GHz Repetition Rates

Amnon Yariv and Steve Sanders
128-95 Caltech, Pasadena, California 91125

It has recently been predicted theoretically [1] and demonstrated experimentally [2,3] that mode-locked quantum well semiconductor lasers can generate picosecond pulse trains with repetition rates exceeding 100 GHz. The demonstration of strong modulation at these high frequencies should open up new applications of semiconductor lasers to millimeter-wave signal generation, processing, and transmission. We will describe *passive* mode-locking of monolithic and external cavity two-section quantum well lasers, which requires no high frequency electrical current to generate the high speed pulse trains.

The structure of a two-section passively mode-locked laser is shown in Figure 1. A single optical cavity is electrically divided by a very shallow etch to remove the highly conductive cap layer between the sections, so that current can be pumped into one region to provide gain while the other region is biased to extract carriers generated by absorption of light. Because the differential gain in quantum well materials decreases as the carrier density increases, the absorber saturation intensity is lower than the gain saturation intensity, as required for passive mode-locking.

The pulse train generated by a monolithic 340 μm long triple quantum well GaAs/AlGaAs laser is shown in Figure 2, as measured by a *single-shot* streak camera. The pulse train was consistently observed from shot to shot and has a repetition rate of 108 GHz, with an average pulsewidth of 2.4 ps, time-bandwidth product of 1.1, and peak power of 30 mw. A more stable pulse train, generated by a 925 μm long double quantum well InGaAs/AlGaAs laser, with a third, unbiased, section is shown in Figure 3 [4]. Consistent with a small signal stability analysis of the average carrier density and photon density of the laser cavity, the longer device is less susceptible to large power fluctuations at the relaxation resonance of a few GHz. The pulses generated by this laser have an average pulsewidth of 5.9 ps and peak power of 80 mW. We have observed strong modulation in shorter two-section lasers at repetition rates up to 130 GHz, but with poor stability. It should be possible to further increase repetition rates, as has been done in InGaAsP lasers [3] using different cavity structures.

While it is difficult to quantitatively measure the stability of millimeter-wave repetition rate pulse trains, it has been shown that stable pulse trains can be generated at lower repetition rates, where the facet of the two-section laser adjacent to the gain region is anti-reflection coated and coupled to an external cavity to increase the pulse round-trip transit time [5,6]. The noise power spectra about the first, second, fourth, and eighth order harmonics of the pulse train intensity are shown in Figure 4 for a quantum well laser passively mode-locked at 546 MHz. Pulses with 8 ps duration are generated, and the RMS timing jitter, which is separated from the pulse energy fluctuations by the quadratic dependence of phase noise power on harmonic order, is 5.5 ps above 50 Hz. The RMS pulse energy fluctuations are determined to be less than 0.52% above 200 Hz.

References

[1] K. Y. Lau, Appl. Phys. Lett., **52**, 2214 (1988).

[2] S. Sanders, L. Eng, J. Paslaski, and A. Yariv, Appl. Phys. Lett., **56**, 310 (1990).

[3] Y. K. Chen, M. C. Wu, T. Tanbun-Ek, R. A. Logan, and M. A. Chin, Appl. Phys. Lett., **58**, 1253 (1991).

[4] S. Sanders, L. Eng, and A. Yariv, Electron. Lett., **26**, 1087 (1990).

[5] S. Sanders, A. Yariv, J. Paslaski, J. E. Ungar, and H. A. Zarem, Appl. Phys. Lett., **58**, 681 (1991).

[6] S. Sanders, T. Schrans, A. Yariv, J. Paslaski, J. E. Ungar, and H. A. Zarem, to be published in Appl. Phys. Lett. **59**.

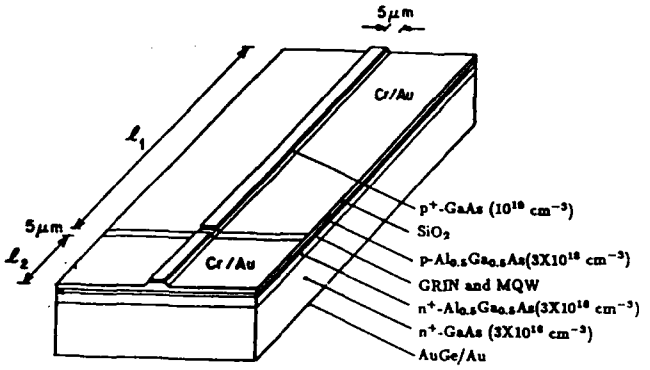

Figure 1: Two-section quantum well laser

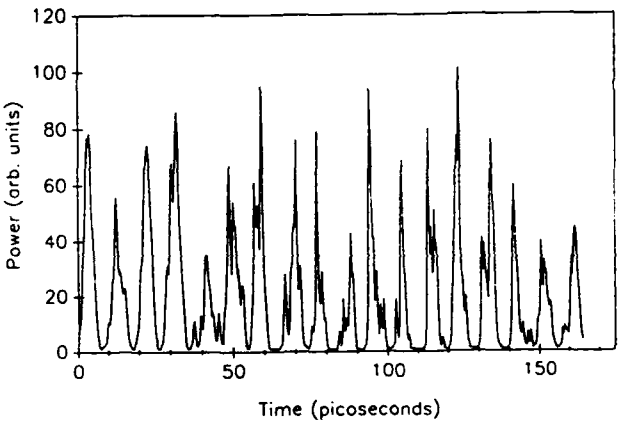

Figure 2: 108 GHz pulse train generated with I_g = 90 mA, V_r = -0.67V

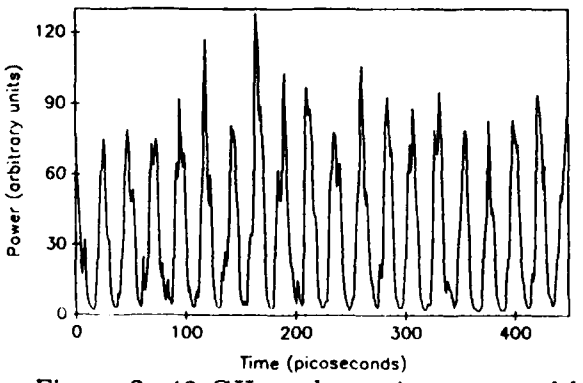

Figure 3: 42 GHz pulse train generated by InGaAs/AlGaAs laser (6 ps resolution)

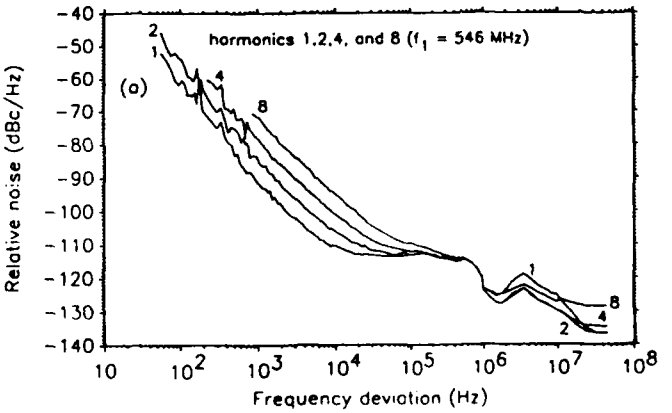

Figure 4: Noise power spectrum for external cavity passively mode-locked quantum well laser at 546 MHz

ThC.1 Microwave and Millimeter Wave Dielectric Measurements with Picosecond Optoelectronics

G. Arjavalingam, W.M. Robertson, J.-M. Halbout, and G.V. Kopcsay.
IBM Research Division, Thomas J. Watson Research Center,
P.O.Box 218, Yorktown Heights, NY 10598.
(914) 945 1359 (ph); (914) 945 2141 (fax).

The generation and detection of picosecond electrical pulses using optoelectronic techniques is now an established field [1]. Coupled with broadband antenna structures these techniques have been extended to the radiation and reception of freely-propagating ultrashort electromagnetic transients [2]. The subject of this talk is the application of these transients to broadband dielectric measurements in the microwave/millimeter wave spectrum [3].

Figure 1 depicts a typical set-up for transmission measurements which has been used to characterize low-loss dielectrics [4]. The radiating and receiving elements in our experiments are exponentially tapered coplanar stripline antennas fabricated on silicon-on-sapphire substrates, with standard photolithographic techniques. The hemispherical fused-silica lenses collimate the radiation diverging from the transmitter, and refocus it onto the receiver [3]. In addition, the high polarization sensitivity of the planar radiating elements in Fig. 1 allow the dielectric properties of anisotropic materials to be determined [5]. Recently, we have utilized the coherent microwave transient spectroscopy (COMITS) technique to measure the dielectric properties of composites, and to explore the validity of mixture theories often used to predict their dielectric response [6].

The "quasi-optical" nature of the COMITS technique can be exploited to characterize samples in reflection as shown in figure 2 [7]. In this case the signal reflected from a gold mirror acts as the reference. The reflection configuration is particularly suited to characterization of lossy materials. Results of recent measurements on silicon substrates with a range of doping densities will be presented, and compared with the predictions of a simple Drude model [8].

REFERENCES

1. See for instance "Picosecond Optoelectronic Devices", edited by Chi H. Lee (Academic Press, Orlando, 1984).
2. A.P. De Fonzo and C. Lutz, Appl. Phys. Lett. vol. 51, pp. 212-214, (1987); Y. Pastol, G. Arjavalingam, J.-M. Halbout, and G.V. Kopcsay, Electron. Lett., vol. 24, pp. 1318-1319, (1988); P.R. Smith, D.H. Auston, and M.C. Nuss, IEEE J. Quantum Electron., vol. 24, pp. 255-260, (1988).
3. Y. Pastol, G. Arjavalingam, J.-M. Halbout, and G.V. Kopcsay, Appl. Phys. Lett., vol. 54, pp. 307-309, (1989); G. Arjavalingam, Y. Pastol, J.-M. Halbout, and G.V. Kopcsay, IEEE Trans. Microwave Theory and Tech., vol. 38, pp. 615-621, (1990).
4. Y. Pastol, G. Arjavalingam, J.-M. Halbout, and G.V. Kopcsay, Electron. Lett., vol. 25, pp. 523-524, (1989); D. Grischkowsky and S. Keiding, Appl. Phys. Lett., vol. 57, pp. 1055-1057, (1990).

5. Y. Pastol, G. Arjavalingam, G.V. Kopcsay, and J.-M. Halbout, Appl. Phys. Lett., vol. 55, pp. 2277-2279 (1989); W.M. Robertson, G. Arjavalingam, and G.V. Kopcsay, Elect. Lett., vol. 27, pp. 175-176, (1991).
6. W.M. Robertson, G. Arjavalingam, and S.L. Shinde, submitted for publication.
7. W.M. Robertson, G. Arjavalingam, and G.V. Kopcsay, Appl. Phys. Lett., vol. 57, pp. 1958-1960, (1990).
8. W.M. Robertson, G. Arjavalingam, G.V. Kopcsay, and J.-M. Halbout, submitted for publication.

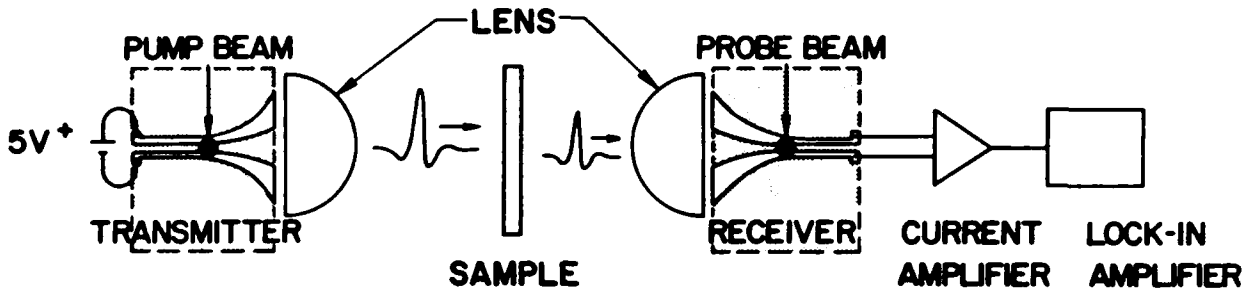

Figure 1. Schematic of the transmission set-up for COMITS experiments.

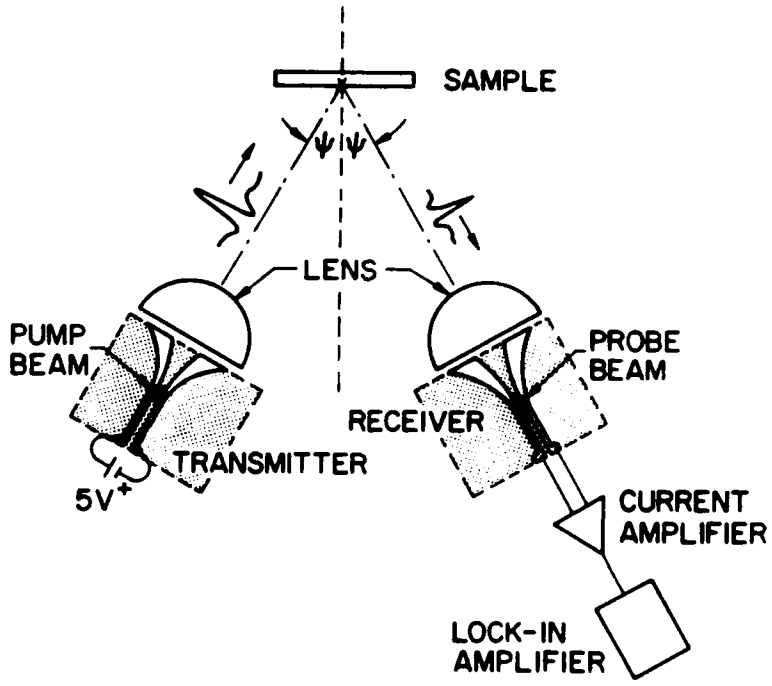

Figure 2. Schematic of the COMITS configuration for reflection measurements.

ThC.2 Submillimeter-Wave Properties of High-Temperature Superconductors and Dielectrics Using Coherent Time-Domain Spectroscopy

James M. Chwalek, John F. Whitaker, and Gerard A. Mourou

University of Michigan, Ultrafast Science Laboratory, Ann Arbor, MI 48109

Coherent time-domain spectroscopy is proving to be an extremely powerful tool in the study of the millimeter-wave and submillimeter-wave properties of materials. Thus far it has been applied to a number of material systems including dielectrics and semiconductors [1,2]. This technique like more conventional techniques such as Fourier-transform infrared (FT-IR) spectroscopy is very broadband. Unlike FT-IR spectroscopy this time-domain technique is a coherent one, *i.e.*, both phase and amplitude information are obtained directly from the measurements.

Studies of the high-frequency properties of superconducting materials based on their response to millimeter- and submillimeter-wave electromagnetic perturbations are of special interest. They can give insight into the nature of quasiparticle excitations and pairing mechanisms, as well as a direct assessment of how the materials would perform as passive microwave devices (*e.g.*, interconnects, resonators, filters, *etc.*). The latter is found via measurements of the complex conductivity or surface impedance.

A schematic of the experimental system is shown in Fig. 1. A CPM laser (λ = 630 nm) provides ~100-fs optical pulses which serve as a trigger for both the transmitter and receiver photoconductive (*Auston*-type) gates. The terahertz radiation is generated by momentarily shorting a dc-biased photoconductive switch with a short laser (pump) pulse. This switch is located at the center of a simple dipole antenna imbedded in a coplanar transmission line. To aid the coupling of the radiation into the air and to provide collimation of the terahertz beam, a hyperhemispherical lens is placed at the back of the substrate as shown in Fig. 1. The terahertz beam is collected and focussed onto an identical receiving antenna. The electric field associated with the collected radiation induces a transient bias voltage across the receiving antenna. Another photoconductive gap at the center of the receiving antenna is gated with a second (probe) pulse train which can be variably delayed with respect to the pump-pulse train. The amplitude and temporal profile of this induced voltage is obtained by measuring the collected charge versus the pump-probe delay time. The addition of a continuous flow cryostat provides sample cooling to ~10 K.

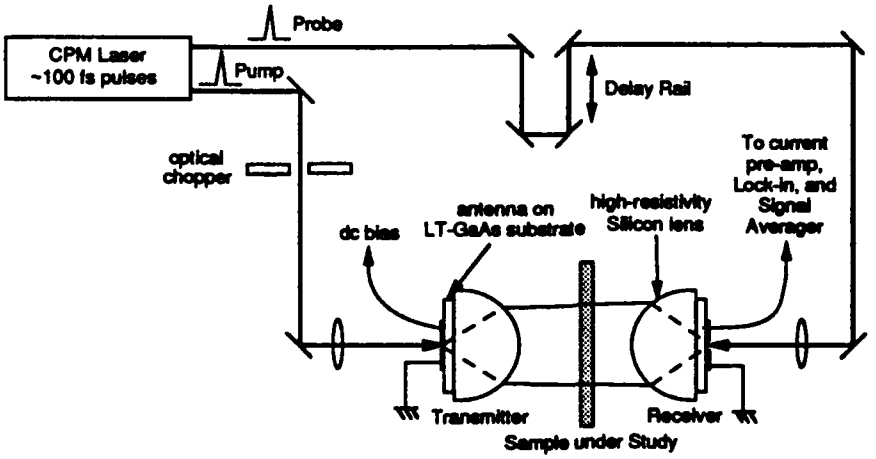

Figure 1. The terahertz spectroscopy system.

We first apply the terahertz spectroscopy technique to assess the characteristics of a magnesium oxide (MgO) substrate on which the high-T_c thin films are later deposited. From a measurement of the transmitted waveforms without (vacuum) and with the sample (see Fig. 2a) the complex index, N can be directly obtained. The results are shown in Fig. 2b. The real part of the index increases only slightly with frequency. Indeed this demonstrates the ability to accurately measure index changes of less than 2% over a bandwidth exceeding 2 THz in thin samples (0.5 mm).

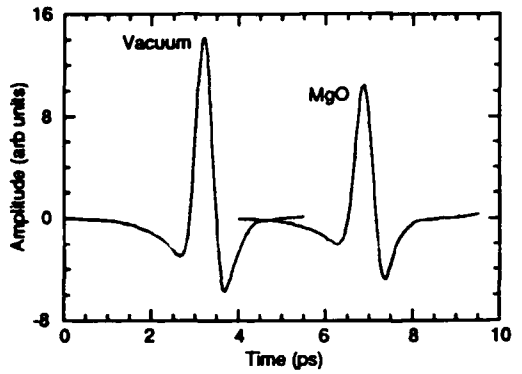

Figure 2a. Transmitted time domain waveforms without and with a 500-μm thick MgO substrate.

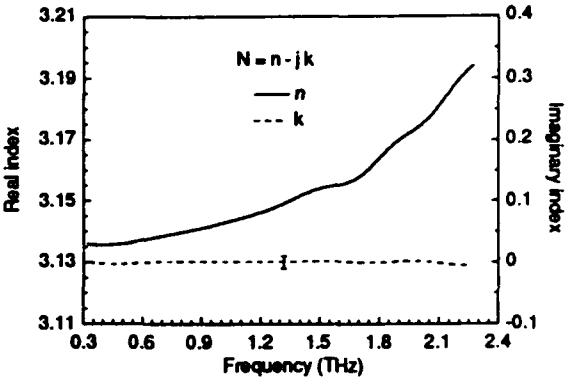

Figure 2b. The measured complex index obtained from the data contained in Fig. 2a.

Next, a superconducting $YBa_2Cu_3O_{7-x}$ (YBCO) thin film (~1000-Å thickness) deposited on a MgO substrate was placed between the antennas. Figure 3a. shows the time-domain response in transmission for temperatures above and below the critical temperature (~80 K). The changes associated with the onset to superconductivity can be directly seen. A dramatic decrease in the transmitted signal amplitude occurred mainly as a result of the increase in the reflection of the incident wave. An even more dramatic change can be seen for temperatures below $\sim T_c/2$. A phase shift and an accompanying change in pulse shape are also identified. This is a direct result of the presence of superconducting electrons.

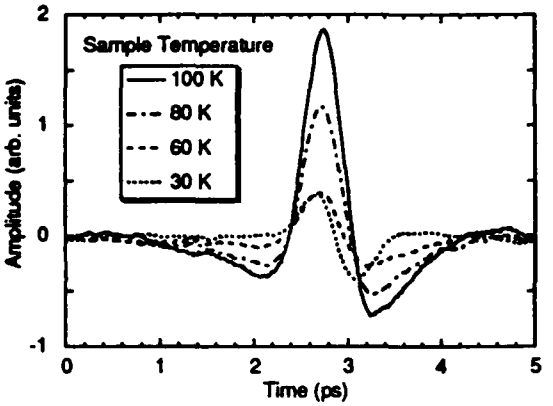

Figure 3a. Transmitted time domain waveforms through a ~1000 Å thick YBCO thin-film above and below T_c.

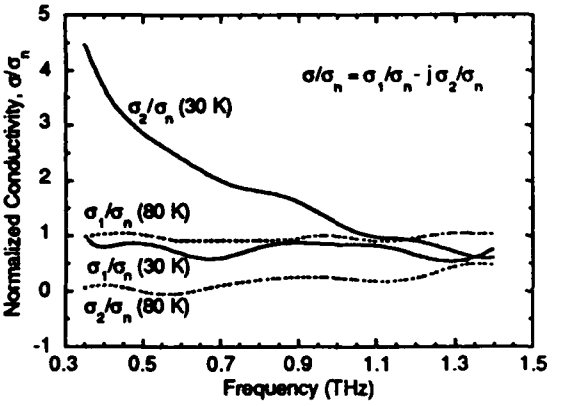

Figure 3b. The complex conductivity obtained from the transmitted waveforms of Fig. 3a.

From the measured transmission function the *complex* conductivity was obtained (see Fig. 3b) [3]. A number of dramatic effects can be seen. The imaginary part of the conductivity, σ_2, nearly zero in the normal state, increases greatly at low frequencies exhibiting a $1/\omega$ frequency dependence, as expected from theory. This behavior of σ_2 is primarily from superconducting pairs. The real part of the conductivity, σ_1, decreases below the normal state value for low temperatures.

In conclusion, from the above examples the coherent time domain technique proves to be an indispensable tool for the assessment of the terahertz properties of a wide variety of materials.

This work has been supported by the AFOSR, University Research Initiative under contract number AFOSR-90-0214 and NASA under contract number NCC3-130.

1. D. Grischkowsky, *et. al.*, *J. Opt. Soc. Am. B*, 7, 2006 (1990).
2. D. Grischkowsky and S. Keiding, *Appl. Phys. Lett.*, 57, 1055 (1990).
3. J. M. Chwalek, J. F. Whitaker, and G. A. Mourou, *Electron. Lett.*, 27, 447 (1991).

ThC.3 Optically Generated 60 GHz Radiation Using InGaAs HEMTs and Quasi-Optical Circuits

D.V. Plant, D.C. Scott, and H.R. Fetterman
Department of Electrical Engineering
University of California, Los Angeles
Los Angeles, California 90024

L.K. Shaw
TRW Electronics & Technology Division,
One Space Park
Redondo Beach, California 90278

Optical-millimeter wave interactions have attracted recent attention because of applications which involve the advantages of both lightwave and microwave technologies. In this paper, we report the generation of 60 GHz cw millimeter wave radiation using pseudomorphic InGaAs HEMTs integrated with printed circuit antennas and illuminated with visible laser radiation. Utilizing three terminal rather than two terminal devices permitted millimeter wave power optimization as a function of bias (V_{ds}, and V_{gs}) and device structure. In addition, the gate terminal provided a means of applying RF sidebands (<500 MHz) to the optically generated carrier for applications in communication systems.

The HEMT was illuminated with light from a Kiton Red dye laser (600nm to 640 nm, 50 mW) and a frequency stabilized HeNe laser (632.8 nm, 0.6 mW). The wavelength of the dye laser was locked to an external temperature stabilized Fabry-Perot reference cavity. Light was brought onto the device active region using single mode polarization preserving optical fibers at 633nm. In order to prevent unwanted optical feedback into the lasers, the fiber was polished with a wedge angle of approximately 10 degrees. The fiber tip was brought to less than 1 mm from the device active region. The millimeter wave output was detected using heterodyne detection techniques. The optical mixing in the device produced mixing currents at the desired re-radiation frequency. Figure 1 is a recording of a received signal at 60.25 GHz. This figure

shows a signal to noise ratio of > 45 dB. Figure 2 is a recording of a received signal with 175 MHz electrical sidebands applied to a 60.1 GHz optically generated carrier. The signal power in the RF sidebands is significantly large, approximately 10 dB down from the carrier.

This technique demonstrates the potential of converting optical frequencies into millimeter-wave signals. Current work includes using a monolithic multistage InGaAs HEMT amplifier to provide amplification to the optical mixing signal prior to driving the twin dipole antenna.

This work was supported by the Air Force Office of Scientific Research and by the National Center for Integrated Photonics Technology.

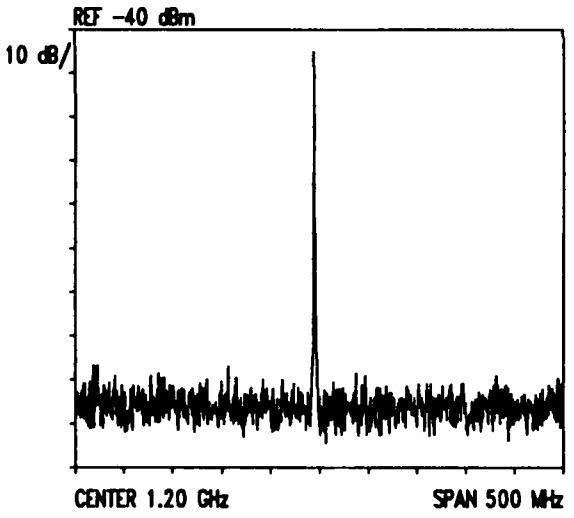

Figure 1

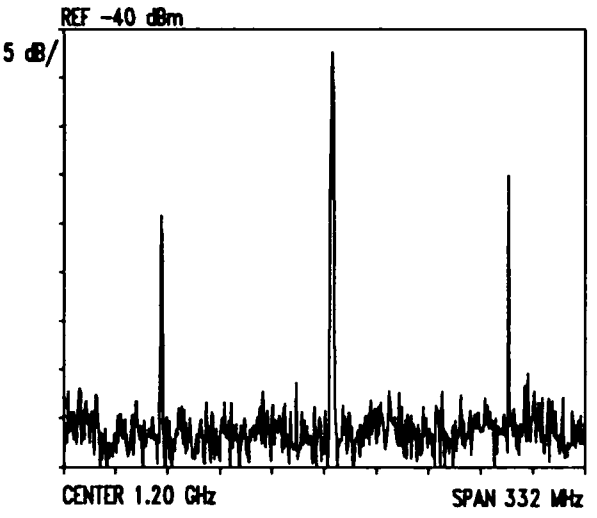

Figure 2

ThC.4

Broadband Microwave Measurement of Water Using Transient Radiation

C. D. Capps, R. A. Falk, S. G. Ferrier, T. R. Majoch
Boeing Aerospace & Electronics Division
P.O. Box 3999, MS 8H-18
Seattle, WA 98124

It has been shown (Ref. 1) that transient radiation from optoelectronically pulsed antennas can be used to measure the complex dielectric function for relatively lossless solid materials in the microwave frequency region. In this work we will show that the technique can be extended to measure the complex dielectric function, or equivalently, the complex refractive index of a very lossy liquid, e.g. water. The principle difference is that in transparent materials, the sample thickness can be made great enough that multiple reflections can be removed by time windowing. For highly absorptive media the samples must be very thin to transmit measureable energy and an alternative method used for analysis.

A formalism is derived based on the Fourier components of the transmitted pulse and the matrix form of the electromagnetic continuity conditions at the window and sample interfaces. Measurements on multiple sample thicknesses generate at each frequency a set of 2N equations in two unknowns, the real and imaginary parts of the refractive index of the material. This overdetermined set of equations is solved numerically to obtain the complex index at each frequency.

A thorough error analysis is performed to quantify contributions from various sources. Uncertainties in the window index, window thickness, and sample thickness are treated with a Monte Carlo analysis. Random noise in the apparatus is examined by analysis of repeated measurements. Finally, the results obtained using transient radiation are compared with values of the complex refractive index from the method of travelling waves (Ref 2). Figures 1 and 2 show our results for the real and imaginary parts of the refractive index plotted as points with error bars and corresponding values from Reference 2 calculated from the parameter values given in Table 1 of that reference and plotted as solid lines. The error bars show the one standard deviation uncertainty. Results from the transient and continuous wave technique are in excellent agreement with no significant statistical or systematic discrepancy.

References:

1. G. Arjavalingam, Y. Pastol, J.-M Halbout, and G. V. Kopcsay, "Broad-Band Microwave Measurements with Transient Radiation from Optoelectronically Pulsed Antennas", IEEE Trans. Microwave Theory Techn., Vol. MTT-38, pp. 615-621, 1990.
2. J. Barthel, K. Bachuber, R. Buchner, H. Hetzenauer, "Dielectric Spectra of Some Common Solvents in the Microwave Region: Water and Lower Alcohols", Chem. Phys. Lett., Vol. 165, pp. 364-373, 1990.

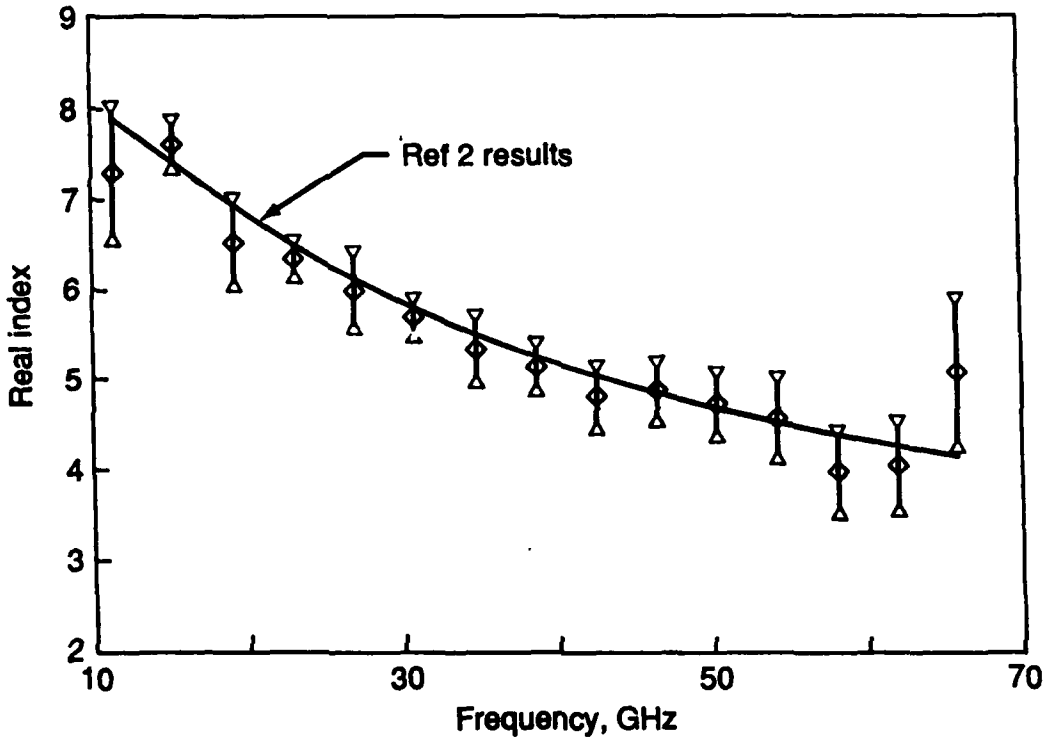

Figure 1. Real part of the complex refractive index of water.

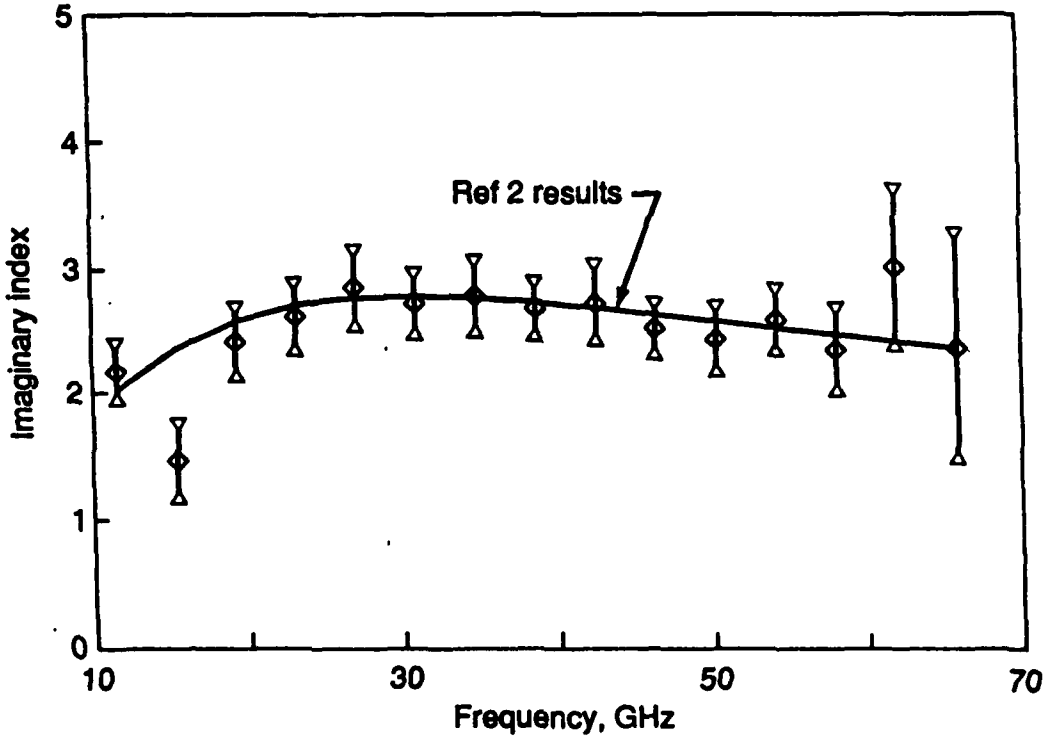

Figure 2. Imaginary part of the complex refractive index of water.

ThC.5 Coherent, Broadband Millimeter-Wave Spectroscopy Using Monolithic GaAs Circuits

M. Kamegawa*, Y. Konishi*, M. Case, R. Yu, and M. J. W. Rodwell

Department of Electrical and Computer Engineering,
University of California, Santa Barbara, CA 93106.
*Presently on leave from Shimadzu Corporation, Kyoto, Japan

Abstract

We report a millimeter-wave spectroscopy system using a nonlinear transmission line stimulus signal generator (NLTL) and a monolithic GaAs diode sampling bridge receiver. Signal to noise ratios greater than 20 dB (1Hz) in the 10 -160 GHz range are achieved. This work is an alternative to Terahertz spectroscopic techniques using mode-locked lasers and femtosecond photoconductors.

Introduction

Recently, several groups have demonstrated broadband TeraHertz spectroscopy [1-5]. In these experiments, a mode-locked laser illuminates a photoconductor, thereby generating a subpicosecond electrical transient which is subsequently radiated by an on-wafer antenna. A similar system is used to receive and sample the radiated signal. NLTL shock-wave generators and NLTL-gated diode sampling circuits are alternative, solid-state technologies for generation and detection of ≈300 GHz-bandwidth signals [6,7]. The combination of an NLTL with an on-wafer broadband antenna provides a monolithic millimeter-wave transmitter, while connecting a similar antenna to the high-speed sampler's input forms a monolithic receiver. There are several potential advantages of this system compared to those using photoconductors. First, the system has fewer components and is very compact without a laser or its optics. Second, there is substantially more transmitted power, since the NLTL output power is ≈50 mW. Third, since the NLTL is driven by a microwave synthesizer, and the NLTL input frequency can be varied by as much as an octave, the system can easily be tuned to any desired mm-wave harmonic frequency.

System Design

The sampling circuit we use has been reported by Yu et al. [6]. Exponentially-tapered coplanar-strip antennas [1,2] are used for both the transmitter and the receiver. To make a transition from the coplanar wave guide of the NLTL to the coplanar strips of the antenna, we used a resistive balun. The antenna has 100 Ω characteristic impedance, and is terminated with a 100 Ω resistor at the output to reduce reflections back into the NLTL's output. The input part of the antenna consists of a pair of 10 μm wide gold lines with a 14 μm space between them, and the lines' width and spacing is exponentially increased until the end of the antenna, where the aperture size is 2 mm. The total length of the antenna is 4 mm. The resistive balun incurs a 3 dB power loss in both the transmitter and receiver.

Wafer Processing

Starting with a semi-insulating GaAs substrate, a heavily doped (6×10^{18} /cm^3, 1μm thick) N^+ layer is grown by molecular beam epitaxy. This serves as a highly conductive diode cathode connection. An N^- active layer (425 nm thickness) is then grown with an exponentially-graded, hyperabrupt doping profile (2×10^{17} /cm^3 surface doping, 225 nm grading constant). Ohmic contacts to the N^+ layer are formed by a 0.5 μm recess etch through the N^- layer, a self-aligned AuGe/Ni/Au liftoff, and a subsequent anneal. Diode junction areas and resistors are patterned by a proton implantation which converts the N+ and N- layers to semi-insulating material in unmasked

areas. During implantation, the diode regions and resistors are protected by a 1.6 μm Au on polyimide mask. After implantation, interconnections, antennas, and Schottky contacts are formed with a 1.1 μm Ti/Pt/Au liftoff. Air-bridge crossovers required in the baluns and in the sampling circuit are then fabricated

Experimental Set-Up and Results

Fig. 1 shows the experimental setup. Two off-axis paraboloidal mirrors collimate and direct the mm-wave signals. The sampling circuit is driven at 10 GHz, and the transmitter NLTL is driven at 10 GHz + 14 Hz. Fig. 2 shows the signal-to-noise ratio of this system with a 1 Hz resolution bandwidth. Fig. 2 also shows the signal-to-noise ratio of an NLTL connected through 26 dB attenuator to an on-wafer sampling circuit, indicating a potential of ≈ 500 GHz bandwidth with optimized antenna design and reflector setup.

This work was supported by the Air Force Office of Scientific Research under grant number AFOSR-89-0394.

References

[1] G.Arjavalingam, Y.Pastol, J.M.Halbout, G.V.Kopcsay, "Broard-band microwave measurements with transient radiation from optoelectronically pulsed antenna", IEEE, Trans. MTT, Vol. 38, No.5 May 1990 pp. 615-621

[2] A.P.DeFonzo, C.R.Lutz, "Optoelectronic transmission and reception of ultrashort electrical pulses", Appl. Phys. Lett., Vol. 51, No.4, 22 July 1987, pp. 212-214

[3] N. Katzenellenbogen and D. Grischkowsky, "Efficient generation of 380 fs pulses of THz radiation by ultrafast laser pulse excitation of a biased metal-semiconductor interface", Appl. Phys. Lett., Vol. 58, No.3, 21 January 1991, pp. 222-224

[4] M.C.Nuss, K.W.Goossen, "Investigation of high-temperature superconductors with terahertz bandwidth electrical pulses", IEEE, J. Quantum Electron., Vol. 25, No.12, December, 1989, pp. 2596-2607

[5] J.T. Darrow, X-C. Zhang, and D.H. Auston, "Power scaling of large-aperture photoconducting antennas", Appl. Phys. Lett., Vol. 58, No.1, 7 January 1991, pp. 25-27

[6] R. Yu, M. Case, M. Kamegawa, M. Sandram, M.J.W.Rodwell and A. Gossard, "275 GHz 3 mask Integrated Sampling Circuit", Electronics Letters, Vol. 26, No.13, 21 June 1990, pp. 949-951.

[7] R.A. Marsland, C.J. Madden, D.W. Van Der Weide, M.S. Shakouri, and D.M. Bloom, "Monolithic Integrated Circuits for MM-Wave Instrumentation", in Technical Digest, 1990 GaAs IC Symposium, Oct. 7-10, New Orleans, La.

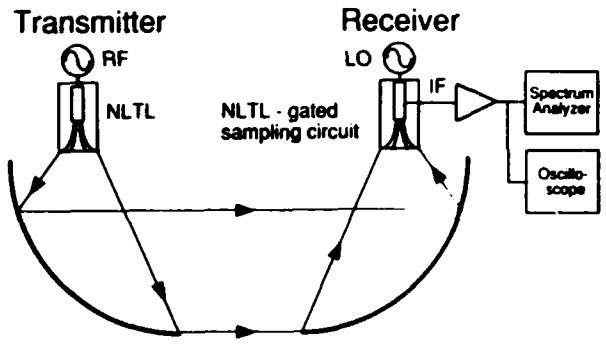

Fig. 1 Schematic of the experimental setup

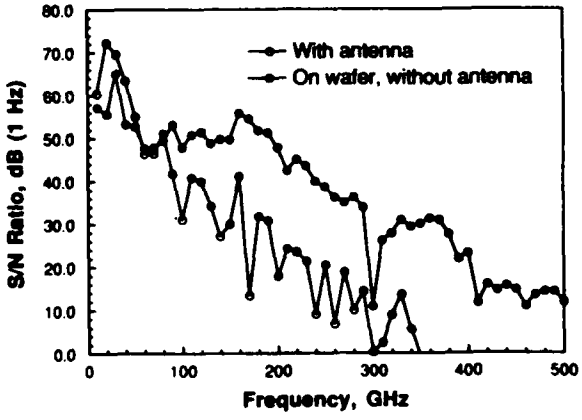

Fig. 2 System signal to noise ratio compared to the S/N ratio observed with an NLTL connected to an on-wafer sampling circuit

ThC.6 Photonically Activated Stored Energy Device Arrays for Microwaves

James B. Thaxter
Capt Richard E. Bell
Rome Laboratory
Hanscom AFB, MA 01731

Many laboratories have shown the energy stored in dielectrics in the form of static electric field and electric polarization can be released via photoconductive switching to create short powerful microwave pulses useful for many communication and radar applications. Static energy densities up to several joules/meter^3 stored in conventional dielectrics can in principle produce radiation power density of severals megawatts from an aperture a few centimeter diameter.

The form of the devices used depends radically on both the frequency range of interest and dictates of scaling laws for both the photoconductive switching processes and impedance matching to the radiation fields. At low frequencies (up to several gigahertz) energy storage in a circuit of transmission line segments connected with lumped photoconductive switches, a so called Frozen Wave (F.W.) generator, is appropriate with wide band horn antennas matching the energy to space. For frequencies in the terahertz range the "circuit" shrinks in size and importance as both a storage and impedance matching structure. Efficient radiation is achieved with simple structures such as a photoconductive spot on the surface of a polarized dielectric.

Large arrays of such structures offer the possibility of a variety of circuit architectures using low cost microelectronic fabrication techniques to distribute the electrical stress over many components. Thereby improving device reliability while obtaining high power by combining radiated power in space. In addition to the possibility of high power, the implementation of a short pulse microwave phased array using F.W. generators located at the array face circumvents the problems of dispersion and loss encountered in the feed structure of conventional corporate fed microwave arrays.

The emphasis of this work is the design and fabrication of an non-optimized experimental C-band F.W source comprising microstrip transmission line segments and lumped photoconductor switches. Both space fed and fiber optic fed optical schemes are being investigated to deliver picosecond pulses to approximates 100 micron diameter photoconductive switches bonded to 50 ohm M.S. lines. Progress in achieving good performance depends on developing an efficient low-resistance ultrafast switch which stays closed for the wareform duration. Both GaAs and Silicon on Sapphire linear photoconducture materials are being investigated.

Circuit modeling to project performance of a five cycle F.W. generator under a variety of circuit parameters including M.S. loss, parasitic, carrier lifetime, impedance match and excitation pulse shape are considered in the model. A scheme for resonant charging of the line segments is also modeled showing methods of voltage amplification and waveform shaping to control the spectral distribution of the synthesized signal. The design allows for the possibility of all optical control of pulse wave form and amplitude using a single low voltage charging source and an appropriate optical pulse train.

ThC.7 Generation of Submillimeter-Wave Pulses from Semiconductor Surfaces and Interfaces with Femtosecond Optics

X.-C. Zhang and D.H. Auston
Electrical Engineering Department and
Center for Telecommunications Research
Columbia University, New York, NY 10027

We describe a novel optoelectronic technique to generate and detect THz electromagnetic waves from semiconductor surfaces and interfaces with femtosecond laser pulses. This approach, utilizing the concept of large-aperture planar photoconductive antennas and antenna arrays, is an effective method of producing directional and steerable millimeter-wave, submillimeter-wave pulses [1].

The physical mechanism for the generation of subpicosecond electromagnetic pulses from large aperture photoconducting antennas is the radiation from a fast time varying current. when a femtosecond laser beam illuminates on a semiconductor surface with the photon energy greater than the bandgap of the semiconductor, photons are absorbed, creating free carriers. The surface field (external bias or the built-in electric fields) drives the surface photocarriers to form a transient photocurrent. The current pulse has a sharp risetime which is on the order of the laser pulse duration. The transient photocurrent radiates inward (transmitted) and outward (pseudoreflected) femtosecond electromagnetic pulses. Since the aperture size of the photoconductor is larger than the spatial pulse duration of the electromagnetic radiation, the electromagnetic wave is directional and diffraction-limited. A half-power beam width of 6 degrees has been measured from a 1 cm aperture photoconducting antenna. The amplitude of the radiated electromagnetic waves is proportional to the first time derivative of the photocurrent. Therefore, if the fall-time of the photocurrent is much longer than the rise-time, the rise-time is found to be more important than the fall-time in determining the relative sensitivity of photoconducting materials. Figure 1 schematically illustrates the geometry of the experiment. The incident angle of the optical beam, and propagating directions of the outward radiated field (pseudoreflected) and inward radiated field (transmitted) satisfy a generalized Fresnel law. A duration of approximately 100 fs laser pulse was used to optically induce and detect electromagnetic radiation. The radiated field is detected by a photoconducting dipole antenna. The temporal measurement is achieved by varying the time-delay between the excited laser pulse illuminated on the semiconductor surface and the trigger laser pulse focused on the photoconducting detector.

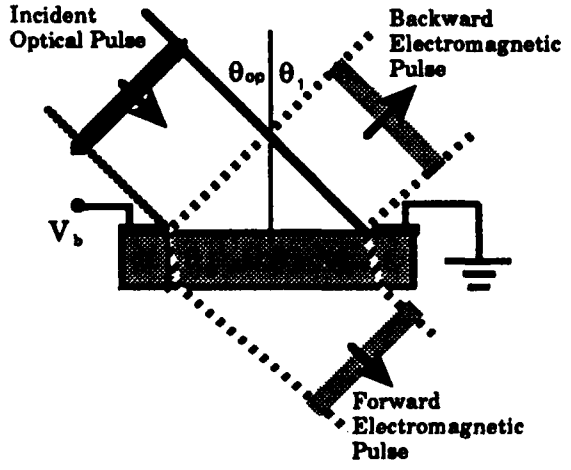

Figure 1.

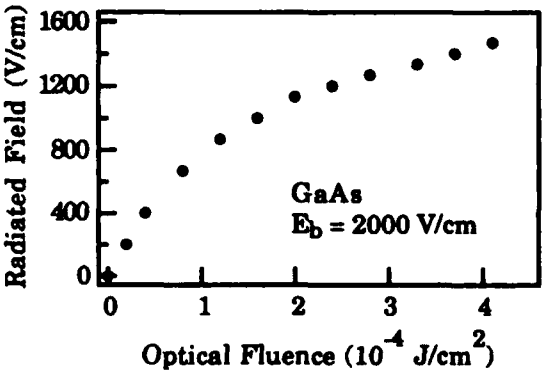

Figure 2.

In addition, the large aperture photoconducting antennas show power scaling and saturation properties. At high optical fluences, the radiated electric field (near field) saturates at a value comparable to the bias field. Figure 2 shows the radiated field versus optical fluence from a GaAs emitter with a bias field of 2 kV/cm. This observation is in agreement with a simple model of the radiation mechanism [2]. With appropriate optical fluence, bias field strength and large semiconductor area, it should be possible to generate an electromagnetic pulses with peak powers up 1 GW and local electric fields greater than 10 MV/cm.

We also present the use of an antenna array to generate electrically-steered electromagnetic waves [3]. When illuminated by a train of properly spaced ultrashort optical pulses, an array of short photoconducting dipole antennas emits a sub-millimeter wave beam which can be electrically steered by varying the periodicity of the voltage bias applied to the individual antenna elements, as shown in Figure 3. We have used a 32-element array to electrically steer a 500 GHz submillimeter wave in free space. Finally,we describe the technique of electrically-controlled frequency scanning. The radiation frequency of an electromagnetic wave from this array at a fixed direction can be electrically scanned if a single optical pulse used. In this case, the number of cycles in a electromagnetic wave packet is proportional to the number of the bias cycles, temporal radiation waveform carries the spatial bias distribution, as shown in Figure 4. Over 900 GHz frequency tuning bandwidth has been demonstrated.

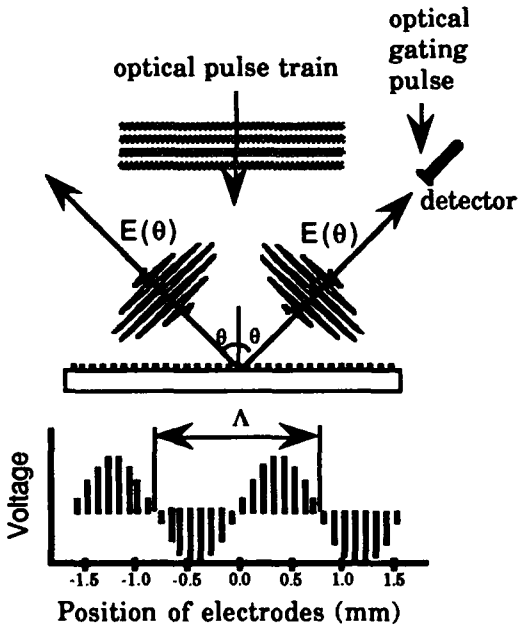

Figure 3.

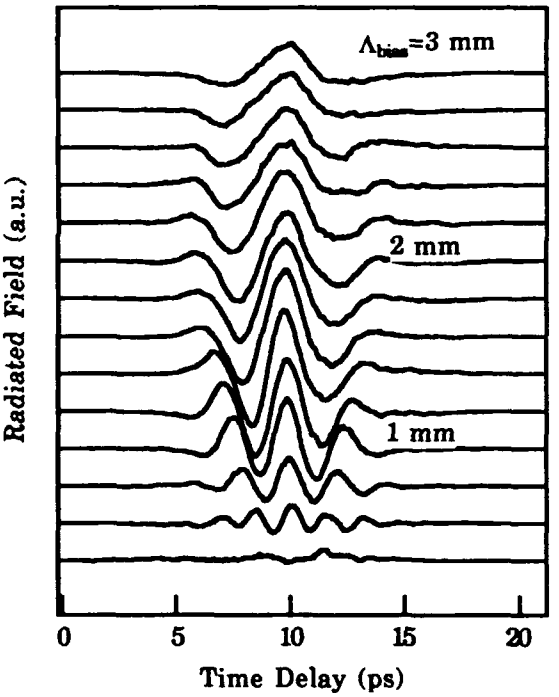

Figure 4.

References:

[1] B.B Hu, J.T. Darrow, X.-C. Zhang, D.H. Auston and P.R. Smith, "Optically-Steerable Photoconducting Antennas," Appl. Phys. Lett. **56**, 886 (1990)

[2] J.T. Darrow, X.-C. Zhang and D.H. Auston, "Power Scaling of Large Aperture Photoconducting Antennas," Appl. Phys. Lett. **58**, 25 (1991)

[3] N. Froberg, M. Mack, B.B. Hu, X.-C. Zhang and D.H. Auston, "Electrically Steerable Photoconducting Antenna Array," Appl. Phys. Lett. **58**, 446 (1991)

Friday

July 26, 1991

FA.1 Laser Heterodyne for Generation Control and Distribution of Millimeter Waves

G. J Simonis and R. G. Hay
LABCOM Harry Diamond Laboratories
2800 Powder Mill Road
Adelphi, MD 20783

The direct modulation at millimeter wave frequencies of a semiconductor laser diode or the use of an external millimeter wave optoelectronic modulator is challenging due to transient effects in current, carrier population and heating as well as packaging limitations and transit time effects. However, the optical mixing of the outputs of two cw lasers operating at somewhat different optical frequencies provides a stable tunable-modulation optical signal which can be delivered to a remote detector where the heterodyne difference frequency can be generated in a square law detector.[1,2] The difference frequency can be nearly arbitrarily large, limited primarily by the tuning ranges of the individual lasers and the ability to detect high frequencies. The highly coherent output of optically-pumped temperature-tunable Nd:YAG 1.06 μm ring lasers[3] can be used to produce a highly coherent (less than 5-kHz 3-dB heterodyne linewidth) tunable microwave signal without any active stabilization.[2] This two-frequency optical signal is readily distributable over optical fibers with minimal frequency dispersion or other distortion. The optical "modulation" depth is large and nearly independent of the heterodyne frequency. Multiple heterodyne signals can be generated by splitting and combining the two laser signals multiple times. The relative phases and amplitudes of these microwave signals can be individually controlled by opto-electronically controlling the phases and amplitudes of the optical signals being mixed at each output .[4,5]

In our original work, both Nd:YAG lasers were frequency tuned by temperature tuning the laser crystal cavities and the neodymium gain frequencies with heater elements (restricted to temperatures above room temperature) which limited the heterodyne frequency range achievable. We have subsequently characterized an extended heterodyne frequency tuning range at 1.06 μm by temperature tuning one of the lasers with a thermo-electric cooler[6] to increase the temperature tuning range. Direct detection of difference frequencies was limited to about 60 GHz maximum in our work by our detector frequency response (30-GHz 3-dB roll-off), the achievable signal-to-noise ratio, and the accessible temperature range. However, by heterodyning first a heated and then a cooled laser against a common reference laser, we were able to demonstrate an overall tuning range greater than 90 GHz, as presented in Fig. 1. Extension somewhat beyond this range should be straightforward. The 10- to 15-GHz breaks observed in the tuning curve are due to mode hopping as the laser crystal cavity modes are tuned at 3.1 GHz/°C, and the Nd:YAG gain band tunes at 1.0 GHz/°C.

We also report the enhancement of several other features of these lasers for the generation, distribution, and control of microwaves and millimeter waves[7] such as fiber optic coupling, amplitude stabilization, relaxation-oscillation supression, rapid piezoelectric frequency tuning and improved electronic control interfaces. These laser enhancements are being developed at the 1.3-μm emission wavelength of Nd:YAG rather than 1.06 μm to provide a good wavelength match for use with low-loss low-dispersion 1.3 μm fiber optics and other optoelectronics under development in the research and development community. The improvements at this wavelength also makes these lasers more useful for a wide range of other applications in the 1.3 μm community such as fiber-optic sensors, 1.3-μm-detector frequency-response characterization, and

frequency-sweep analysis of 1.3-μm optical waveguide circuits.

References

1. H. Fettermann, C. Liew, and W. L. Hgai, "Millimeter-visible injection locking and testing," Optical Technology for Microwave Applications II, SPIE **545**, pp. 26-28 (1985), D. K. Donald, D. M. Bloom, and F. K. David, "Efficient, simple optical heterodyne receiver: DC to 80 GHz," ibid, pp. 29-34.

2. G. J. Simonis and K. G. Purchase, "Optical generation, distribution, and control of microwaves using laser heterodyne," IEEE Trans. Microwave Theory Tech. **MTT-38**, pp. 667-9 (1990).

3. T. J. Kane and R. L. Byer, "Monolithic, unidirectional single-mode Nd:YAG ring laser," Opt. Lett. **10**, pp. 65-67 (1985).

4. R. A. Soref, "Voltage-controlled optical/RF phase shifter," J. Lightwave Technol. **LT-3**, pp. 992-998 (1985), M. Tamburrini, M. Parent, L. Goldberg, and D. Stillwell, "Optical feed for a phased array microwave antenna," Electron. Lett. **23**, pp. 680-681 (1987).

5. G. J. Simonis, R. G. Hay and K. G. Purchase, "Optical control of microwaves with III-V semiconductor optical waveguides," Optoelectronic Signal Processing for Phased-Array Antennas II, SPIE **1217**, pp. 83-91 (1990).

6. Laser provided by Lightwave Electronics, Mountain View, CA, E. A. P. Cheng et al.

7. Harry Diamond Laboratories, Small Business Innovative Research Phase II Contract , Lightwave Electronics, Mountain View, CA..

Figure 1. 1.06-μm laser-heterodyne temperature tuning curve.

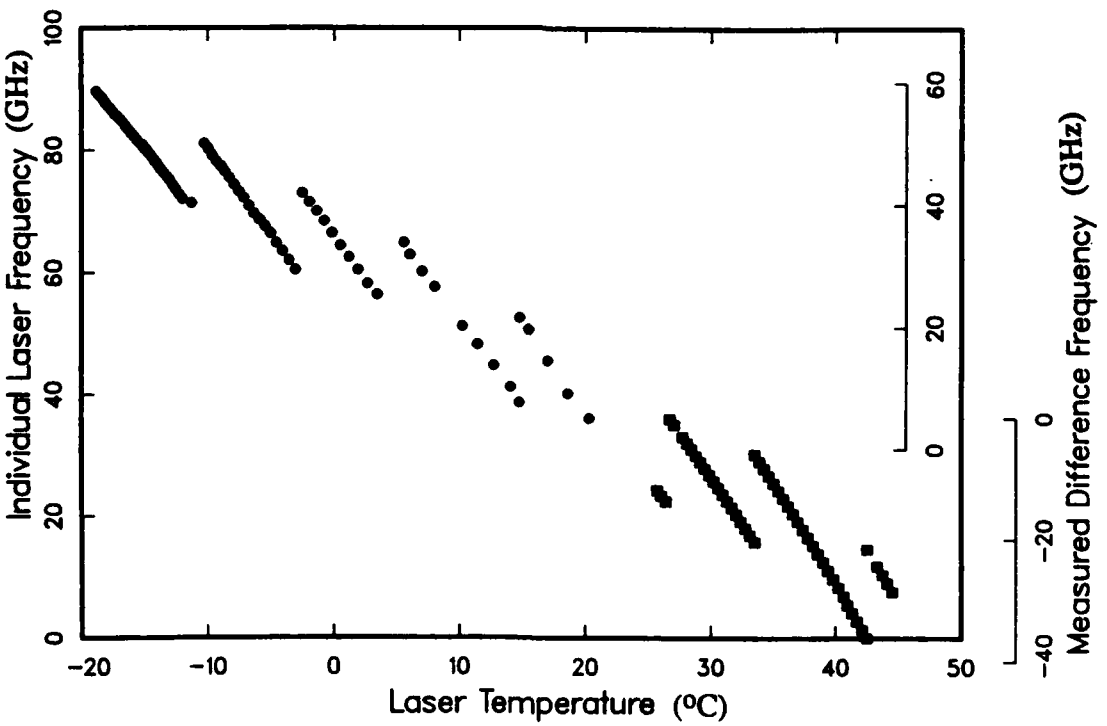

FA.2 Optical Generation of Microwave Signals by the Use of Phase Locked Semiconductor Lasers

U. Gliese, E. Lintz Christensen, T.N. Nielsen and K. Stubkjær

Center for Broadband Telecommunications
Electromagnetics Institute, Technical University of Denmark
Building 348, DK-2800 Lyngby, Denmark

Future satellite antennas may be implemented as active phased array antennas based on a large number of active microwave array elements. The signal distribution is a difficult task and conventional feeds using waveguides or coaxial cables will not be feasible for antennas with a large number of beams. By contrast, fibre optic links offer an attractive solution for the distribution of the signals in a phased array antenna system [1].

The basic principle of the coherent optical beam forming network (OBFN) is the generation of the microwave carrier by the beating of two lasers as shown in Fig. 1. Unfortunately, the carrier phase stability requirements in a microwave satellite link are very high [2]. It is therefore, important to know the influence of the laser phase noise. Consequently, the required total laser linewidth were calculated by relating the rms phase error in the microwave receiver to the phase noise of the lasers in the coherent OBFN [3]. Results are listed in Table 1 for two of the bit rates normally used in satellite links. Clearly, these requirements are not easily fulfilled with semiconductor lasers.

When the two lasers are phase locked, as shown in Fig. 1, the phase fluctuations of the difference frequency will be modified with the transfer function of the locking loop [4]. Consequently, the phase noise reduction (PNR) obtained with ideal first and second order phase locked loops (PLLs) has been calculated. The results are shown in Fig. 2 together with the maximum theoretical limit of the PNR.

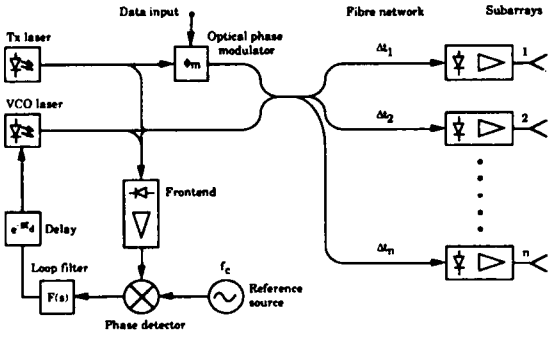

Figure 1: Schematic of a coherent optical beam forming network (OBFN) consisting of an optical phase locked transmitter module, an optical phase modulator, a fibre optic distribution network, and an active phased array antenna with n subarrays.

QPSK bit rate Mbit/s	Required linewidth in KHz	
	1° rms phase error	2° rms phase error
33	1.2	4.8
131	4.8	19

Table 1: Total laser linewidth requirements in coherent OBFNs.

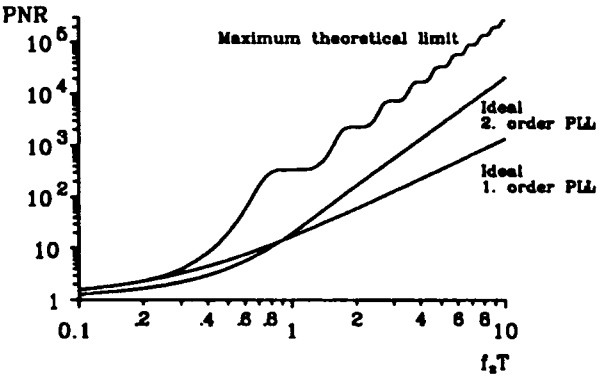

Figure 2: Phase noise reduction as a function of normalized loop bandwidth $f_z T$.

The limit of the PNR is reached when all the phase noise below the normalized loop bandwidth $f_z T$ is removed. Here f_z is the open loop zero dB frequency and T is the symbol time which corresponds to the bit rate as $R_b = \frac{2}{T}$ (QPSK modulation).

From Fig. 2 it is seen that a large amount of phase noise can be suppressed by the use of broadband PLLs. However, when designing broadband PLLs the loop propagation delay τ_d may have a large influence on both the PNR and the loop stability. Therefore, the PNR has been calculated taking the loop propagation delay into account. The PNR is shown in Fig. 3 for the second order loop, which seems the most interesting for obtaining high PNRs. In addition, the demand placed on the laser linewidth to ensure stable locked loop operation has been calculated and is shown in Fig. 4. It is obvious that the loop propagation delay has a large influence on the PNR obtained with broadband PLLs. Furthermore, the loop propagation delay drastically limits the area of stable locked loop operation. Therefore, the loop propagation delay cannot be neglected, making careful loop design very important.

The results from Fig. 3 and Fig. 4 shows that it is possible to optically generate highly stable microwave carriers by the use of phase locked semiconductor lasers with linewidths in the order of MHz. Unfortunately, DFB lasers tend to have a dip in the frequency response at low frequencies which will disturb the PLL. Multi-electrode DFB lasers on the other hand seem very promising since both narrow linewidth, uniform frequency response and high modulation sensitivity can be obtained [5].

In conclusion the strict demands placed on linewidth of the lasers in a coherent OBFN seem possible to fulfil with narrow linewidth semiconductor DFB lasers when using PLLs, thereby making the coherent approach realistic for optical generation of high quality microwave signals.

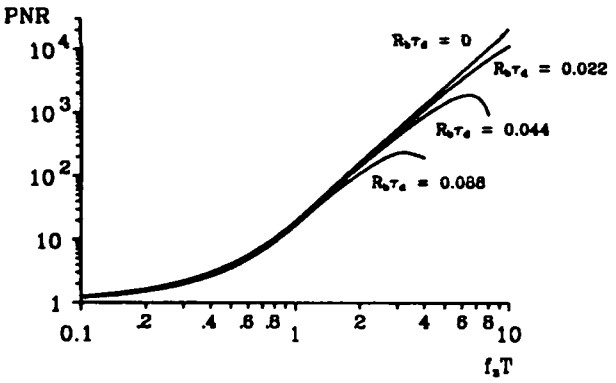

Figure 3: Phase noise reduction obtained with a second order loop as a function of normalized loop bandwidth for different values of normalized loop propagation delay.

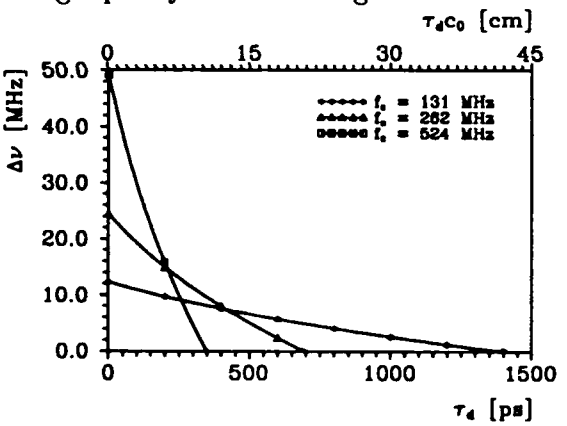

Figure 4: Laser linewidth demand for stable locked loop operation as a function of propagation delay and loop bandwidth for an average time to cycle slip of 10 years.

References

[1] A. Daryoush et al: Microwave Journal, vol. 30, no. 3, pp. 97-104, 1987.

[2] Intelsat earth station standards (IESS), Document IESS-309 (Rev. 2), 1990, p. 14.

[3] U. Gliese et al: In Proceedings of CLEO, 1991, paper CWM5.

[4] A. Blanchard: Phase-Locked Loops, John Wiley & Sons, New York 1976.

[5] R. J. S. Pedersen et al: In Proceedings of ECOC, 1990, paper TuF3.3.

FA.3 Optical Control of Microwave Circuits

Yukio Yamamoto and Tatsuo Itoh

Electrical Engineering Department, University of California, Los Angeles, 405 Hilgard Av., Los Angeles, CA 90024-1594

ABSTRACT

The simulation of the MESFET controlled active band-pass filter shows that loss of a tuning end-coupled filter is compensated by a negative resistance circuit in the frequency range over the cutoff frequency. In the region of low gate bias, the center frequency of the filter is changed well either by a gate bias or by a laser illumination. It is shown that the tuning ranges due to the gate bias and the laser illumination are 133 MHz and 43 MHz in X-band, respectively.

INTRODUCTION Recently, the active band-pass filter which was composed of a varactor tuned end coupled filter and a negative resistance circuit using a MESFET was developed [1]. It is well known that the capacitance of a MESFET can be changed either by the gate bias or by the light illumination. Therefore, it was proposed by the authors that another MESFET could also be used for tuning and controlled either by a gate-to-source voltage or by a laser illumination [2]. Use of the same elements, i.e. MESFETs, simplifies fabrication of the circuit, especially MMIC. The present paper shows the functions of the filter by simulation and the experimental results about the possible tuning range.

FILTER STRUCTURE AND MEASUREMENT PROCEDURE Fig.1 shows the microstrip pattern of the one-pole active band-pass filter. The thickness and the relative dielectric constant of the substrate are 0.737 mm and 2.55, respectively. The filter is composed of an end-coupled band-pass filter and a negative resistance (N.R.) circuit.

The characteristic impedance of the circuit is 82 Ω. The end-coupled filter is separated to two equal-length (L) microstrip lines, called two half-resonators, by a gap. The gate and source of a tuning MESFET bridge the gap. The drain is open circuited. The cover of the tuning MESFET is removed and the gate-source area is illuminated by a focused laser light of which wavelength is 788 nm. The N.R. circuit is connected to the end coupled filter through a quarter-wavelength coupler. The MESFETs are NE72084Bs(NEC). The circuit was simulated by Touchstone simulator. HP-8510 vector network analyzer was used for measurement of S_{21} of the filter. The capacitance of MESFETs was measured by HP-4275A LCR-meter at 400 kHz.

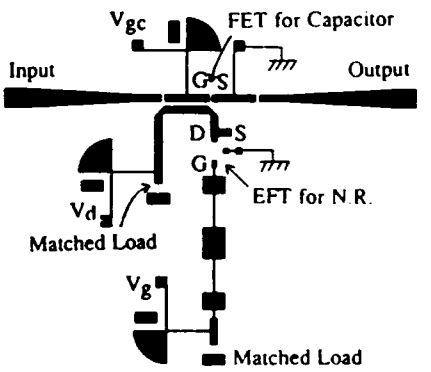

Fig.1. The circuit pattern of the filter.

RESULTS Fig.2 shows that simulated S21 of the end-coupled filter depends on the capacitance (C) connecting two half-resonators (L= 5.8mm in this case) instead of a MESFET. The center frequencies considerably shift with the variation of the capacitance. The losses in the passband are 1.9dB without N.R. In the case using the N.R., the transmission gain is observed only in the frequency region over 8.85 GHz because the filter has a low pass filter at its gate.

The relation between the gate-to-source capacitance of the MESFET and the applied gate bias (V_{gc}) was measured with and without laser illumination. The results are shown

in Fig.3. It can be seen that the capacitance is increased when V_{gc} increases from -2.2V to -0.2 V. In the same region of V_{gc}, the laser illumination with the power of 14.4mW increases the capacitance.

It is shown in Fig.4 that the center frequencies of the filters with and without the N.R. circuit depend on Vgc. In these cases, L is 4.97 mm. At the maximum Vgc points of the curves, the filter transmission losses come up to 3dB. In both cases, the maximum frequency shifts are about 132 MHz.

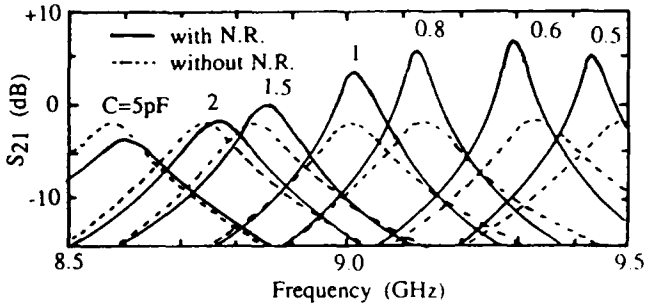

Fig.2. Simulated shift of the pass-band center frequency with the variations of the capacitance bridging the center gap.

The results shown in Fig.3 indicate that the center frequency is considerably changed in the Vgc range over -2.5 V in Fig.4. The increase of the transmission loss prevents the filter from being used in the region (Vgc>-1.5V) where the capacitance still changes significantly. The difference between curves (a) and (b) for a given Vgc indicate the possible optical tuning range, and the maximum value is 43 MHz.

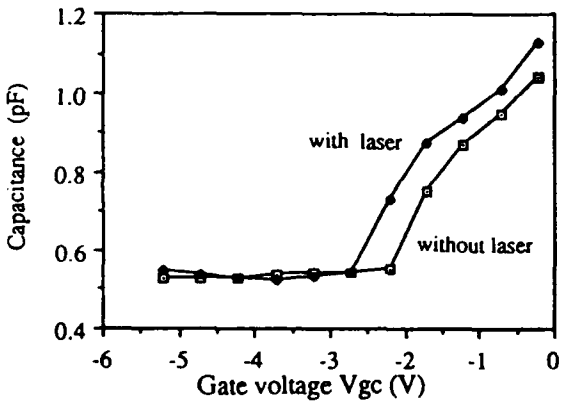

Fig 3. Measured capacitance of NE72084B MESFET vs V_{gc}.

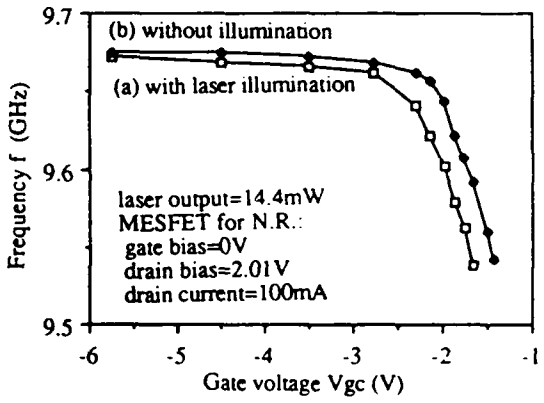

Fig.4. Center frequency of the filter pass-band vs V_{gc}.

CONCLUSIONS The results of the filter simulation show the tuning effect and the compensation of the filter loss due to the tuning capacitance and the MESFET negative resistance circuit, respectively. It is found experimentally that, in the low gate bias region, the center frequency of the pass-band changes substantially either by the gate bias or by the laser illumination experimentally. The possible tuning ranges are 43MHz optically and 132 MHz electrically.

ACKNOWLEDGMENT This work was supported by US Army Research Office under contract DAAL-03-88-K-0005.

REFERENCES

[1]C.Y.Chang and T.Itoh,*IEEE Microwave Theory Tech.*,vol.MTT-38,pp.1979-1884,1990

[2]Y.Yamamoto, K.Kawasaki and T.Itoh,*IEEE Microwave and Guided Wave Lett.* vol.1,No.5 (1991) to be published.

FA.4 Fabrication, Packaging, and Testing of 60 GHz GaAs and InGaAs Photodetectors

R.A. Marsland and T. Day
New Focus, Inc. Mountain View, CA 94041

E.Özbay, D M. Bloom
E.L. Ginzton Laboratory, Stanford University

Although dramatic speeds have been reported for photodetectors in the laboratory [1][2], the frequency response of commercially available photodetectors has been limited to date by the difficulty of manufacturing these units and verifying their performance in production. We have developed a coplanar-waveguide based package which allows low-parasitic interface to the coplanar-waveguide transmission line patterned on the photodiode chip. This package also provides a means of aligning a fiber pigtail to either the front or the back side of the photodiode chip. Testing of the photodiodes is achieved by frequency locking two infrared lasers with a difference frequency up to 60 GHz to generate the mm-wave signal and simultaneously doubling the lasers to translate the signal into the visible region of the spectrum.

Both the GaAs and InGaAs photodiodes are Schottky barrier type. The GaAs photodiode consists of a semi-transparent (100Å) Au Schottky contact on an N- GaAs active layer. A heavily doped N+ layer below the active layer provides a low resistance back contact for the photodiode. The substrate is semi-insulating to allow patterning a low loss transmission line on the photodiode chip. Active areas are isolated using proton damage. The InGaAs photodiode uses a thin InAlAs layer to raise the Schottky barrier height [3] and a heavily doped InAlAs layer beneath the active layer to provide the ohmic back contact. The substrate is semi-insulating Fe:InP. Active areas are isolated using a mesa etch, and an airbridge is used to make a low-capacitance connection to the Schottky contact. Because the airbridge used to make contact to the Schottky contact on the InGaAs photodiode is opaque, this photodiode must be back illuminated. Thus the wafer is thinned and polished to 0.005" after processing and the fiber is attached to the back side.

Coplanar-waveguide (CPW) was chosen for the planar transmission lines connecting the microwave launcher to the photodiode because backside metal is not required. A lack of backside metal not only simplifies processing of the photodiode chip (all contacts are on one side) but also makes both the front and back sides of the chip readily accessible. The photodiode and a bias circuit are bonded to a fused quartz carrier which is in turn bonded into the microwave housing. The fused-quartz carrier for the InGaAs chips has a 0.015" hole beneath the photodiode to allow plenty of room for aligning the fiber to the backside of the chip (Fig 1). Once the fiber is epoxied to the chip, it is strain-relieved and epoxied to one of the lids on the microwave housing.

Testing of the photodiodes was accomplished by offset locking two Lightwave Electronics model 120 single frequency lasers with a difference frequency up to 60 GHz. The lasers are locked to adjacent axial modes of an externally resonant doubling cavity [4] as shown in Figure 2. Locking to adjacent axial modes of a cavity serves two purposes. First, the locking process allows for careful control of the difference frequency between the lasers, and second, locking is required for efficient doubling the lasers which allows for simultaneous characterization of the visible GaAs photodiodes. The doubling material was a 5 mm long piece of KTP. The cavity free spectral range is 1.00 GHz and is resonant at 1.06 μm. The difference frequency is therefore stepped in 1 GHz increments in the IR and 2.0 GHz in the green. The frequency response of the diodes is shown in Figure 3 and was obtained in three steps. From 0-21 GHz a μwave spectrum analyzer was used to analyze the output from the V connector on the photodiode housing. From 26-40 GHz and from 40-60 GHz mm-wave mixers are used. In all cases the optically generated

mm-wave signal was obtained by focusing the offset locked lasers into the fiber pigtailed directly on the photodiode housing.

In summary, packaged diodes with response to 60 GHz in the visible and near IR have been demonstrated. Coplanar Schottky structures provide a robust packaging scheme and testing of the diodes using offset locked lasers has proven to be very reliable technique.

References

1. E. Özbay, K.D. Li, and D.M. Bloom, "2.0ps, 150 GHz GaAs Monolithic Photodiode and All-Electronic Sampler," *Picosecond Electronics and Optoelectronics*, March 13-15, 1991.
2. R.S. Tucker, A.J. Taylor, C.A. Burrus, G. Eisentstein, and J.M. Wiesenfeld, "Coaxially mounted 67 GHz bandwidth InGaAs PIN photodiode," *Electron. Lett.*, **22**. pp. 917-918, 1986.
3. O.Wada, H. Nobuhara, H. Hamaguchi, T. Mikawa, A. Tackeuchi, and T. Fujii, "Very high speed GaInAs metal-semiconductor-metal photodiode incorporating and AlInAs/GaInAs graded superlattice," *Appl. Phys. Lett.*, **54**, pp. 16-17, 1988.
4. W. J. Kozlovsky, C. D. Nabors, and R. L. Byer, "Efficient second harmonic generation of a diode-laser-pumped cw Nd:YAG laser using monolithic MgO:$LiNbO_3$ external resonant cavities," *IEEE J. Quantum Electron.*, **24**, pp. 913-917, 1988

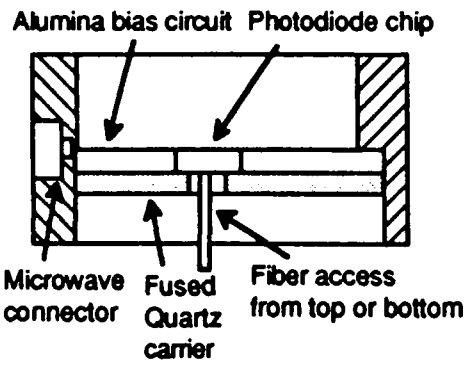

Figure 1. Cross section of the coplanar-waveguide based package.

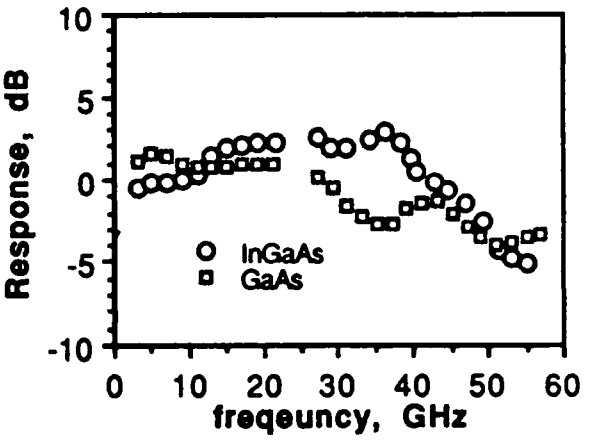

Figure 2. Frequency response of the GaAs and InGaAs packaged photodiode

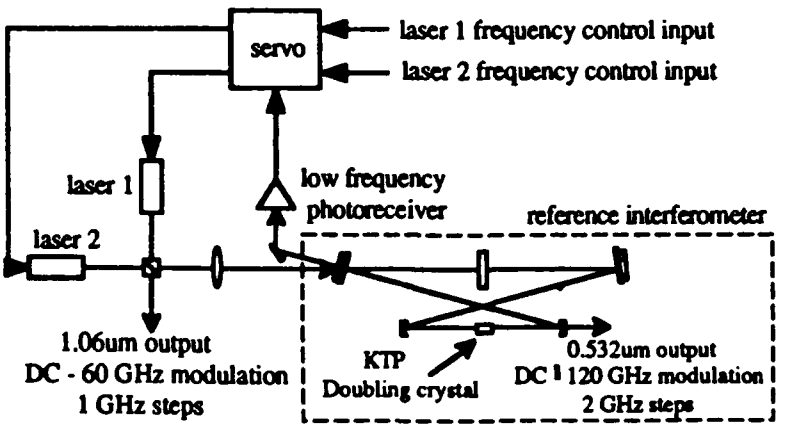

Figure 3. Optical layout for characterization of the InGaAs and GaAs photodiodes.

FA.5 Microwave-Optical Mixing and Harmonic Generation

G.K. Gopalakrishnan and K. Chang

Department of Electrical Engineering, Texas A&M University
College Station, Texas 77843-3128

Optoelectronic integrated circuit (OEIC) technology has been intensely investigated in the recent past for application in multi-gigabit/second fiber-optic communication systems [1]. Concomitantly, considerable research in optoelectronic devices and systems for generation of microwave signals [2], control of microwave oscillators [3] and transmission of microwave signals over a fiber-optic cable [4] have also been carried out. In future microwave systems where signal and local oscillator waveforms are transmitted over optical fibers, analog OEICs with complexity comparable to the present digital OEICs will be needed. In this paper we present a study of the interaction of microwave and optical signals in a semiconductor substrate.

To study microwave-optical interactions in the context of mixing and harmonic generation, we have built a microwave OEIC [5] by integrating a Schottky diode photodetector into a microstrip ring resonator. The flexibility afforded by this approach is that both resistive and reactive changes of the photodetector, due to absorption of modulated light, can be independently availed to study microwave-optical interactions. When the interaction involves a resistive change, the circuit is said to be operated in the resistive mixing mode; studies pertaining to reactive changes involve operation of the circuit in the parametric mode. It is found that the interaction efficiency of the circuit is enhanced when the microwave and modulated optical signals are near a ring's resonance. Details pertaining to the operation and performance of the circuit will be presented. It is expected that this type of optoelectronic resonator circuit can be used for generating IF signals in receivers for analog fiber optic communication and in OEICs for optically controlled microwave oscillators.

REFERENCES

1. T. Horimatsu and M. Sasaki, "OEIC technology and its application to subscriber loops," *Journal of Lightwave Technology*, vol. LT-7, pp. 1612-1622, November 1989.

2. C.H. Lee, "Picosecond optics and microwave technology," *IEEE Trans. on Microwave Theory and Techniques*, vol. MTT-38, pp. 596-607, May 1990.

3. A.J. Seeds and A.A.A de Salles, "Optical control of microwave semiconductor devices," *IEEE Trans. on Microwave Theory and Techniques*, vol. MTT-38, pp. 577-585, May 1990.

4. W.E. Stephens and T.R. Joseph, "A 1.3 μm fiber-optic link using a direct modulated laser transmitter," *Journal of Lightwave Technology*, vol. LT-3, pp. 308-315, April 1985.

5. G.K. Gopalakrishnan, B.W. Fairchild, C.L. Yeh, C.S. Park, K. Chang, M.H. Weichold and H.F. Taylor, "Microwave performance of a nonlinear optoelectronic microstrip ring resonator," *Electronics Letters*, vol. 27, pp. 121-123, January 1991.

FB.1

Application of Photonics to Microwave and Millimeter-Wave Systems

B. Hendrickson, *USAF Rome Laboratory, Griffiss AFB, NY*

Photonics provides a new dimension in microwave (MW) and millimeter-wave (MMW) systems. By placing MW-MMW signals on the optical carrier, processes at the MW-MMW frequency become much simpler at the optical frequency. This is particularly true in phased array antenna systems. Beneficial impacts also exist in signal distribution and processing. This paper will discuss applications, system impacts, and technology issues to achieve those impacts.

FB.2 A High Performance Integrated Optic System to Control RF Phase and Amplitude for Phased Array Antennas

J.F. Coward, T.K. Yee, C.H. Chalfant, P.H. Chang
Lockheed Missiles and Space Co.
P.O.Box 3504
Sunnyvale, CA 94088-3504

The practical application of phased arrays is limited by their need for complex corporate feed structures and active phase shifting elements which drive system cost, weight, and power consumption beyond acceptable limits for most potential space applications. Much of the development has focussed on MMIC technology in an attempt to minimize cost and weight. Although significant progress has been made on wideband phase and amplitude controllers, the RF peak and amplitude taper errors are far above the typical requirements of 3° for phase and 0.5 dB for amplitude. Furthermore, coaxial cable is still required in the distribution of RF signals thus adding to the system weight. Photonic technologies have been extensively investigated for weight and power reduction and increased bandwidth.[1,2]. Our study has shown that photonic system can also significantly improve RF phase and amplitude performance. As a result of our investigations, we have developed a high performance RF vector modulators that can control RF phase amplitude and also convert the electrical signal to an optical signal. The modulator which is modulo-2π in nature can be connected to optical time delay units to allow very wide instantaneous bandwidth.

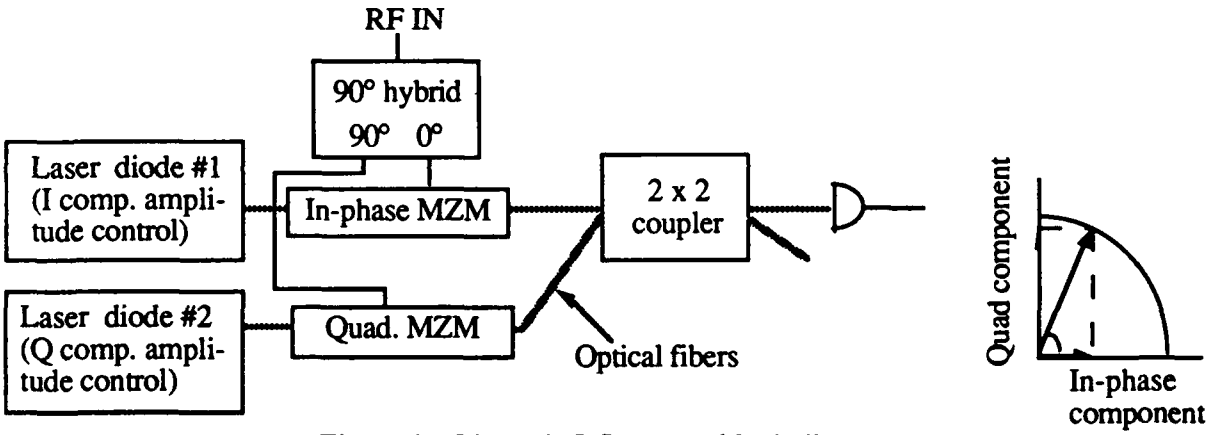

Figure 1. Photonic I-Q system block diagram.

Figure 1 shows the block diagram for a Photonic In-Phase/Quadrature (I-Q) Microwave Phase and Amplitude control system. The microwave signal is split by a 90° hybrid into in-phase (I) and quadrature (Q) components which drive two integrated optic Mach-Zehnder Modulators (MZMs). The intensity modulated light from the I and Q legs is combined by the 2x2 optical coupler and directed to an optical detector. The detector performs the vector addition of the I and Q intensities and converts the optical signal into an electrical signal. Adjusting the relative and absolute I and Q intensities hitting the detector results in RF phase and amplitude adjustment of the electrical signal out of the detector. By weighting the optical intensity modulated signal out of each MZM, it is possible to achieve 0° to 90° phase control as shown in the phasor diagram. The weighting can be accomplished by several means including adjusting the laser diode output powers.

The Photonic I-Q system can achieve 360° phase control by utilizing a characteristics of the MZM. When biased at the $-\pi/4$ point the modulated optical intensity will be in phase with the input RF signal. If the MZM is biased at the $+\pi/4$ point, the intensity is 180° out of phase with the RF

input. By permutations of the $-\pi/4$ and $\pi/4$ bias points for the I and Q MZMs, it is possible to extend the operation into the other 3 quadrants and thus achieve 360° phase control.

A Photonic I-Q system was assembled using discrete integrated-optic components. The system had excellent phase performance with errors less than 1° (Figure 2). Amplitude taper tests were performed on the individual I and Q links with RF phase errors less than 1° over a 25 dB attenuation range (Figure 3). Additionally, temperature testing was performed on the individual links that demonstrated less than 2° error over a 25 °C temperature range. The results of the temperature tests are also shown in Figure 4.

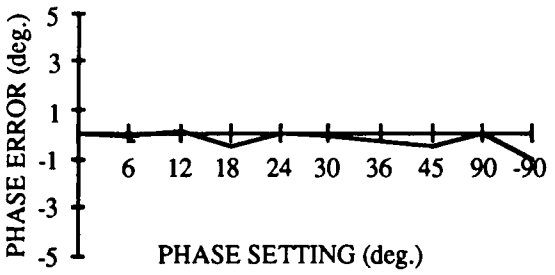

Figure 2. Phase errors as a function of phase setting.

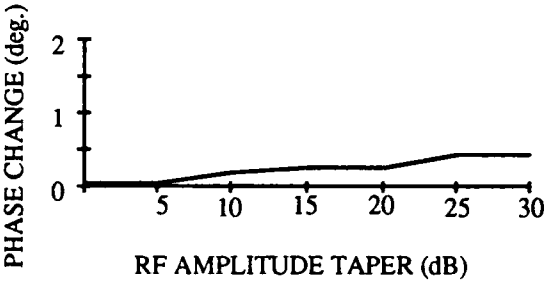

Figure 3. Phase errors as a function of amplitude taper and temperature.

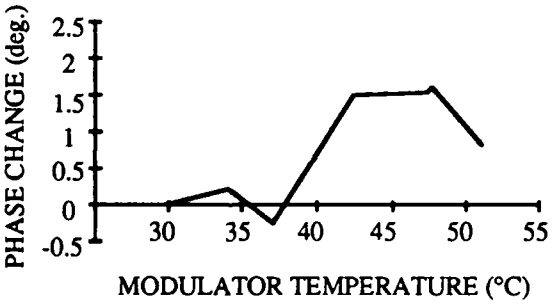

Figure 4. Phase errors as a function of temperature

We have also demonstrateed that the system can be configured such that the phase adjustment is proportional to a single input control voltage. Finally, we are integrating all the components into chip form to attain the normal advantages of electronic integration, i.e. lower cost, better reliability, etc.

[1] R. R. Kunath and K. B. Bhasin, SPIE vol.886, Optoelectronic Sig. Processing for Phase Array Antennas, 1988.

[2] G. L. Tangonan, SPIE vol.1102, Opt. Tech. for Microwave Appl. IV, 1989.

FB.3 Scattering of Transient Radiation by Three-dimensional Objects

W. M. Robertson, G. V. Kopcsay, and G. Arjavalingam

IBM T. J. Watson Research Center
P.O. Box 218, Yorktown Heights, NY 10598

The scattering of electromagnetic radiation by three-dimensional objects is a fundamental topic in both optics and microwave engineering. Although the theoretical description of scattering has been well explored, accurate experimental results in well-defined scattering configurations are difficult to obtain and thus are far less numerous. In this presentation we demonstrate that the technique of coherent microwave transient spectroscopy (COMITS)[1] provides a valuable new method of performing electromagnetic scattering experiments. COMITS offers a number of features that make it particularly suited to scattering measurements: broad frequency coverage (15 GHz - 140 GHz) in a single experiment; radiation which is freely propagating and linearly polarized; coherence, i.e. both amplitude and phase information are preserved; and finally, the data is acquired in the time-domain which offers an unusual perspective on the scattering process as well as permitting the exclusion of spurious reflections by time windowing.

COMITS is based on the radiation and detection of ultrashort electromagnetic transients by optoelectronically pulsed antennas.[1] The freely propagating transients have frequency components in the range 15 GHz to 140 GHz, facilitating broadband microwave measurements, in a single experiment. Figure 1 shows the experimental configuration for COMITS scattering experiments.

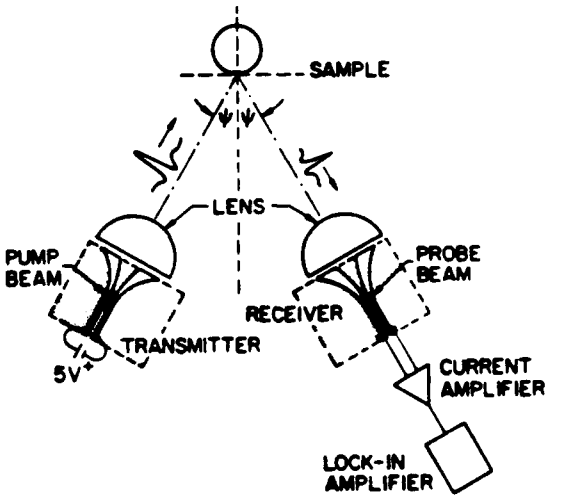

Figure 1. COMITS configuration for scattering measurements.

The transmitting and receiving antennas are exponentially tapered coplanar strip antennas photolithographically fabricated on silicon-on-sapphire. The transmitter is excited, and the received signal photoconductively sampled, by 1.5 ps optical pulses at 527

nm from a mode-locked, pulse-compressed, and frequency-doubled Nd:YLF laser. The optical pulses are arranged in a pump-probe configuration such that the signal arriving at the receiver is measured as a function of the delay time between the pump and probe. As shown, hemispherical fused silica lenses are used to collimate the transient radiation from the transmitter and to focus the scattered radiation onto the receiver. Absolute scattering cross-sections are obtained by referencing the scattered signal to that recorded by specular reflection from a gold mirror (an essentially perfect reflector at microwave frequencies).

Time domain waveforms scattered from a series of different diameter aluminum cylinders were recorded. The waveforms contain two pulses, an initial strong pulse at a time delay corresponding to specular reflection from the cylinder, and a second weaker pulse which is delayed with respect to the initial pulse by a time proportional to the diameter of the rod. When Fourier transformed and analyzed in the frequency domain, the results are in reasonable agreement with the theory for plane wave scattering from a perfectly conducting cylinder.[2] As an example Figure 2 shows the corresponding results for a 0.250" diameter cylinder. Scattering from a series of spheres was also measured and these results will be presented.

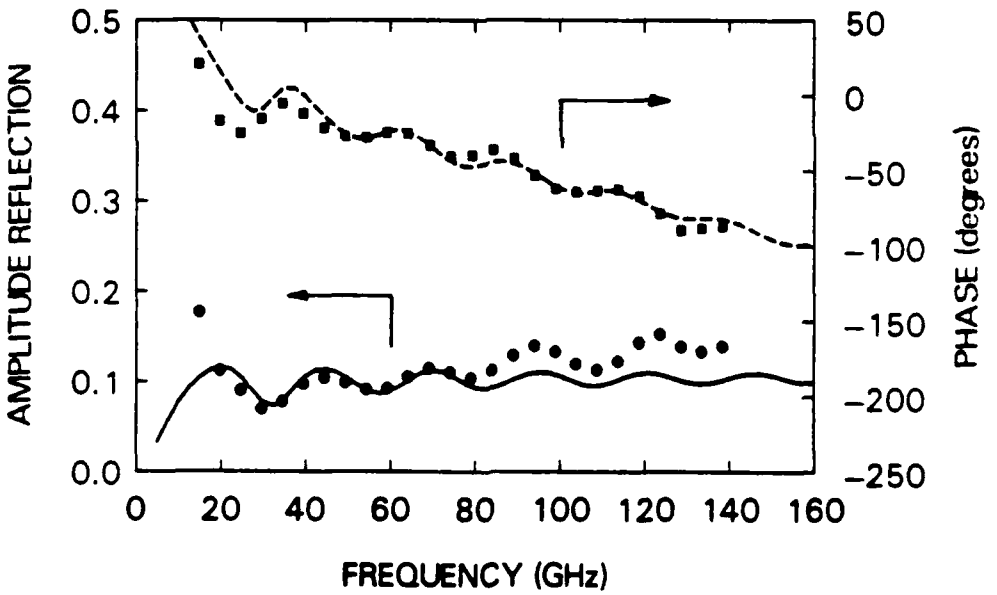

Figure 2. Frequency-domain results of scattering by a 0.250" aluminum cylinder.

References

1. W. M. Robertson, G. Arjavalingam, and G. V. Kopcsay, Appl. Phys. Lett. **57**, 1958 (1990).

2. "Time-Harmonic Electromagnetic Fields", R. Harrington (New York, McGraw-Hill, 1961) pp. 232-235.

FB.4 Phased Array Antenna Beamforming Using Optical Processor

L.P.Anderson, F. Boldissar, D.C.D.Chang
Hughes Aircraft Company, Space and Communications Group
P.O.Box 92919, El Segundo, California 90245

1. INTRODUCTION

Phased array antennas are playing an increasingly important role in current and anticipated radar and communications applications.RF distribution manifolds used to furnish the required aperture excitation can become prohibitively bulky for space applications.

Problems with conventional beamforming for large arrays makes it imperative to develop a proposed technology that performs array beamforming via alternative approaches. A novel method utilizing an optical signal processor to furnish these excitations has been proposed.

Previous work has described the operational principles of such a processor [1,2] and have established a simple analytical model for the network.

This work will describe refinements to the originally proposed model which include errors in the spatial path. The effect of the processor on the microwave signal to noise quality at the antenna output will also be considered.

2. SPATIAL PROCESSING MODEL

The model for the optical processor is based on the Fourier transform relationship between the front and rear focal planes of the optical lens of focal length f [3]. Here a two dimensional image formed in the rear focal plane can be expressible as an electric field distribution in the forward focal plane. The input field distribution is expressed as:

$$E(x_1, y_1) = t_o(x_1, y_1)\, E_o \qquad (1)$$

where $t_o(x_1, y_1) =$ image transmittance function of the SLM

The field formed in the front focal plane of the lens via diffraction are thus expressible through a Fourier transform i.e.,

$$E(x_2, y_2) \sim \iint_{-\infty}^{+\infty} t_o(x_1, y_1) \exp\left\{\frac{-j2\pi}{\lambda f}(x_1 x_2 + y_1 y_2)\right\} dx_1 dy_1 \qquad (2)$$

The pupil function is assumed to be unity for the lens. A digitized image of the desired far field footprint is provided in the form of light and dark contrasting elements (pixels). A discreet Fourier transform is thus formed for a NxM matrix scene of area axa (square) constant transmittance pixels. Thus the front focal field are now expressible by the double summation:

$$E_{focal}(x_2, y_2) \sim \sum_{n=1}^{N} \sum_{m=1}^{M} t_{mn}(x_1, y_1)\, sinc(a f_{x_n})\, sinc(a f_{y_m})\, e^{-j2\pi(b_n f_{x_n} + c_m f_{y_m})} \qquad (3)$$

where f_x, f_y are spatial frequencies and bm, cn are offsets of the m, nth pixel in the x , y , directions respectively.The function

$$sinc(z) = \frac{\sin(\pi z)}{\pi z}$$

Thus both amplitutde and phase (i.e. pixel "brightness" and location relative to a central axis) is contained in equation (3). The distribution E(x2,y2) now represents the complex

aperture excitation, once downconverted, of the array antenna. The far zone fields resulting from such excitations may be obtained via standard Fraunhoffer diffraction evaluation of the array aperture.

Deterministic errors (i.e. axial defocussing of F.T.L.) can be approximated by the addition of a quadratic phase term to the incident wavefront i.e.

$$E_{nm}(x_1, y_1) = E_0\left(t_{nm}(x_1, y_1)\, e^{-j\delta_{nm}}\right) \qquad (4)$$

Here the quadratic phase term is defined as:

$$\delta_{nm}(x_1, y_1) = k\left\{\frac{x_{1n}^2 + y_{1m}^2}{2R_0}\right\} \qquad (5)$$

where k is the free space wavenumber and Ro is the axial displacement of pixel from image plane. The effect of the error was evaluated using a one dimensional model to simplify understanding of the resultant Fourier transform spectra. For progressive values of phase error, the presence of grating lobes of increasing intensity is observed in the spatial frequency output plane. The element pattern presented by the individual pixels in the SLM serve to modulate the amplitude of the grating lobe formation. The existence of these lobes in the complex aperture distribution of the antenna array will serve to create secondary beams in the far field. Albeit in most applications, these lobes will not exist in visible space due to finite array aperture; they will tend to decrease main lobe directivity.

3. TEMPORAL PROCESSING MODEL

An essential element of consideration in the utilization of the processor is the evaluation of signal quality in the communications link. The underlying basis of the analysis is the development of the expression for processor output signal to noise ratio.It can be shown that exclusive of input and output amplifiers and their associated matching circuits, the expression for processor (S/N) out is found to be

$$\left(\frac{S}{N}\right)_{out} = \frac{P_{in}\left(\frac{\tau P_n \eta_d e}{2V_\pi L_0 h\nu}\right)^2 R_0 R_M}{\left(\frac{P_n \eta_d e}{2L_0 h\nu}\right)^2 R_0 (R_{IN})\Delta\nu + \frac{P_n \eta_d e^2}{h\nu L_0}\left(1 - \frac{\eta_d}{2L_0}\right) R_0 \Delta\nu + kT\Delta\nu} \qquad (6)$$

here the variables have been defined in [2]. The noise contributions in the denominator can be attributed to three major categories [4]; (1) Laser noise (2) partition noise (quantum effects) and (3) detector noise. Note that this general equation will be weighted accordingly with the individual amplitude coefficients assocated withs the F.T. spectra at the fiber optic input.

4. References

1. L.P.Anderson et. al "Antenna Beamforming Using Optical Processing" SPIE Vol. 886 p.228 Jan. 1988.

2. "Antenna Beamforming Using Optical Techniques - Follow-On Study" NASA LeRc Final Report Contract #NAS 3-25720 Feb. 1991.

3. Goodman Introduction to Fourier Optics p. 86-87 McGraw Hill N.Y. Cpy 1968.

4. R.H.Buckley "Progress in Mcrowave Modulated Fiber Optic Links SPIE Vol. 1101 Jan. 1979.

Optical Millimeter-Wave Interactions
AUTHOR INDEX